Mechanisms of antibody-mediated neutralization targeting viral glycoproteins

James A. Williams

A dissertation

submitted in partial fulfillment of the

requirements for the degree of

Doctor of Philosophy

University of Washington

2018

Reading Committee:

Kelly Lee, Chair

Abhinav Nath

William Atkins

Program Authorized to Offer Degree:

Medicinal Chemistry

University of Washington

Abstract

Mechanisms of antibody-mediated neutralization targeting viral glycoproteins

James A. Williams

Chair of the Supervisory Committee:

Kelly Lee

Medicinal Chemistry

The antibody response against viral glycoproteins is important for preventing many viral infections but we lack a comprehensive understanding of the mechanisms by which antibodies act. Furthermore, the immense antigenic variability of glycoproteins complicates the design of immunogens that must elicit broadly neutralizing antibodies (bnAbs) capable of neutralizing a range of circulating isolates. The objective of this dissertation is to shed light on the mechanisms of antibody-mediated neutralization of enveloped viruses and the ability of nAbs to inhibit glycoprotein function by examining two significant human pathogens, influenza and HIV-1. Firstly, in Chapter 2, I investigate the effect of nAb binding and the role of IgG bivalency on inhibition of influenza's hemagglutinin (HA) glycoprotein function for nAbs targeting distinct epitopes. I observe that the Ab-mediated inhibition of HA function occurs by multiple complementary mechanisms, and is largely dependent on the specific epitope that is targeted and on the bivalent nature of IgG molecules. My work reveals that the ability of nAbs to aggregate influenza virus particles enhances the inhibition of HA at an early stage of fusion peptide-induced membrane disruption through the occlusion of infectious virions. Epitopes further down the HA stem do not exhibit cross-linking across separate particles, but the findings here support a model of neutralization where bivalent binding to a sufficient amount of antigen is needed to disrupt the cooperative network of HA required for fusion. These results demonstrate that IgG bivalency enhances HA inhibition through functionally important modes not evident in pared-down Fab-soluble HA

structures. In Chapter 3, I solve the cryo-EM structure of the first, and currently best described, infant-derived broadly neutralizing antibody against the HIV-1 envelope (Env) glycoprotein. We reveal that BF520.1 binds an epitope commonly targeted by adult-derived bnAbs, namely the V3-glycan region of HIV-1 Env. In addition, we highlight an important role in variable light chain development for BF520.1, which occurs early during lineage maturation and makes extensive contacts with the N332 glycan. Overall, the identification of a rapidly developed, infant bnAb is encouraging for vaccination strategies that aim to elicit bnAbs without the requirement for a long-term maturation pathway. Finally, Chapter 4 begins to explore BF520.1's development through characterization of early antibody lineage intermediates. We propose that early light chain mutations help to establish the antibody's epitope early in development, allowing focusing of heavy chain contacts. Overall, it is clear that future development of vaccination strategies will require in-depth knowledge of the critical interactions between antibody and virus, a comprehensive understanding of the mechanisms by which nAbs act, as well as familiarity with the developmental pathways bnAbs undergo in response to a rapidly evolving, antigenically diverse virus.

Table of Contents

List of Figures

Acknowledgements

I would like to take this opportunity to express my gratitude to the following individuals who have contributed towards the success and completion of this dissertation.

My sincere appreciation goes to my supervisor and mentor, Dr. Kelly Lee, who provided tremendous support and guidance during my graduate research. You have always been a voice of encouragement and inspiration, even when things seemed at their most difficult. You always reminded me to think big when considering my research—to boldly ask questions and courageously seek answers. There are many moments from my time here that I will always remember. This has truly been an amazing journey.

I would also like to extend thanks to my committee members for all their guidance during this process: Dr. William Atkins, Dr. Abhinav Nath, Dr. Shiu-Lok Hu and Dr. David Veesler. Dr. Atkins, thank you for reminding me that sometimes frustration is part of the process towards something wonderful. This helped me to maintain focus and excitement throughout graduate school. Dr. Nath, thank you for helping me think critically about my project. Your thoughtful questions always offered a new perspective that I may not have otherwise considered. Dr. Hu, you motivated me to reflect on the broader context of the questions I attempted to answer. Thank you for helping me to look for meaning far beyond the data that was right in front of me. And to Dr. Veesler, thank you for always being willing to help answer technical questions I had. Your advice and generous assistance greatly improved my understanding of cryo-electron microscopy.

Also, I extend gratitude to Julie Overbaugh for allowing me to partner with her lab over the past few years. It has been a privilege to work alongside such a motivated and excited group. And to Cassie Simonich and Laura Noges, thank you both for every interesting discussion we had about the project. I learned so much from you both and your enthusiasm brought joy into collaborative research.

Thank you to all my colleagues and friends at the University of Washington over the years: Long Gui, Natalie Garcia, Tad Davenport, Mark Benhaim, Eddie Hodge, Nancy Hom, Rachel Kinzelman, Alex Mileant, Gajendra Naika, Vidya Magala Prasad, Adam Nguyen, and Klaus Lovendahl. You all made this experience more enjoyable than I could have imagined and I am thankful for your friendships. Also, thank you to my classmates, Michelle Redhair and Robert Pelletier. There are so many great memories during our time here and I look forward to more.

I would have never even attempted, let alone completed this dissertation, had it not have been for my parents, Steven Williams and Brenda Williams, who have always supported me and believed in my abilities. You taught me from a young age to work hard and to be kind to others. Those two things shaped my experience here in Seattle and for that I am thankful. And to my wife, Nicole, thank you for your patience and your support. I don't know how I managed to survive here without you so long. This dissertation is as much yours as it is mine.

Dedication

To my loving wife, Nicole, for always encouraging me to relax more and laugh often; for being a constant source of comfort and peace.

Chapter 1. Introduction

1.1 Overview

Viruses that infect humans present an immense challenge for global healthcare systems and account for extremely high morbidity and mortality across multiple populations (1-3). As a result, the development of effective vaccination strategies is of great importance. During natural infection, neutralizing antibodies (nAbs) play a key role in the immune response against viral pathogens by binding to viral surface proteins and preventing them from mediating cell entry and infection. Broadly neutralizing antibodies (bnAbs) are of significant interest because they provide protection against most strains of a given virus. Consequently, these bnAbs could serve as potential therapeutic agents and as guides for designing an effective vaccine to confer long-lasting immunity. Human immunodeficiency virus (HIV-1) and influenza A virus (IAV) are two noteworthy human pathogens that complicate the design of an effective vaccine due to the vast global diversity among circulating strains (4-7). Nevertheless, there has been achievement in the isolation of bnAbs that exhibit broad and potent neutralization. Demonstrated success of protection in animal models and the suppression of HIV-1 viremia in chronically infected individuals has given hope that suitable immunogens capable of eliciting a broad and potent antibody response can be designed (8-13). However, the future development of such an immunogen will require in-depth knowledge of the critical interactions between antibody and virus, a comprehensive understanding of the mechanisms by which neutralizing antibodies act, as well as familiarity with the developmental pathways bnAbs undergo in response to a rapidly evolving, antigenically diverse virus. Below, the major antigenic targets of nAbs for IAV and HIV will be discussed, as will the challenges associated with eliciting a broadly neutralizing antibody response.

1.2 The role of viral glycoproteins in virus entry

In its simplest description, viruses are infectious agents composed of nucleic acid, either RNA or DNA, that are encapsulated by a protective protein coat. The distinguishing feature of an enveloped virus is a host-derived lipid bilayer that is acquired when newly formed particles are released via budding at a host-cell membrane. Considering that the lipid bilayer is derived from the host, the viral envelope acts as

an additional barrier to shield the internal components from the host immune system. As a result, the enveloped virus must deliver the genetic cargo through fusion of the viral and host-cell membrane for continuous rounds of replication to occur. Viral glycoproteins are presented on the surface of all enveloped viruses. These protein machines facilitate delivery of the genetic material by functioning as a catalyst to overcome the kinetic barrier of merging two membranes together (14, 15). The roles of viral glycoproteins in mediating attachment to host cells and catalyzing the subsequent fusion event have been well described for many enveloped viruses. Pre-fusion structures of attachment glycoproteins bound to their cognate receptors have revealed the architecture of various glycoproteins that help determine the host-cell tropism, while post-fusion structures of fusion domains highlight the dramatic conformational changes that drive the merging of viral and target membranes. Although the overall variation amongst glycoproteins is diverse, all act within common stages, involving attachment and triggering, leading to subsequent fusion of two membranes. Given that viral glycoproteins are the earliest viral components detected by the host immune system and that they have a critical role in initiating viral pathogenesis, vaccines that can elicit antibodies, which block the glycoprotein's functions are a highly desirable means of gaining protection against infection. However, for viruses such as influenza and HIV-1, where vaccines that provide protection against a broad range of viral strains (a universal vaccine) remain unavailable, the immune response is tasked with overcoming the many evasion strategies evolved by these viruses.

1.3 Architecture of the influenza A virus

Influenza A virus is a member of the *Orthomyxoviridae* family of enveloped viruses that is composed of a segmented, single-stranded, negative-sense RNA genome (16). The RNA genome is packaged as a complex of viral polymerases and nucleoproteins, and is encapsulated by a lipid-bilayer that is acquired from the host plasma membrane during egress from the cell (17). Two glycoproteins project outward from the viral envelope and are the primary targets for the humoral immune system (Figure 1.1A). Hemagglutinin (HA) is the most abundant glycoprotein on the viral surface and mediates virus attachment through interactions with sialic acid on the host-cell surface, leading to endocytosis of the particle (18, 19). The second surface glycoprotein, neuraminidase (NA), cleaves sialic acid from the surface of glycoproteins, allowing egress of newly formed influenza particles from infected cells. Variation in antigenicity of these

glycoproteins has been used to classify influenza A virus into 16 HA and 9 NA subtypes. HA and NA are divided phylogenetically into two groups, and viruses of varying combinations of HA and NA have been isolated in avian species with potential for crossover into humans (20, 21). Both glycoproteins are the targets of antibodies that can prevent spread of the virus; however, in contrast to anti-NA antibodies, which act by preventing the release of progeny virus from already infected cells, only anti-HA antibodies can effectively prevent viral entry (22). Therefore, structural characterization of HA has been the focus of extensive research aimed at understanding the mechanisms of fusion and inhibition by neutralizing antibodies.

1.4 Overview of influenza hemagglutinin structure

Influenza HA is initially synthesized as a single polypeptide precursor (HA0) that is activated by cellular proteases into a receptor binding domain, HA1, that is connected by a single disulfide linkage to the fusion subunit HA2 (23). Binding of HA1 to sialic acid on the cell surface results in internalization of the virus via endocytosis. Acidification of the maturing endosome directs fusion peptide release and triggers a cascade of conformational changes, leading to fusion of the viral envelope and host-cell membrane (Figure 1.1B).

HA was the first viral antigen for which high resolution structural information was achieved, setting a standard for how other viral glycoproteins would be studied (23). The reported crystal structure of the soluble ectodomain of HA at neutral pH revealed a 225 kDa HA trimer made up of a globular domain of antiparallel beta sheets (HA1), nestled atop a coiled-coil of alpha helices (HA2) (Figure 1.1). The globular domain of each protomer forms a trimeric interface at the distal end of the glycoprotein and is thought to stabilize HA in its prefusion conformation at neutral pH. This premise was supported by the observed difficulty in expression of soluble forms of the HA2 fusion domain, which often spontaneously triggered into the post-fusion conformation (24). A highly conserved, shallow groove at the apex of each HA1 subunit forms the receptor binding domain (RBS). At the base of the RBS exist several conserved amino acids (Tyr98, Trp153, His183, and Tyr195), two loops (130 and 220 loop), and the 190-alpha helix forming the edges of the RBS. Mutations around the RBS are thought to be responsible for differences in receptor affinity and specificity amongst influenza variants, and mutagenesis of as few as one amino acid has been

shown to alter receptor specificity from avian to human-like sialic acid (25-27). HA2, as it exists within the HA trimer at neutral pH, forms the majority of the membrane proximal domain and is composed of a coiled coil of helices connected by a linear peptide linker that forms electrostatic interactions with the base of HA1. A series of HA2 helices and the N-terminus of HA1 form a negatively charged cavity that functions to stabilize the fusion peptide.

More than a decade passed before the post-fusion form of HA2 would be solved. This striking structure of a trimer of HA2 subunits illustrated the dramatic reorganization that occurs especially in this fusion machinery subunit (28). The HA2 subunits reorganize into a six-helix bundle, juxtaposing the fusion peptides on the same side as the transmembrane domains (29). The pH-induced refolding of HA2 has been suggested to provide the mechanism for catalyzing membrane fusion. Although the exact number of HA trimers required for fusion is not well understood, it is widely accepted that a functional network of several HA trimers is required (30-33).

1.5 Neutralizing antibodies against HA

Influenza virus vaccines currently represent our best strategy for protection against influenza infection. The majority of antibodies generated through vaccination target the membrane-distal HA1 subunit and block attachment of HA to sialylated host receptors, suggesting that neutralization primarily interferes with receptor engagement (22, 34, 35). The receptor binding site of HA is surrounded by several antigenic sites that are targeted by neutralizing antibodies designated as sites A, B, C, D and E for group 2 and Sa, Sb, Ca1, Ca2, and Cb for group 1 HA subtypes (Figure 1.2B). Although the antibodies directed against these antigenic sites possess potent neutralizing activity, they are generally strain specific due to the rapid evolution of influenza virus and the frequent amino acid changes occurring near the receptor binding site of HA1. As these mutations accumulate in a process referred to as antigenic drift, the virus strain is no longer neutralized by host antibodies, leaving the host susceptible to infection by the drifted variant. In rare cases, it has been observed that antibodies against HA1 have the capability of cross-reactive neutralization (36, 37). These rare antibodies target relatively invariant features within the receptor binding site; however, they exhibit narrow specificity and are often group specific (38-41).

In contrast to the high sequence variability within the globular head domain, the membrane proximal stalk domain of HA is highly conserved among both group 1 and group 2 influenza viruses and is composed of the N- and C-terminal parts of HA1 and the N-terminal part of HA2 (42, 43). Antibodies against the HA stalk are rare in humans and are generally not induced by vaccination (44, 45). It was long thought that the HA stalk was not a significant target of the immune response, and it was not until 1993 that the first antibody against the stalk domain, C179, was isolated after immunizing rats with an H2N2 influenza strain (46). C179 showed broad neutralizing activity against multiple group 1 viruses and rather than blocking receptor binding, C179 inhibited HA's fusion activity, suggesting an alternative mechanism of neutralization, specifically by inhibiting pH dependent conformational changes necessary for fusion (47-49). Since the discovery of C179, several mAbs against the HA stalk have been isolated from both humans and mice, many of which show broad neutralizing activity against a range of influenza virus subtypes. Stalk-directed antibodies such as CR6261 and F10 can neutralize a range of group 1 HA strains and share a common epitope as C179, where the recognized epitope involves residues in both HA1 and HA2 (50). Group 2 specific antibody CR8020 has a distinct conformational epitope that appears further down towards the membrane proximal region of HA and almost exclusively interacts with the C-terminal portion of the fusion peptide and the short helix of HA2 (48).

It is speculated that differences in sequence conservation and variation of glycosylation patterns between group 1 and 2 viruses prevent binding of C179 and F10 to group 2 viruses, as well as binding of CR8020 to group 1 viruses. Furthermore, interactions between group 1 specific nAbs and HA are dominated by interactions with the antibody heavy chain. In contrast, CR8020 interacts with HA using both heavy and light chain contacts and the CR8020 epitope may be sterically occluded in group 1 isolates by an HA1 N-linked glycan at N21. Similarly, it has been speculated that the HA1 N-linked glycan N38 in group 2 isolates prevents binding of CR6261 and F10 (48, 51). In a remarkable finding, stalk-directed antibody F16v3 was isolated and found to possess neutralizing capability against nearly all subtypes of influenza A virus. Structures of FI6v3 with HAs from both groups indicated that the stem epitope has some sequence overlap with all the other stem-directed bnAbs. The long flexible loop from the CDRH3 targets a hydrophobic groove in the HA stem while the light chain CDRL1 targets the fusion peptide from an adjacent monomer. A unique

feature of FI6v3 is that it can also bind to the uncleaved HA0 trimer, providing an additional mechanism of neutralization against newly synthesized virions that rely on cell surface proteolysis for HA priming.

The antibody response against viral glycoproteins is important for preventing many viral infections, but we lack a comprehensive understanding of the mechanisms by which antibodies act. The available high resolution structures of antigen binding fragments (Fab) bound to soluble antigen constructs have generated structural models of neutralization that mainly involves antibody/receptor competition or inhibition of conformational changes necessary for fusion. Although these static structures reveal antibody-antigen recognition in detail, they do not necessarily enable the functional consequences of these interactions to be assessed. In addition, relatively few studies have characterized the interactions between full-length IgG and whole virions, where bivalency of full-length IgG may prevent viral entry through crosslinking of antigenic sites on the surface of a virus and through aggregation of virus particles, imparting additional complexity not easily characterized by traditional structural methods (Figure 1.2C). These additional modes of action may be responsible for observations that high levels of virus neutralization are often observed even when saturation of binding sites by antibodies is not achieved (30, 52, 53). A comprehensive understanding of the mechanisms by which Fab and full-length IgG act to inhibit glycoprotein function are necessary to improve the design of therapeutic strategies.

1.6 Architecture of the human immunodeficiency virus

The human immunodeficiency virus (HIV) is categorized as a lentivirus within the family, *retroviridae* (54). It is an enveloped virus that contains a cone-shaped core of viral capsid proteins, which holds two copies of viral RNA and closely associated nucleoproteins. Like other retroviruses, the HIV genome codes for structural proteins (Gag), replication enzymes (Pol), and a surface glycoprotein that is required for cell entry (Env). In addition, HIV also codes for several regulatory proteins, including Tat and Rev, that are necessary to initiate HIV replication, and Nef, Vif, Vpr and Vpu, that have an impact on viral replication, virus budding and pathogenesis (54).

Assembly of an HIV virion occurs at the host-cell plasma membrane with the HIV Gag polyprotein, mediating all essential steps for particle assembly. Initially, the Gag polyprotein helps to form an immature virus particle that becomes cleaved after budding by viral protease (PR) into MA, CA, NC, and p6 proteins.

This proteolysis step is essential to form a mature HIV virion that can enter and replicate in a new host cell (55, 56). Each mature virion is spherical, with an approximate diameter of 150 nm and an estimated 10-20 Env spikes decorating the envelope surface (57, 58).

1.7 Overview of HIV-1 envelope glycoprotein structure

The HIV-1 envelope (Env) glycoprotein is the only virally encoded protein at the surface of the virus (Figure 1.3A). It plays a central role in viral entry and is the sole antigenic target of neutralizing antibodies. Like influenza HA and other class I fusion proteins, Env is first synthesized as a polypeptide precursor, referred to as gp160. gp160 contains a signaling sequence at the N-terminus that directs Env to the rough endoplasmic reticulum (59, 60). During translation, gp160 becomes extensively glycosylated with N-linked side chains (61). Monomers of gp160 oligomerize into a trimeric glycoprotein that is further trafficked through the secretory pathway, where high-mannose oligosaccharides undergo modifications within the trans-Golgi network. Furin, or furin-like proteases, cleave gp160 in the Golgi, which serves as an essential step for activation of Env fusion activity. This proteolytic processing yields a surface glycoprotein, gp120, and the transmembrane glycoprotein, gp41, that are associated by noncovalent interactions. Therefore, the mature Env glycoprotein exists as a homotrimer of heterodimers, consisting of gp120 and gp41 on the virus surface. Env mediates entry into host immune cells through sequential binding of primary receptor CD4, and co-receptor CCR5 or CXCR4. Engagement of co-receptor allows insertion of the gp41 fusion peptide into the target membrane, followed by dramatic refolding of gp41 into a highly stable six-helix bundle that results in the fusion of the viral and host membrane (Figure 1.3B).

The gp120 subunit exhibits a high degree of sequence variability, specifically within hypervariable loops (V1-V5) that are interspersed with constant domains (C1-C5). Variability is driven by the rapid reproduction of HIV-1 and the high error rate of nucleotide substitutions by the reverse transcriptase enzyme, which is responsible for converting the viral RNA into the double-stranded DNA that is integrated into the host chromosome (62, 63). Additionally, gp120 is highly glycosylated with glycans accounting for approximately half of the mass. At the trimer apex are the V1/V2 loops, which are highly variable in loop length and glycosylation sites between strains. Nestled below the V1/V2 loops is another variable loop, V3, which forms part of the Env apex and is thought to contain part of the co-receptor binding site upon binding

CD4 (64, 65). The conserved domains, specifically C1, C3 and C4 form the major portions of the CD4 receptor binding site, and the overall architecture of gp120 can be viewed in terms of a membrane distal outer domain and an inner domain that interacts with gp41 transmembrane domain.

The gp41 fusion domain mediates the fusion of the viral and host membrane and is organized into three major subdomains: an extracellular domain, a transmembrane domain, and a C-terminal cytoplasmic tail. The extracellular domain contains an α-helical coiled-coil structure referred to as heptad repeat regions HR1 and HR2. The fusion peptide, thought to be associated within the gp120/gp41 quaternary complex, becomes released in response to conformational changes associated with co-receptor binding. Upon refolding that occurs during fusion, the three HR1 helices form a core helical bundle, and the three HR2 domains dock into the hydrophobic groove around the core, forming a stable six-helix bundle that promotes fusion of the viral and target membrane.

1.8 Broadly neutralizing antibodies targeting the Env glycoprotein

During natural infection with HIV-1, the immune response generates antibodies against Env; however, these antibodies are specific to the infecting strain (66-68). Rapid evolution of the virus allows escape variants to continue to proliferate, despite this initial antibody response, causing the immune system to battle rounds of increasing antigenic diversity. In a subset of chronically infected adults, the continuous interplay of 'antibody response' and 'immune evasion' results in the production of antibodies that can neutralize a broad range of these antigenically diverse viruses. Over the past several years, these potent bnAbs have been isolated and characterized from multiple subjects and can be categorized into five groups, targeting distinct epitopes (Figure 1.4A) (69-76). The first epitope is the CD4 binding site, where bnAbs such as VRCO1 block Env binding to the primary receptor (72, 77-80). Antibodies targeting the V1/V2 apex region of Env represent a second commonly targeted bnAb epitope. These antibodies include PGT145 and PG9-like antibodies that recognize both protein and glycan elements in V1/V2 (73, 81-83). The third epitope is the V3 region, which is a glycan-rich patch centered around the N332 glycan and has been referred to as a supersite of immune vulnerability due to the epitope's accessibility at the perimeter of Env, which allows multiple binding modes and various angles of approach (84). This class of bnAbs make significant contacts with V3 glycans as well as a conserved GDIR sequence within the V3 loop (76, 84-87). The fourth

group targets the gp120/gp41 interface and includes the PGT151 series of bnAbs and 8ANC195 bnAb (88-90). Finally, the last group of broadly neutralizing antibodies target the membrane proximal external region (MPER) of gp41. MPER-specific bnAbs, such as 10E8, bind to protein segments adjacent to the viral membrane and are suggested to inhibit refolding of gp41 (71, 91). For many bnAbs, binding the closed prefusion form of Env has been suggested to be a correlate of neutralization potency and it is likely that stabilization of the prefusion structure is the primary mechanism for how bnAbs act (92).

Together with the identification of commonly targeted broadly neutralization epitopes, characterization of the isolated bnAbs revealed common features associated with bnAb development that pose a challenge towards vaccine design meant to elicit similar antibodies (Figure 1.4B). One such challenge is that adult-derived bnAbs develop over years of chronic infection and acquire significant levels of somatic hypermutation (SHM) during antibody maturation (93). Furthermore, in rare cases, bnAb development includes insertions or deletions (Indels) that are localized to antibody CDR-loops—most commonly within CDRH3, which is thought to allow penetration through glycans in order to contact conserved protein epitopes (94, 95). Although the frequency of indels among somatic mutations in the normal human B cell repertoire is small, they are found in high frequency among bnAbs isolated from HIV-1 infected adults (96-98). However, the potential auto-reactivity of highly mutated antibodies is yet another challenge when attempting to induce similar bnAbs due to negative selection of such antibodies in normal B-cell development (99-101). It has recently been observed that infants are capable of mounting a bnAb response against HIV-1 and do so rapidly, within the first year of infection (102, 103). This unique ability of infants to generate a rapid response may suggest that bnAbs responsible for breadth have distinct features relative to adult HIV-1-specific bnAbs such as lower somatic hypermutation. BF520.1 is a bnAb isolated from a HIV-1 infected infant that contributed to plasma breadth within the first year of infection (102). BF520.1 developed rapidly, exhibits low levels of SHM (6%), and neutralized 58% of isolates tested. Prior to our work herein, it was unclear if infant-derived bnAbs bind to novel epitopes or to similar epitopes of highly matured bnAbs isolated from adults. While adult HIV-1 bnAbs have been extensively characterized, high resolution information of the interactions between infant bnAbs is not known. Identification of bnAbs such as BF520.1 provides hope that a similar response can be induced by vaccination through germline targeting immunogen design; however, the future development of such an immunogen requires a

comprehensive understanding of critical interactions between infant-derived bnAbs and Env, and an in-depth knowledge of the developmental pathway during infection.

1.9 Cryo-electron microscopy single-particle techniques

Cryo-electron microscopy (Cryo-EM) has become one of the most widely used tools for the structural determination of biological samples at near-atomic resolution. This structural technique can be used to solve structures across a wide range of molecular mass from individual proteins and protein complexes, to virus particles and to whole cells. Developed in the 1980s, the specimen preparation method by Dubochet and colleagues involved the rapid vitrification of biological specimens by exposing the sample to liquid nitrogen cooled ethane (104). The vitrified sample was found to be preserved in a near-native state and appeared free from damage associated with dehydration and absorption to a support layer that was commonly observed in earlier electron microscopy approaches.

Achieving high resolution structures using single-particle cryo-EM requires that thousands of high-quality images of identical copies of the sample are collected and computationally averaged together. These requirements have recently been met with advances in data collection and image processing algorithms, resulting in thousands of generated three dimensional structures (105-108). Specifically, the development of direct-electron detector devices (DDD) made a tremendous impact within the field of cryo-EM. As the name suggests, a DDD can directly detect incident electrons and read their occurrence at a high frame rate (109, 110). Concomitant with data collected using DDD is the implementation of motion correction algorithms to correct for beam-induced movement of the specimen that occurs during image acquisition, elegantly illustrated by Grigorieff and colleagues using rotavirus particles (111, 112). Furthermore, powerful classification methods have been developed to segregate heterogeneous samples, allowing more precise alignment of identical proteins, resulting in higher resolution structures (105, 106).

In addition to the heterogeneity in protein structure, glycosylated proteins have been especially difficult to structurally characterize due to the nature of glycan composition, which can be extremely diverse, and may contain a significant degree of conformational flexibility. For this reason, structures determined by X-ray crystallography often involve the removal of glycans through mutagenesis or by treatment with glycosidases (113, 114). However, glycan density can be resolved in instances where the glycan is

stabilized by interactions, such as the case with Env and antibody Fab domains (76, 85). Cryo-EM has made strides in overcoming limitations associated with glycan flexibility. A major achievement in Env glycoprotein structure was made in 2013, when structural elements of a fully glycosylated Env construct were visualized and density corresponding to glycans could be observed (115). Due to flexibility, not only of glycans, but also in the inherent dynamics of the Env protein, the resolution of Fab:Env complexes has been limited to ~4 Å to 6 Å; however, a recent 3.1 Å cryo-EM was obtained of a highly stable complex (87, 115-117).

1.10 Cryo-electron tomography of complex biological specimens

Cryo-electron tomography (Cryo-ET) has been instrumental in the visualization of enveloped viruses that exhibit pleomorphic structure unsuitable for traditional single-particle techniques with the resolution being sufficient to distinguish different forms of viral surface glycoproteins alone and in complex with antibody (31, 118-121). Much like single-particle approaches, the technique first requires vitrification of the biological specimen to ensure the preservation of the specimen in a frozen hydrated state prior to transferring the specimen into the electron microscope. The specimen is then rotated around a defined tilt axis, and a series of two dimensional projections are collected over a maximal range of 140° between ±70°. The inability to collect a full ±90° tilt range, due to mechanical constraints in the microscope and hardware that holds the grid, results in loss of structural information, leading to an artifact called the 'missing wedge'. Furthermore, because a single specimen is being imaged multiple times throughout the tilt collection, low dose imaging is used to avoid radiation damage to the sample, and for many biological specimens, a total dose of <120 $e^-/Å^2$ is a common target. The missing wedge effect, along with damage to the specimen from prolonged exposure to incident electrons, reduces the achievable resolution by cryo-ET which is estimated to be ~ 1nm. Alignment of the projection images is commonly performed using fiducial markers such as 10 nm colloidal gold beads. Once aligned, the tilt-series is used to reconstruct the final 3D volume, or tomogram, using weighted back-projection algorithms.

In the study of influenza viruses, cryo-ET has been widely used in observing particle morphology, glycoprotein distribution on the surface of the virus, and the arrangement of internal viral components. Furthermore, budding of influenza particles from cellular membranes has been informative about the

influence of viral proteins on particle morphology, as well as the organization of assembled particles upon release of progeny virus (118, 122-124). Use of cryo-ET has also furthered our understanding of HA-mediated membrane fusion itself. Recent studies have shed light on transitions that occur at low pH, such as matrix layer dissociation and thinning of the HA stalk, suggesting capture of intermediate HA conformations (125). In addition, a recent study characterized the sequence of events occurring at different stages of fusion at low pH, from initial contact between virus and target membrane to fusion pore formation (31, 125-130).

Where single-particle analysis has revealed in detail the interactions between antibody Fab fragments and isolated antigens, cryo-ET provides an opportunity to observe interactions that occur between full-length antibodies with whole particles. Although a few studies have investigated the binding of antibodies and the accessibility of epitopes on the virus surface, the functional consequence of binding as it relates to neutralization has been largely unexplored (131, 132). A major focus of this dissertation employs cryo-ET to visualize the complex interactions that occur between full-length antibodies and whole-virus particles. Together with biophysical methods, cryo-ET is used to discern the mechanisms by which neutralizing antibodies targeting distinct HA epitopes act to inhibit HA function.

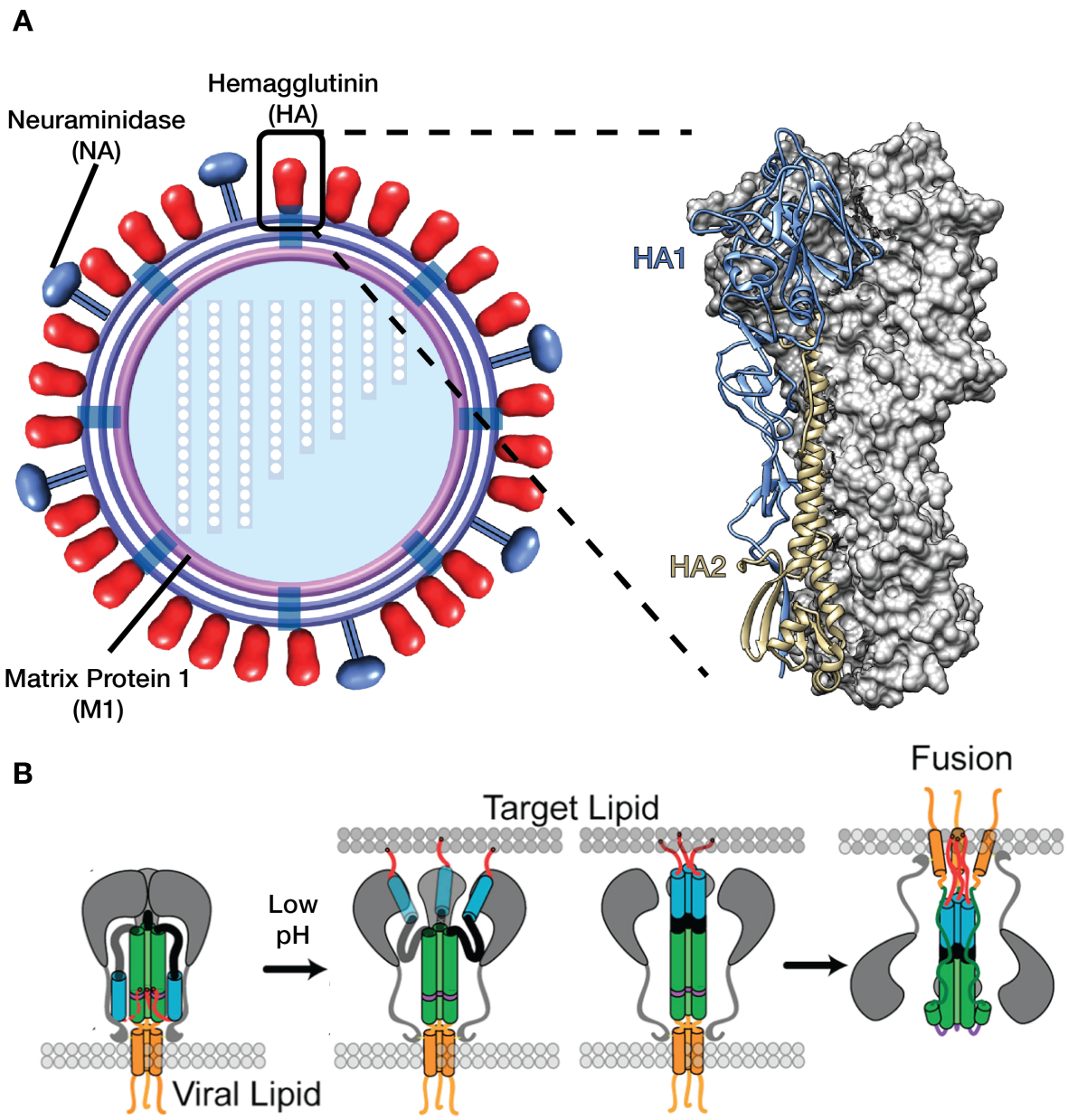

Figure 1.1: Architecture of the influenza A virus. **(A)** The virus surface is coated with a dense layer of hemagglutinin (HA) glycoproteins. Neuraminidase, although at much lower density, is also present on the virus surface. A single HA trimer is expanded to highlight the receptor binding domain (HA1) and the fusion subunit (HA2). **(B)** HA fusion is triggered by low pH. Upon exposure to low pH, the fusion peptide inserts into the target lipid. Upon uncaging of the HA1 trimeric interface, HA2 undergoes dramatic refolding that results in the fusion of the viral and target membrane.

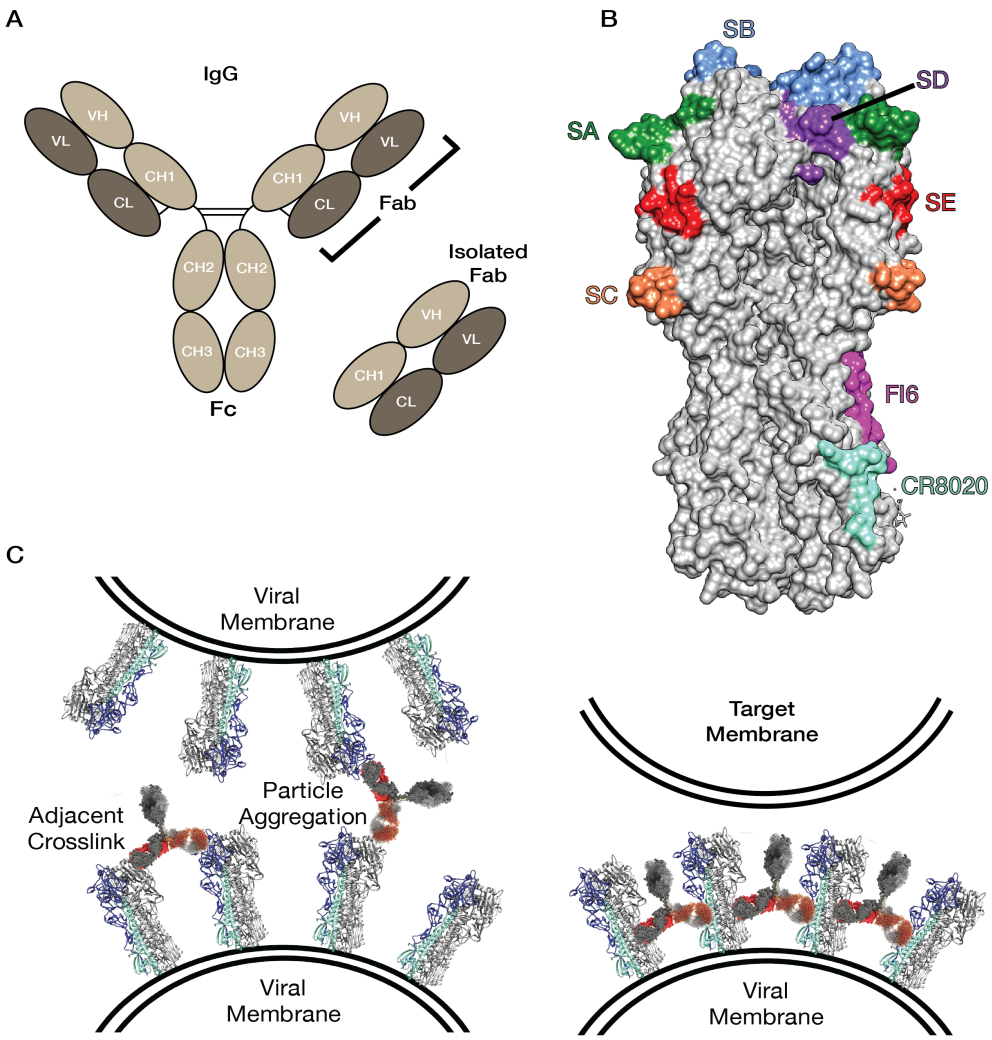

Figure 1.2: Complex binding of IgG to HA depends on the epitope targeted. **(A)** Illustration of the bivalent Fab presentation of full-length IgG. Heavy chains (tan) and light chains (dark brown) are shown for clarity with constant (CH and CL) and variable domains (VH and VL) labeled. Isolated Fab fragments are traditionally complexed with antigen for high resolution structure determination. **(B)** Antigenic sites of HA trimer from H3 subtype used in this study. HA1 epitopes SA (green), SB (blue), SC (orange), SD (purple), SE (red) are highlighted for clarity. HA2 epitopes targeted by FI6 (pink) and CR8020 (aqua marine) are also shown. **(C)** Bivalent Fab presentation by IgG allows complex binding that enhances IgG mediated neutralization. Depending on the epitope targeted, IgG may crosslink HA on a single particle, or aggregate particles together (left). HA2 directed antibodies only crosslink adjacent HAs on single particles (right) due to the epitopes location further down the HA stem.

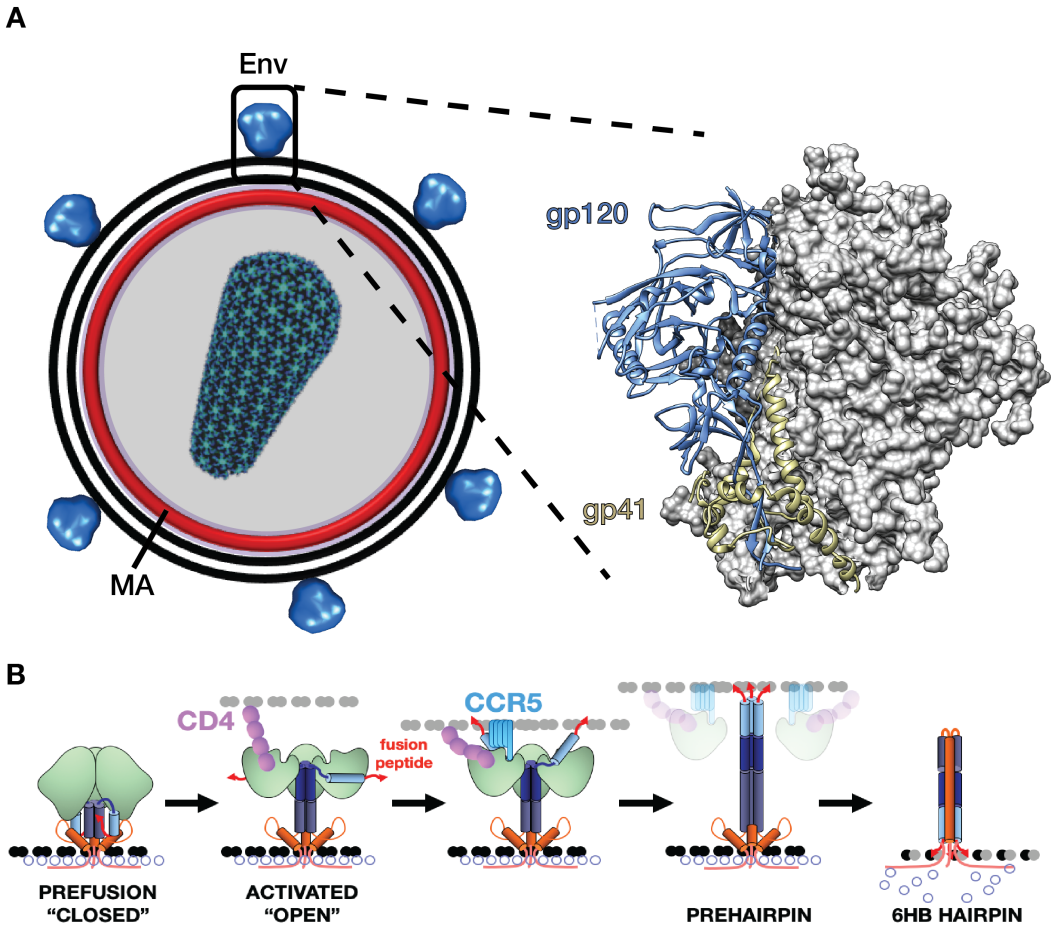

Figure 1.3 Architecture of HIV-1. **(A)** The HIV-1 virus nucleocapsid is surrounded by an internal matrix layer (MA) bound to the lipid bilayer. The surface of HIV-1 is sparsely decorated with Env proteins. A single Env trimer is expanded to highlight the receptor binding domain (gp120) and the fusion subunit (gp41). **(B)** Fusion by Env is triggered by co-receptor engagement. Env first binding to primary receptor CD4, which exposes the co-receptor binding site. Upon engagement with co-receptor (CCR5), gp41 undergoes dramatic refolding into a six-helix bundle hairpin (6HB), resulting in the fusion of the viral and target membrane.

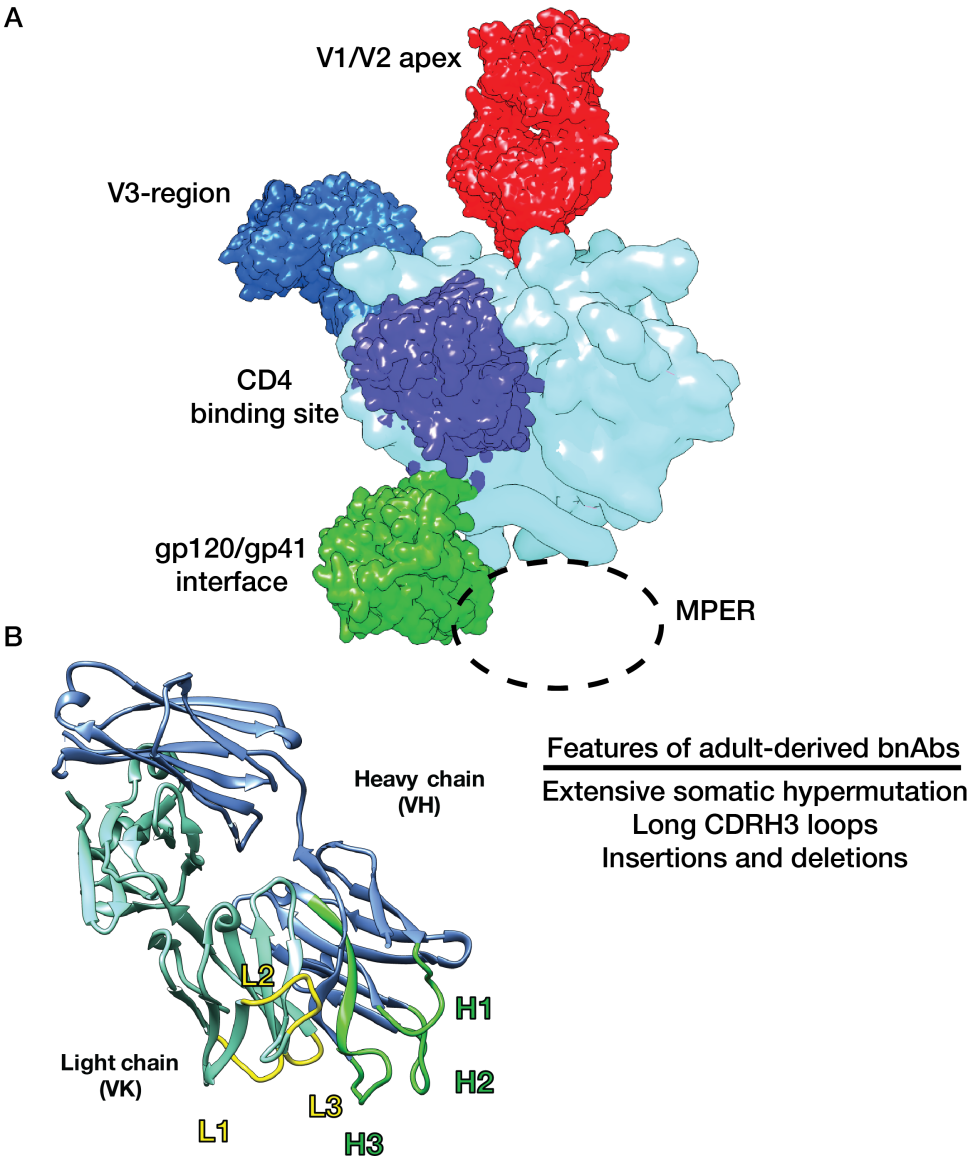

Figure 1.4: Broadly neutralizing antibodies targeted HIV-1 Env. **(A)** Isolation of bnAbs from chronically infected adults reveal five common epitopes that are targeted. These sites are the V1/V2 apex (red), V3-region (blue), CD4 binding site (purple), gp120/gp41 interface (green), and the membrane proximal external region (MPER). The MPER epitope is truncated on most Env trimer constructs; therefore, the domain is represented as a dashed circle before Env, adjacent to the lipid bilayer. **(B)** The crystal structure of PGT128 is shown to highlight both the heavy (blue) and light chain (aqua marine) domains. CDRH Loops are shown in green and CDRL loops are shown in yellow. The majority of adult-derived bnAbs occur after several years of infection and exhibit high degrees of somatic hypermutation (SHM), long CDRH3 loops, as well as insertions and deletions.

References

1. Collaborators GL. 2017. Estimates of the global, regional, and national morbidity, mortality, and aetiologies of lower respiratory tract infections in 195 countries: a systematic analysis for the Global Burden of Disease Study 2015. Lancet Infect Dis 17:1133-1161.
2. Hung IF, Zhang AJ, To KK, Chan JF, Zhu SH, Zhang R, Chan TC, Chan KH, Yuen KY. 2017. Unexpectedly Higher Morbidity and Mortality of Hospitalized Elderly Patients Associated with Rhinovirus Compared with Influenza Virus Respiratory Tract Infection. Int J Mol Sci 18.
3. Alonso WJ, Laranjeira BJ, Pereira SA, Florencio CM, Moreno EC, Miller MA, Giglio R, Schuck-Paim C, Moura FE. 2012. Comparative dynamics, morbidity and mortality burden of pediatric viral respiratory infections in an equatorial city. Pediatr Infect Dis J 31:e9-14.
4. Dampier W, Nonnemacher MR, Mell J, Earl J, Ehrlich GD, Pirrone V, Aiamkitsumrit B, Zhong W, Kercher K, Passic S, Williams JW, Jacobson JM, Wigdahl B. 2016. HIV-1 Genetic Variation Resulting in the Development of New Quasispecies Continues to Be Encountered in the Peripheral Blood of Well-Suppressed Patients. PLoS One 11:e0155382.
5. Lazniewski M, Dawson WK, Szczepinska T, Plewczynski D. 2017. The structural variability of the influenza A hemagglutinin receptor-binding site. Brief Funct Genomics doi:10.1093/bfgp/elx042.
6. Rejmanek D, Hosseini PR, Mazet JA, Daszak P, Goldstein T. 2015. Evolutionary Dynamics and Global Diversity of Influenza A Virus. J Virol 89:10993-1001.
7. Taylor BS, Hammer SM. 2008. The challenge of HIV-1 subtype diversity. N Engl J Med 359:1965-6.
8. Burton DR, Hessell AJ, Keele BF, Klasse PJ, Ketas TA, Moldt B, Dunlop DC, Poignard P, Doyle LA, Cavacini L, Veazey RS, Moore JP. 2011. Limited or no protection by weakly or nonneutralizing antibodies against vaginal SHIV challenge of macaques compared with a strongly neutralizing antibody. Proc Natl Acad Sci U S A 108:11181-6.
9. Caskey M, Klein F, Lorenzi JC, Seaman MS, West AP, Jr., Buckley N, Kremer G, Nogueira L, Braunschweig M, Scheid JF, Horwitz JA, Shimeliovich I, Ben-Avraham S, Witmer-Pack M, Platten M, Lehmann C, Burke LA, Hawthorne T, Gorelick RJ, Walker BD, Keler T, Gulick RM, Fatkenheuer G, Schlesinger SJ, Nussenzweig MC. 2015. Viraemia suppressed in HIV-1-infected humans by broadly neutralizing antibody 3BNC117. Nature 522:487-91.
10. Caskey M, Schoofs T, Gruell H, Settler A, Karagounis T, Kreider EF, Murrell B, Pfeifer N, Nogueira L, Oliveira TY, Learn GH, Cohen YZ, Lehmann C, Gillor D, Shimeliovich I, Unson-O'Brien C, Weiland D, Robles A, Kummerle T, Wyen C, Levin R, Witmer-Pack M, Eren K, Ignacio C, Kiss S, West AP, Jr., Mouquet H, Zingman BS, Gulick RM, Keler T, Bjorkman PJ, Seaman MS, Hahn BH, Fatkenheuer G, Schlesinger SJ, Nussenzweig MC, Klein F. 2017. Antibody 10-1074 suppresses viremia in HIV-1-infected individuals. Nat Med 23:185-191.
11. Marjuki H, Mishin VP, Chai N, Tan MW, Newton EM, Tegeris J, Erlandson K, Willis M, Jones J, Davis T, Stevens J, Gubareva LV. 2016. Human Monoclonal Antibody 81.39a Effectively Neutralizes Emerging Influenza A Viruses of Group 1 and 2 Hemagglutinins. J Virol 90:10446-10458.
12. Saunders KO, Pegu A, Georgiev IS, Zeng M, Joyce MG, Yang ZY, Ko SY, Chen X, Schmidt SD, Haase AT, Todd JP, Bao S, Kwong PD, Rao SS, Mascola JR, Nabel GJ. 2015. Sustained Delivery of a Broadly Neutralizing Antibody in Nonhuman Primates Confers Long-Term Protection against Simian/Human Immunodeficiency Virus Infection. J Virol 89:5895-903.
13. Zhang Z, Liu M, Zheng S. 2015. Protection Against H7 Subtype Influenza Virus Infection in Mice by Passive Transfer of Neutralizing Monoclonal Antibody. Monoclon Antib Immunodiagn Immunother 34:360-5.
14. Parsegian VA, Fuller N, Rand RP. 1979. Measured work of deformation and repulsion of lecithin bilayers. Proc Natl Acad Sci U S A 76:2750-4.

15. Rand RP, Parsegian VA. 1984. Physical force considerations in model and biological membranes. Can J Biochem Cell Biol 62:752-9.

16. Andrewes CH, Bang FB, Burnet FM. 1955. A short description of the Myxovirus group (influenza and related viruses). Virology 1:176-84.

17. Bouvier NM, Palese P. 2008. The biology of influenza viruses. Vaccine 26 Suppl 4:D49-53.

18. Huang RT, Rott R, Klenk HD. 1981. Influenza viruses cause hemolysis and fusion of cells. Virology 110:243-7.

19. Maeda T, Ohnishi S. 1980. Activation of influenza virus by acidic media causes hemolysis and fusion of erythrocytes. FEBS Lett 122:283-7.

20. Munster VJ, Baas C, Lexmond P, Waldenstrom J, Wallensten A, Fransson T, Rimmelzwaan GF, Beyer WE, Schutten M, Olsen B, Osterhaus AD, Fouchier RA. 2007. Spatial, temporal, and species variation in prevalence of influenza A viruses in wild migratory birds. PLoS Pathog 3:e61.

21. Olsen B, Munster VJ, Wallensten A, Waldenstrom J, Osterhaus AD, Fouchier RA. 2006. Global patterns of influenza a virus in wild birds. Science 312:384-8.

22. Gerhard W. 2001. The role of the antibody response in influenza virus infection. Curr Top Microbiol Immunol 260:171-90.

23. Wilson IA, Skehel JJ, Wiley DC. 1981. Structure of the haemagglutinin membrane glycoprotein of influenza virus at 3 A resolution. Nature 289:366-73.

24. Lu Y, Welsh JP, Swartz JR. 2014. Production and stabilization of the trimeric influenza hemagglutinin stem domain for potentially broadly protective influenza vaccines. Proc Natl Acad Sci U S A 111:125-30.

25. Skehel JJ, Wiley DC. 2000. Receptor Binding and Membrane Fusion in Virus Entry: The Influenza Hamagglutinin. Annual Review of Biochemistry:531-569.

26. Sauter NK, Bednarski MD, Wurzburg BA, Hanson JE, Whitesides GM, Skehel JJ, Wiley DC. 1989. Hemagglutinins from two influenza virus variants bind to sialic acid derivatives with millimolar dissociation constants: a 500-MHz proton nuclear magnetic resonance study. Biochemistry 28:8388-96.

27. Sauter NK, Hanson JE, Glick GD, Brown JH, Crowther RL, Park SJ, Skehel JJ, Wiley DC. 1992. Binding of influenza virus hemagglutinin to analogs of its cell-surface receptor, sialic acid: analysis by proton nuclear magnetic resonance spectroscopy and X-ray crystallography. Biochemistry 31:9609-21.

28. Bullough PA, Hughson FM, Skehel JJ, Wiley DC. 1994. Structure of influenza haemagglutinin at the pH of membrane fusion. Nature 371:37-43.

29. Chen J, Skehel JJ, Wiley DC. 1999. N- and C-terminal residues combine in the fusion-pH influenza hemagglutinin HA(2) subunit to form an N cap that terminates the triple-stranded coiled coil. Proc Natl Acad Sci U S A 96:8967-72.

30. Otterstrom JJ, Brandenburg B, Koldijk MH, Juraszek J, Tang C, Mashaghi S, Kwaks T, Goudsmit J, Vogels R, Friesen RHE, Van Oijen AM. 2014. Relating influenza virus membrane fusion kinetics to stoichiometry of neutralizing antibodies at the single-particle level. Proceedings of the National Academy of Sciences of the United States of America 111:E5143-E5148.

31. Lee KK. 2010. Architecture of a nascent viral fusion pore. The EMBO Journal 29:1299-1311.

32. Ivanovic T, Choi JL, Whelan SP, van Oijen AM, Harrison SC. 2013. Influenza-virus membrane fusion by cooperative fold-back of stochastically induced hemagglutinin intermediates. Elife 2:e00333.

33. Danieli T, Pelletier SL, Henis YI, White JM. 1996. Membrane fusion mediated by the influenza virus hemagglutinin requires the concerted action of at least three hemagglutinin trimers. J Cell Biol 133:559-69.

34. Gerhard W, Yewdell J, Frankel ME, Webster R. 1981. Antigenic structure of influenza virus haemagglutinin defined by hybridoma antibodies. Nature 290:713-7.

35. Wiley DC, Wilson IA, Skehel JJ. 1981. Structural identification of the antibody-binding sites of Hong Kong influenza haemagglutinin and their involvement in antigenic variation. Nature 289:373-8.

36. Lee PS, Yoshida R, Ekiert DC, Sakai N, Suzuki Y, Takada A, Wilson IA. 2012. Heterosubtypic antibody recognition of the influenza virus hemagglutinin receptor binding site enhanced by avidity. Proc Natl Acad Sci U S A 109:17040-5.

37. Ekiert DC, Kashyap AK, Steel J, Rubrum A, Bhabha G, Khayat R, Lee JH, Dillon MA, O'Neil RE, Faynboym AM, Horowitz M, Horowitz L, Ward AB, Palese P, Webby R, Lerner RA, Bhatt RR, Wilson IA. 2012. Cross-neutralization of influenza A viruses mediated by a single antibody loop. Nature 489:526-32.

38. Yoshida R, Igarashi M, Ozaki H, Kishida N, Tomabechi D, Kida H, Ito K, Takada A. 2009. Cross-protective potential of a novel monoclonal antibody directed against antigenic site B of the hemagglutinin of influenza A viruses. PLoS Pathog 5:e1000350.

39. Lee PS, Ohshima N, Stanfield RL, Yu W, Iba Y, Okuno Y, Kurosawa Y, Wilson IA. 2014. Receptor mimicry by antibody F045-092 facilitates universal binding to the H3 subtype of influenza virus. Nat Commun 5:3614.

40. Ohshima N, Iba Y, Kubota-Koketsu R, Asano Y, Okuno Y, Kurosawa Y. 2011. Naturally occurring antibodies in humans can neutralize a variety of influenza virus strains, including H3, H1, H2, and H5. J Virol 85:11048-57.

41. Whittle JR, Zhang R, Khurana S, King LR, Manischewitz J, Golding H, Dormitzer PR, Haynes BF, Walter EB, Moody MA, Kepler TB, Liao HX, Harrison SC. 2011. Broadly neutralizing human antibody that recognizes the receptor-binding pocket of influenza virus hemagglutinin. Proc Natl Acad Sci U S A 108:14216-21.

42. Hai R, Krammer F, Tan GS, Pica N, Eggink D, Maamary J, Margine I, Albrecht RA, Palese P. 2012. Influenza viruses expressing chimeric hemagglutinins: globular head and stalk domains derived from different subtypes. J Virol 86:5774-81.

43. Steel J, Lowen AC, Wang TT, Yondola M, Gao Q, Haye K, Garcia-Sastre A, Palese P. 2010. Influenza virus vaccine based on the conserved hemagglutinin stalk domain. MBio 1.

44. Wrammert J, Smith K, Miller J, Langley WA, Kokko K, Larsen C, Zheng NY, Mays I, Garman L, Helms C, James J, Air GM, Capra JD, Ahmed R, Wilson PC. 2008. Rapid cloning of high-affinity human monoclonal antibodies against influenza virus. Nature 453:667-71.

45. Moody MA, Zhang R, Walter EB, Woods CW, Ginsburg GS, McClain MT, Denny TN, Chen X, Munshaw S, Marshall DJ, Whitesides JF, Drinker MS, Amos JD, Gurley TC, Eudailey JA, Foulger A, DeRosa KR, Parks R, Meyerhoff RR, Yu JS, Kozink DM, Barefoot BE, Ramsburg EA, Khurana S, Golding H, Vandergrift NA, Alam SM, Tomaras GD, Kepler TB, Kelsoe G, Liao HX, Haynes BF. 2011. H3N2 influenza infection elicits more cross-reactive and less clonally expanded anti-hemagglutinin antibodies than influenza vaccination. PLoS One 6:e25797.

46. Okuno Y, Isegawa Y, Sasao F, Ueda S. 1993. A common neutralizing epitope conserved between the hemagglutinins of influenza A virus H1 and H2 strains. J Virol 67:2552-8.

47. Ekiert DC, Bhabha G, Elsliger MA, Friesen RH, Jongeneelen M, Throsby M, Goudsmit J, Wilson IA. 2009. Antibody recognition of a highly conserved influenza virus epitope. Science 324:246-51.

48. Ekiert DC, Friesen RH, Bhabha G, Kwaks T, Jongeneelen M, Yu W, Ophorst C, Cox F, Korse HJ, Brandenburg B, Vogels R, Brakenhoff JP, Kompier R, Koldijk MH, Cornelissen LA, Poon LL, Peiris

M, Koudstaal W, Wilson IA, Goudsmit J. 2011. A highly conserved neutralizing epitope on group 2 influenza A viruses. Science 333:843-50.

49. Wang TT, Tan GS, Hai R, Pica N, Petersen E, Moran TM, Palese P. 2010. Broadly protective monoclonal antibodies against H3 influenza viruses following sequential immunization with different hemagglutinins. PLoS Pathog 6:e1000796.

50. Dreyfus C, Ekiert DC, Wilson IA. 2013. Structure of a classical broadly neutralizing stem antibody in complex with a pandemic H2 influenza virus hemagglutinin. J Virol 87:7149-54.

51. Sui J, Hwang WC, Perez S, Wei G, Aird D, Chen LM, Santelli E, Stec B, Cadwell G, Ali M, Wan H, Murakami A, Yammanuru A, Han T, Cox NJ, Bankston LA, Donis RO, Liddington RC, Marasco WA. 2009. Structural and functional bases for broad-spectrum neutralization of avian and human influenza A viruses. Nat Struct Mol Biol 16:265-73.

52. Klasse P. 2014. Neutralization of Virus Infectivity by Antibodies: Old Problems in New Perspectives. Advances in Biology.

53. Taylor H, Armstrong S, Dimmock N. 1987. Quantitative relationships between an influenza virus and neutralizing antibody. Virology:288-298.

54. Levy JA. 1993. Pathogenesis of human immunodeficiency virus infection. Microbiol Rev 57:183-289.

55. Konvalinka J, Krausslich HG, Muller B. 2015. Retroviral proteases and their roles in virion maturation. Virology 479-480:403-17.

56. Lee SK, Potempa M, Swanstrom R. 2012. The choreography of HIV-1 proteolytic processing and virion assembly. J Biol Chem 287:40867-74.

57. Chrystie IL, Almeida JD. 1988. The morphology of human immunodeficiency virus (HIV) by negative staining. J Med Virol 25:281-8.

58. Zhu P, Liu J, Bess J, Jr., Chertova E, Lifson JD, Grise H, Ofek GA, Taylor KA, Roux KH. 2006. Distribution and three-dimensional structure of AIDS virus envelope spikes. Nature 441:847-52.

59. Hunter E, Swanstrom R. 1990. Retrovirus envelope glycoproteins. Curr Top Microbiol Immunol 157:187-253.

60. Freed EO, Martin MA. 1995. The role of human immunodeficiency virus type 1 envelope glycoproteins in virus infection. J Biol Chem 270:23883-6.

61. Cao L, Diedrich JK, Kulp DW, Pauthner M, He L, Park SR, Sok D, Su CY, Delahunty CM, Menis S, Andrabi R, Guenaga J, Georgeson E, Kubitz M, Adachi Y, Burton DR, Schief WR, Yates JR, III, Paulson JC. 2017. Global site-specific N-glycosylation analysis of HIV envelope glycoprotein. Nat Commun 8:14954.

62. Araujo LA, Almeida SE. 2013. HIV-1 diversity in the envelope glycoproteins: implications for viral entry inhibition. Viruses 5:595-604.

63. Roberts JD, Bebenek K, Kunkel TA. 1988. The accuracy of reverse transcriptase from HIV-1. Science 242:1171-3.

64. Wang WK, Dudek T, Zhao YJ, Brumblay HG, Essex M, Lee TH. 1998. CCR5 coreceptor utilization involves a highly conserved arginine residue of HIV type 1 gp120. Proc Natl Acad Sci U S A 95:5740-5.

65. Suphaphiphat P, Essex M, Lee TH. 2007. Mutations in the V3 stem versus the V3 crown and C4 region have different effects on the binding and fusion steps of human immunodeficiency virus type 1 gp120 interaction with the CCR5 coreceptor. Virology 360:182-90.

66. Richman DD, Wrin T, Little SJ, Petropoulos CJ. 2003. Rapid evolution of the neutralizing antibody response to HIV type 1 infection. Proc Natl Acad Sci U S A 100:4144-9.

67. Li B, Decker JM, Johnson RW, Bibollet-Ruche F, Wei X, Mulenga J, Allen S, Hunter E, Hahn BH, Shaw GM, Blackwell JL, Derdeyn CA. 2006. Evidence for potent autologous neutralizing antibody titers and compact envelopes in early infection with subtype C human immunodeficiency virus type 1. J Virol 80:5211-8.

68. Gray ES, Moore PL, Choge IA, Decker JM, Bibollet-Ruche F, Li H, Leseka N, Treurnicht F, Mlisana K, Shaw GM, Karim SS, Williamson C, Morris L, Team CS. 2007. Neutralizing antibody responses in acute human immunodeficiency virus type 1 subtype C infection. J Virol 81:6187-96.

69. Bonsignori M, Hwang KK, Chen X, Tsao CY, Morris L, Gray E, Marshall DJ, Crump JA, Kapiga SH, Sam NE, Sinangil F, Pancera M, Yongping Y, Zhang B, Zhu J, Kwong PD, O'Dell S, Mascola JR, Wu L, Nabel GJ, Phogat S, Seaman MS, Whitesides JF, Moody MA, Kelsoe G, Yang X, Sodroski J, Shaw GM, Montefiori DC, Kepler TB, Tomaras GD, Alam SM, Liao HX, Haynes BF. 2011. Analysis of a clonal lineage of HIV-1 envelope V2/V3 conformational epitope-specific broadly neutralizing antibodies and their inferred unmutated common ancestors. J Virol 85:9998-10009.

70. Corti D, Langedijk JP, Hinz A, Seaman MS, Vanzetta F, Fernandez-Rodriguez BM, Silacci C, Pinna D, Jarrossay D, Balla-Jhagjhoorsingh S, Willems B, Zekveld MJ, Dreja H, O'Sullivan E, Pade C, Orkin C, Jeffs SA, Montefiori DC, Davis D, Weissenhorn W, McKnight A, Heeney JL, Sallusto F, Sattentau QJ, Weiss RA, Lanzavecchia A. 2010. Analysis of memory B cell responses and isolation of novel monoclonal antibodies with neutralizing breadth from HIV-1-infected individuals. PLoS One 5:e8805.

71. Huang J, Ofek G, Laub L, Louder MK, Doria-Rose NA, Longo NS, Imamichi H, Bailer RT, Chakrabarti B, Sharma SK, Alam SM, Wang T, Yang Y, Zhang B, Migueles SA, Wyatt R, Haynes BF, Kwong PD, Mascola JR, Connors M. 2012. Broad and potent neutralization of HIV-1 by a gp41-specific human antibody. Nature 491:406-12.

72. Liao HX, Lynch R, Zhou T, Gao F, Alam SM, Boyd SD, Fire AZ, Roskin KM, Schramm CA, Zhang Z, Zhu J, Shapiro L, Program NCS, Mullikin JC, Gnanakaran S, Hraber P, Wiehe K, Kelsoe G, Yang G, Xia SM, Montefiori DC, Parks R, Lloyd KE, Scearce RM, Soderberg KA, Cohen M, Kamanga G, Louder MK, Tran LM, Chen Y, Cai F, Chen S, Moquin S, Du X, Joyce MG, Srivatsan S, Zhang B, Zheng A, Shaw GM, Hahn BH, Kepler TB, Korber BT, Kwong PD, Mascola JR, Haynes BF. 2013. Co-evolution of a broadly neutralizing HIV-1 antibody and founder virus. Nature 496:469-76.

73. Walker LM, Huber M, Doores KJ, Falkowska E, Pejchal R, Julien JP, Wang SK, Ramos A, Chan-Hui PY, Moyle M, Mitcham JL, Hammond PW, Olsen OA, Phung P, Fling S, Wong CH, Phogat S, Wrin T, Simek MD, Protocol GPI, Koff WC, Wilson IA, Burton DR, Poignard P. 2011. Broad neutralization coverage of HIV by multiple highly potent antibodies. Nature 477:466-70.

74. Barnes CO, Gristick HB, Freund NT, Escolano A, Lyubimov AY, Hartweger H, West AP, Jr., Cohen AE, Nussenzweig MC, Bjorkman PJ. 2018. Structural characterization of a highly-potent V3-glycan broadly neutralizing antibody bound to natively-glycosylated HIV-1 envelope. Nat Commun 9:1251.

75. Julien JP, Sok D, Khayat R, Lee JH, Doores KJ, Walker LM, Ramos A, Diwanji DC, Pejchal R, Cupo A, Katpally U, Depetris RS, Stanfield RL, McBride R, Marozsan AJ, Paulson JC, Sanders RW, Moore JP, Burton DR, Poignard P, Ward AB, Wilson IA. 2013. Broadly neutralizing antibody PGT121 allosterically modulates CD4 binding via recognition of the HIV-1 gp120 V3 base and multiple surrounding glycans. PLoS Pathog 9:e1003342.

76. Kong L, Torrents de la Pena A, Deller MC, Garces F, Sliepen K, Hua Y, Stanfield RL, Sanders RW, Wilson IA. 2015. Complete epitopes for vaccine design derived from a crystal structure of the broadly neutralizing antibodies PGT128 and 8ANC195 in complex with an HIV-1 Env trimer. Acta Crystallogr D Biol Crystallogr 71:2099-108.

77. Scheid JF, Mouquet H, Ueberheide B, Diskin R, Klein F, Oliveira TY, Pietzsch J, Fenyo D, Abadir A, Velinzon K, Hurley A, Myung S, Boulad F, Poignard P, Burton DR, Pereyra F, Ho DD, Walker BD, Seaman MS, Bjorkman PJ, Chait BT, Nussenzweig MC. 2011. Sequence and structural convergence of broad and potent HIV antibodies that mimic CD4 binding. Science 333:1633-7.

78. Li Y, O'Dell S, Walker LM, Wu X, Guenaga J, Feng Y, Schmidt SD, McKee K, Louder MK, Ledgerwood JE, Graham BS, Haynes BF, Burton DR, Wyatt RT, Mascola JR. 2011. Mechanism of neutralization by the broadly neutralizing HIV-1 monoclonal antibody VRC01. J Virol 85:8954-67.

79. Zhou T, Georgiev I, Wu X, Yang ZY, Dai K, Finzi A, Kwon YD, Scheid JF, Shi W, Xu L, Yang Y, Zhu J, Nussenzweig MC, Sodroski J, Shapiro L, Nabel GJ, Mascola JR, Kwong PD. 2010. Structural basis for broad and potent neutralization of HIV-1 by antibody VRC01. Science 329:811-7.

80. Wu X, Zhang Z, Schramm CA, Joyce MG, Kwon YD, Zhou T, Sheng Z, Zhang B, O'Dell S, McKee K, Georgiev IS, Chuang GY, Longo NS, Lynch RM, Saunders KO, Soto C, Srivatsan S, Yang Y, Bailer RT, Louder MK, Program NCS, Mullikin JC, Connors M, Kwong PD, Mascola JR, Shapiro L. 2015. Maturation and Diversity of the VRC01-Antibody Lineage over 15 Years of Chronic HIV-1 Infection. Cell 161:470-485.

81. Lee JH, Andrabi R, Su CY, Yasmeen A, Julien JP, Kong L, Wu NC, McBride R, Sok D, Pauthner M, Cottrell CA, Nieusma T, Blattner C, Paulson JC, Klasse PJ, Wilson IA, Burton DR, Ward AB. 2017. A Broadly Neutralizing Antibody Targets the Dynamic HIV Envelope Trimer Apex via a Long, Rigidified, and Anionic beta-Hairpin Structure. Immunity 46:690-702.

82. McLellan JS, Pancera M, Carrico C, Gorman J, Julien JP, Khayat R, Louder R, Pejchal R, Sastry M, Dai K, O'Dell S, Patel N, Shahzad-ul-Hussan S, Yang Y, Zhang B, Zhou T, Zhu J, Boyington JC, Chuang GY, Diwanji D, Georgiev I, Kwon YD, Lee D, Louder MK, Moquin S, Schmidt SD, Yang ZY, Bonsignori M, Crump JA, Kapiga SH, Sam NE, Haynes BF, Burton DR, Koff WC, Walker LM, Phogat S, Wyatt R, Orwenyo J, Wang LX, Arthos J, Bewley CA, Mascola JR, Nabel GJ, Schief WR, Ward AB, Wilson IA, Kwong PD. 2011. Structure of HIV-1 gp120 V1/V2 domain with broadly neutralizing antibody PG9. Nature 480:336-43.

83. Pejchal R, Walker LM, Stanfield RL, Phogat SK, Koff WC, Poignard P, Burton DR, Wilson IA. 2010. Structure and function of broadly reactive antibody PG16 reveal an H3 subdomain that mediates potent neutralization of HIV-1. Proc Natl Acad Sci U S A 107:11483-8.

84. Kong L, Lee JH, Doores KJ, Murin CD, Julien JP, McBride R, Liu Y, Marozsan A, Cupo A, Klasse PJ, Hoffenberg S, Caulfield M, King CR, Hua Y, Le KM, Khayat R, Deller MC, Clayton T, Tien H, Feizi T, Sanders RW, Paulson JC, Moore JP, Stanfield RL, Burton DR, Ward AB, Wilson IA. 2013. Supersite of immune vulnerability on the glycosylated face of HIV-1 envelope glycoprotein gp120. Nat Struct Mol Biol 20:796-803.

85. Garces F, Lee JH, de Val N, de la Pena AT, Kong L, Puchades C, Hua Y, Stanfield RL, Burton DR, Moore JP, Sanders RW, Ward AB, Wilson IA. 2015. Affinity Maturation of a Potent Family of HIV Antibodies Is Primarily Focused on Accommodating or Avoiding Glycans. Immunity 43:1053-63.

86. Garces F, Sok D, Kong L, McBride R, Kim HJ, Saye-Francisco KF, Julien JP, Hua Y, Cupo A, Moore JP, Paulson JC, Ward AB, Burton DR, Wilson IA. 2014. Structural evolution of glycan recognition by a family of potent HIV antibodies. Cell 159:69-79.

87. Lee JH, de Val N, Lyumkis D, Ward AB. 2015. Model Building and Refinement of a Natively Glycosylated HIV-1 Env Protein by High-Resolution Cryoelectron Microscopy. Structure 23:1943-1951.

88. Blattner C, Lee JH, Sliepen K, Derking R, Falkowska E, de la Pena AT, Cupo A, Julien JP, van Gils M, Lee PS, Peng W, Paulson JC, Poignard P, Burton DR, Moore JP, Sanders RW, Wilson IA, Ward AB. 2014. Structural delineation of a quaternary, cleavage-dependent epitope at the gp41-gp120 interface on intact HIV-1 Env trimers. Immunity 40:669-80.

89. Scharf L, Wang H, Gao H, Chen S, McDowall AW, Bjorkman PJ. 2015. Broadly Neutralizing Antibody 8ANC195 Recognizes Closed and Open States of HIV-1 Env. Cell 162:1379-90.

90. Falkowska E, Le KM, Ramos A, Doores KJ, Lee JH, Blattner C, Ramirez A, Derking R, van Gils MJ, Liang CH, McBride R, von Bredow B, Shivatare SS, Wu CY, Chan-Hui PY, Liu Y, Feizi T, Zwick MB, Koff WC, Seaman MS, Swiderek K, Moore JP, Evans D, Paulson JC, Wong CH, Ward AB, Wilson IA, Sanders RW, Poignard P, Burton DR. 2014. Broadly neutralizing HIV antibodies define

a glycan-dependent epitope on the prefusion conformation of gp41 on cleaved envelope trimers. Immunity 40:657-68.

91. Chen J, Frey G, Peng H, Rits-Volloch S, Garrity J, Seaman MS, Chen B. 2014. Mechanism of HIV-1 neutralization by antibodies targeting a membrane-proximal region of gp41. J Virol 88:1249-58.

92. Guttman M, Cupo A, Julien JP, Sanders RW, Wilson IA, Moore JP, Lee KK. 2015. Antibody potency relates to the ability to recognize the closed, pre-fusion form of HIV Env. Nat Commun 6:6144.

93. Landais E, Moore PL. 2018. Development of broadly neutralizing antibodies in HIV-1 infected elite neutralizers. Retrovirology 15:61.

94. Yu L, Guan Y. 2014. Immunologic Basis for Long HCDR3s in Broadly Neutralizing Antibodies Against HIV-1. Front Immunol 5:250.

95. Mascola JR, Haynes BF. 2013. HIV-1 neutralizing antibodies: understanding nature's pathways. Immunol Rev 254:225-44.

96. Wilson PC, de Bouteiller O, Liu YJ, Potter K, Banchereau J, Capra JD, Pascual V. 1998. Somatic hypermutation introduces insertions and deletions into immunoglobulin V genes. J Exp Med 187:59-70.

97. Briney BS, Willis JR, Crowe JE, Jr. 2012. Location and length distribution of somatic hypermutation-associated DNA insertions and deletions reveals regions of antibody structural plasticity. Genes Immun 13:523-9.

98. Reason DC, Zhou J. 2006. Codon insertion and deletion functions as a somatic diversification mechanism in human antibody repertoires. Biol Direct 1:24.

99. Koff WC. 2012. HIV vaccine development: challenges and opportunities towards solving the HIV vaccine-neutralizing antibody problem. Vaccine 30:4310-5.

100. Stamatatos L. 2012. HIV vaccine design: the neutralizing antibody conundrum. Curr Opin Immunol 24:316-23.

101. Ivanov, II, Schelonka RL, Zhuang Y, Gartland GL, Zemlin M, Schroeder HW, Jr. 2005. Development of the expressed Ig CDR-H3 repertoire is marked by focusing of constraints in length, amino acid use, and charge that are first established in early B cell progenitors. J Immunol 174:7773-80.

102. Simonich CA, Williams KL, Verkerke HP, Williams JA, Nduati R, Lee KK, Overbaugh J. 2016. HIV-1 Neutralizing Antibodies with Limited Hypermutation from an Infant. Cell 166:77-87.

103. Goo L, Chohan V, Nduati R, Overbaugh J. 2014. Early development of broadly neutralizing antibodies in HIV-1-infected infants. Nat Med 20:655-8.

104. Dubochet J, Adrian M, Chang JJ, Homo JC, Lepault J, McDowall AW, Schultz P. 1988. Cryo-electron microscopy of vitrified specimens. Q Rev Biophys 21:129-228.

105. Scheres SH. 2012. RELION: implementation of a Bayesian approach to cryo-EM structure determination. J Struct Biol 180:519-30.

106. Punjani A, Rubinstein JL, Fleet DJ, Brubaker MA. 2017. cryoSPARC: algorithms for rapid unsupervised cryo-EM structure determination. Nat Methods 14:290-296.

107. Kuhlbrandt W. 2014. Biochemistry. The resolution revolution. Science 343:1443-4.

108. Cheng Y, Grigorieff N, Penczek PA, Walz T. 2015. A primer to single-particle cryo-electron microscopy. Cell 161:438-449.

109. Faruqi AR, McMullan G. 2011. Electronic detectors for electron microscopy. Q Rev Biophys 44:357-90.

110. Li X, Mooney P, Zheng S, Booth CR, Braunfeld MB, Gubbens S, Agard DA, Cheng Y. 2013. Electron counting and beam-induced motion correction enable near-atomic-resolution single-particle cryo-EM. Nat Methods 10:584-90.

111. Zheng SQ, Palovcak E, Armache JP, Verba KA, Cheng Y, Agard DA. 2017. MotionCor2: anisotropic correction of beam-induced motion for improved cryo-electron microscopy. Nat Methods 14:331-332.

112. Brilot AF, Chen JZ, Cheng A, Pan J, Harrison SC, Potter CS, Carragher B, Henderson R, Grigorieff N. 2012. Beam-induced motion of vitrified specimen on holey carbon film. J Struct Biol 177:630-7.

113. Julien JP, Cupo A, Sok D, Stanfield RL, Lyumkis D, Deller MC, Klasse PJ, Burton DR, Sanders RW, Moore JP, Ward AB, Wilson IA. 2013. Crystal structure of a soluble cleaved HIV-1 envelope trimer. Science 342:1477-83.

114. Kwong PD, Wyatt R, Robinson J, Sweet RW, Sodroski J, Hendrickson WA. 1998. Structure of an HIV gp120 envelope glycoprotein in complex with the CD4 receptor and a neutralizing human antibody. Nature 393:648-59.

115. Lyumkis D, Julien JP, de Val N, Cupo A, Potter CS, Klasse PJ, Burton DR, Sanders RW, Moore JP, Carragher B, Wilson IA, Ward AB. 2013. Cryo-EM structure of a fully glycosylated soluble cleaved HIV-1 envelope trimer. Science 342:1484-90.

116. Rantalainen K, Berndsen ZT, Murrell S, Cao L, Omorodion O, Torres JL, Wu M, Umotoy J, Copps J, Poignard P, Landais E, Paulson JC, Wilson IA, Ward AB. 2018. Co-evolution of HIV Envelope and Apex-Targeting Neutralizing Antibody Lineage Provides Benchmarks for Vaccine Design. Cell Rep 23:3249-3261.

117. Lee JH, Ozorowski G, Ward AB. 2016. Cryo-EM structure of a native, fully glycosylated, cleaved HIV-1 envelope trimer. Science 351:1043-8.

118. Harris A, Cardone G, Winkler DC, Heymann JB, Brecher M, White JM, Steven AC. 2006. Influenza virus pleiomorphy characterized by cryoelectron tomography. Proc Natl Acad Sci U S A 103:19123-7.

119. Ortiz JO, Brandt F, Matias VR, Sennels L, Rappsilber J, Scheres SH, Eibauer M, Hartl FU, Baumeister W. 2010. Structure of hibernating ribosomes studied by cryoelectron tomography in vitro and in situ. J Cell Biol 190:613-21.

120. Liljeroos L, Huiskonen JT, Ora A, Susi P, Butcher SJ. 2011. Electron cryotomography of measles virus reveals how matrix protein coats the ribonucleocapsid within intact virions. Proc Natl Acad Sci U S A 108:18085-90.

121. Chang JT, Schmid MF, Rixon FJ, Chiu W. 2007. Electron cryotomography reveals the portal in the herpesvirus capsid. J Virol 81:2065-8.

122. Vijayakrishnan S, Loney C, Jackson D, Suphamungmee W, Rixon FJ, Bhella D. 2013. Cryotomography of budding influenza A virus reveals filaments with diverse morphologies that mostly do not bear a genome at their distal end. PLoS Pathog 9:e1003413.

123. Chlanda P, Schraidt O, Kummer S, Riches J, Oberwinkler H, Prinz S, Krausslich HG, Briggs JA. 2015. Structural Analysis of the Roles of Influenza A Virus Membrane-Associated Proteins in Assembly and Morphology. J Virol 89:8957-66.

124. Calder LJ, Wasilewski S, Berriman JA, Rosenthal PB. 2010. Structural organization of a filamentous influenza A virus. Proc Natl Acad Sci U S A 107:10685-90.

125. Fontana J, Steven AC. 2015. Influenza virus-mediated membrane fusion: Structural insights from electron microscopy. Arch Biochem Biophys 581:86-97.

126. Gui L, Ebner JL, Mileant A, Williams JA, Lee KK. 2016. Visualization and Sequencing of Membrane Remodeling Leading to Influenza Virus Fusion. J Virol 90:6948-62.

127. Fontana J, Cardone G, Heymann JB, Winkler DC, Steven AC. 2012. Structural changes in Influenza virus at low pH characterized by cryo-electron tomography. J Virol 86:2919-29.

128. Calder LJ, Rosenthal PB. 2016. Cryomicroscopy provides structural snapshots of influenza virus membrane fusion. Nat Struct Mol Biol 23:853-8.

129. Chlanda P, Zimmerberg J. 2016. Protein-lipid interactions critical to replication of the influenza A virus. FEBS Lett 590:1940-54.

130. Garcia NK, Guttman M, Ebner JL, Lee KK. 2015. Dynamic changes during acid-induced activation of influenza hemagglutinin. Structure 23:665-76.

131. Harris AK, Meyerson JR, Matsuoka Y, Kuybeda O, Moran A, Bliss D, Das SR, Yewdell JW, Sapiro G, Subbarao K, Subramaniam S. 2013. Structure and accessibility of HA trimers on intact 2009 H1N1 pandemic influenza virus to stem region-specific neutralizing antibodies. Proc Natl Acad Sci U S A 110:4592-7.

132. Tran EE, Podolsky KA, Bartesaghi A, Kuybeda O, Grandinetti G, Wohlbold TJ, Tan GS, Nachbagauer R, Palese P, Krammer F, Subramaniam S. 2016. Cryo-electron Microscopy Structures of Chimeric Hemagglutinin Displayed on a Universal Influenza Vaccine Candidate. MBio 7:e00257.

Chapter 2. Dissection of epitope-specific mechanisms of neutralization of virus by intact IgG and Fab fragments

The text in this chapter has been modified slightly from © American Society for Microbiology, Journal of Virology, Vol. 92(6), 2018. doi: 10.1128/JVI.02006-17.

2.1 Introduction

Neutralizing antibodies (nAbs) play a key role in the immune response against viral pathogens by binding to viral surface proteins and preventing them from mediating cell entry and infection. The influenza virus hemagglutinin (HA) fusion glycoprotein is the dominant surface antigen and primary target of nAbs with an estimated abundance of ~300 to 500 HA glycoproteins per virion (1-3). HA is expressed as a single polypeptide chain, HA0, which trimerizes to form a 225-kDa spike on the virus surface (4). Each HA0 chain is cleaved by host proteases into the receptor binding domain, HA1, and the fusion subunit, HA2 (Fig. 2.1). HA mediates cell entry by binding to sialic acid on cellular glycoproteins and glycolipids, initiating internalization through endocytosis (4). As the endosomes mature, their lumens acidify, triggering HA to undergo a large-scale conformational change that drives the fusion of viral and endosomal membranes and generates a fusion pore through which the viral genetic material is delivered to the cytosol (4-7).

We are beginning to shed light on the mechanisms of antibody (Ab)-mediated neutralization, yet much of our understanding is based upon high resolution structural studies of antigen binding (Fab) fragments in complex with soluble, isolated antigen constructs (8). Structures for several neutralizing antibodies against HA have been reported (9-13). Based upon high resolution structures of Fab-HA complexes, it is usually inferred that the blockage of receptor binding sites or inhibition of conformational changes required for membrane fusion is responsible for neutralization. The static structures reveal antibody-antigen recognition in detail but do not necessarily enable the functional consequences of these interactions to be assessed. Recent structural and biophysical studies have begun to reveal the nature of the structural calisthenics performed by the HA fusion protein as well as the sequence of HA-induced membrane remodeling that leads to membrane fusion (5-7, 14, 15). With these new insights into fusion machinery function, it is possible to analyze mechanisms of the antibody-mediated disruption of these

dynamic events that are essential for virus entry into cells. In addition, relatively few studies have characterized the interactions between full-length IgG and whole virions, where these modes of interaction are distinct from the picture provided by isolated Fab fragments due to the bivalency of IgG molecules and the multivalent display of antigens on the surface of most virus particles. Although the binding of IgG to antigens presented on the surface of the virus has been observed in some previous studies (16, 17), we are left with an incomplete picture of the relationship between IgG bivalency and mechanisms of inhibition of virus function. Interactions between intact IgG and proteins on the surface of the virus may increase binding avidity as well as expand the modes of neutralization through the cross-linking of antigenic sites on the same viral particle or on separate particles that lead to aggregation. These additional modes of action may be responsible for observations that high levels of virus neutralization are often observed even when saturation of binding sites by antibodies is not achieved (18-20).

Here, we examine the interaction of two nAbs targeting different sites on the HA fusion protein presented on intact influenza virus. HC19 targets the receptor binding domain (RBD) on membrane-distal HA1, while FI6v3 targets the HA2 fusion subunit on the HA stalk (10, 13). We hypothesize that due to the location of the HC19 epitope on the highly-exposed end of HA, the bivalency of IgG could enhance its mechanism of action by aggregating virus particles and by cross-linking adjacent HA trimers on a virion. In contrast, the epitope for FI6v3 is located further down along the HA spike, where it may be unable to reach across to HA on a separate particle (Fig. 2.1B) (13). More specifically, we seek to investigate the effect of antibodies targeting these distinct epitopes on the ability of HA to undergo the conformational changes required to drive membrane fusion to completion. In addition, we examine the impact of bivalency on the ability of IgG to arrest infectivity by comparing the neutralization of virus by intact IgG and monovalent Fab domains. We report that the inhibition of specific stages of HA-mediated fusion, starting with membrane disruption caused by fusion peptide insertion and followed by lipid mixing, leading to pore formation as well as virus infectivity, showed dramatic differences for Fabs and intact IgG. These results suggest a pivotal and complex role for bivalency in effecting antibody neutralization of virus entry.

2.2 Materials and Methods

2.2.1 IgG purification and Fab preparation

nAb HC19 was transiently expressed by using the FreeStyle 293F expression system (Life Technologies), while FI6v3 was constitutively expressed from a stable HEK293F cell line. Plasmids encoding HC19 IgG and the stable cell line expressing FI6v3 IgG were kindly provided by Jesse Bloom at Fred Hutchinson Cancer Research Center (Seattle, WA). After production in HEK293F cells, secreted IgGs were isolated by centrifugation and further purified from the cell culture supernatant by gravity flow over protein A-agarose resin. IgGs were eluted from protein A by using 100 mM glycine buffer (pH 2.0). Fractions were analyzed by SDS-PAGE, pooled, and concentrated by using Vivaspin 2 centrifugal concentrators. Purified IgG was further digested into Fab domains by papain digestion (Pierce Fab preparation kit), and purified from Fc fragments and undigested IgG by gravity flow over protein A resin. Fractions were pooled and analyzed by SDS-PAGE to assess purity.

2.2.2 Influenza virus purification

X31 (H3N2) influenza A virus grown in allantoic fluid of embryonated chicken eggs and purified by density gradient centrifugation was purchased from Charles River Laboratories. Virus stocks (2 mg/ml) were centrifuged at 2,320 relative centrifugal force (rcf) at 4°C for 5 min to remove residual egg protein contaminants. Virus in the supernatant was pelleted by centrifugation at 25,000 rcf for 60 min at 4°C and resuspended in HEPES-buffered saline (HBS) (pH 7.5) (150 mM NaCl, 50 mM citrate, 10 mM HEPES, 0.02% NaN_3). For influenza virus used in fluorescence assays, the supernatant containing the virus was mixed with lipophilic tracer dye Vybrant DiD (1,1′-dioctadecyl-3,3,3′,3′-tetramethyl-indodicarbocyanine,4-chlorobenzenesulfonate salt) cell-labeling solution (Invitrogen) at a final dye concentration of 2.5% (vol/vol) for 60 min at 37°C prior to the final centrifugation.

2.2.3 HA quantitation

The concentration of trimeric HA in influenza virus stocks was determined by Western blot analysis using bromelain-released HA ectodomain (BHA) as a protein standard. X31 virus and known quantities of BHA (quantified by the A280) were run on NuPAGE 4% to 12% Bis-Tris gels and subsequently transferred to Immobilon-P polyvinylidene difluoride (PVDF) membranes (Millipore). After transfer, membranes were

blocked with 5% nonfat dry milk buffered in Tris-buffered saline (TBS) (pH 7.2)–150 mM NaCl–0.1% Tween 20 (TBST). Anti-HA-tagged antibody (Millipore) was diluted in blocking buffer at a 1:2,000 dilution and incubated with membranes for 1 h at room temperature. After incubation with primary antibody, membranes were washed with TBST. After washing, horseradish peroxidase (HRP)-conjugated protein G was diluted in blocking buffer at a 1:5,000 dilution and incubated with membranes for 1 h. Membranes were washed with TBS and developed by using enhanced chemiluminescence (ECL) detection methods. The band density for HA was measured and the concentration was calculated by using ImageJ software for gel analysis (21).

2.2.4 Antibody-mediated neutralization of virus measured by a TCID50 assay

X31 (H3N2) influenza A virus mixed with either IgG at a 1:1 molar ratio or Fab at a 2:1 molar ratio to the HA trimer presented on the surface of the virus was incubated for 10 min at 37°C. The use of a 2:1 (Fab/HA) ratio offers a better comparison in our assay by accounting for the bivalent presentation of Fab on IgG and the number of potential interactions with the antigen. Samples of influenza virus without antibody were treated identically as a control. Neutralization was measured by a TCID50 assay in a 96-well-plate format. In the initial well of a column, 10 µl of the sample was added to 90 µl of influenza growth medium (IGM) (20 ml bovine serum albumin [BSA], 5 ml penicillin-streptomycin, 500 µl of 100 mg/ml $CaCl_2$, 50 µl fetal bovine serum [FBS], and up to 500 ml of Opti-MEM). The total amount of HA from the virus in each initial well was 14.4 µg. The sample was then serially diluted 1:10 down the column of the plate. A 50 µl volume of 105 MDCK-SIAT1-TMPRSS2 cells/ml (referred to as “MDCK cells”) was added to each well. Four columns were used per sample in each replicate. Plates were incubated at 37°C and scored for cytopathic effects at 72 h post-infection. Viral titers were calculated by Reed-Muench analysis implemented by the Python script at https://github.com/jbloom/reedmuenchcalculator. A total of 4 to 5 replicates for each sample was used for the statistical calculation of P values between groups by analysis of variance (ANOVA).

2.2.5 Dynamic light scattering

Dynamic light scattering measurements were performed by using a Dynapro Nanostar instrument (Wyatt Technologies, Santa Barbara, CA). IgG or Fab was titrated into purified X31 influenza virus at the desired molar ratios of Ab to HA prior to addition to a low-volume quartz cuvette. For DLS measurements,

the HA concentration was kept constant at 100 μg/ml. Concentrations of polyclonal Ab in serum in response to infection are estimated to be on the order of 1 mg/ml (22); however, concentrations of monoclonal Ab are not easily quantified. Therefore, concentrations of IgG ranging from 0.1 to 100 μg/ml, consistent with quantities used in previous neutralization assays, were examined (23, 24). Measurements were taken over the course of an hour at 25°C, and the mean estimated radius at each time point was calculated from 10 individual measurements.

2.2.6 Liposome preparation

Liposomes composed of 1,2-dioleoyl-sn-glycero-3-phosphocholine (DOPC) lipid and 25% cholesterol (molar ratio to DOPC), and decorated with 5% ganglioside (molar ratio), aNeu5Ac(2-3)bDGalp(1-3)bDGalNAc(1-4)[aNeu5Ac(2-3)]bDGalp(1-4)bDGlcp(1-1)Cer (gD1a), serving as a sialic acid receptor for the HA glycoprotein, were prepared by lipid extrusion, according to a previously described protocol (5). DOPC, cholesterol, and gD1a were combined from chloroform stock solutions and dried under nitrogen gas. The lipid films were resuspended in buffer containing 25 mM SRB dye, 150 mM NaCl, 10 mM HEPES, 50 mM sodium citrate (pH 7.5), and 0.02% NaN_3. After 10 freeze-thaw cycles in liquid nitrogen, liposomes were extruded 29 times through a 100-nm polycarbonate membrane (Avanti Polar Lipids). Extruded liposomes were passed over a PD-10 desalting column (GE Healthcare) and stored in pH 7.5 HEPES-citrate buffer. DLS was used to measure the average diameter and polydispersity of the liposomes at room temperature. The liposome diameter ranged from 165 nm to 182 nm, with low polydispersity.

2.2.7 Biolayer interferometry

Binding kinetics of HC19 and FI6v3 IgGs and Fabs with trimeric BHA were determined by using BLI on an Octet Red system (FortéBio). Hydrated anti-human Fab-CH1 biosensors were immobilized for 4 min with purified IgG or Fab diluted to 10 μg/ml in phosphate-buffered saline (PBS) (pH 7.4) supplemented with 1% BSA, 0.03% Tween 20, and 0.02% NaN_3. After reaching a stable baseline, antibody-immobilized tips were moved to wells containing a 2-fold dilution series of trimeric BHA to monitor association for 4 min. Tips were moved back to wells containing buffer to monitor dissociation for 8 min. Kinetic data were analyzed by using FortéBio Data Analysis 7.0 software. Average measurements from reference wells were

subtracted, and data were processed by Savitzky-Golay filtering prior to fitting using a 1:1 binding model. Reported values are averages of data from experiments repeated in triplicate.

2.2.8 Fluorescence spectroscopy

For fluorescence-monitored membrane fusion assays, DiD-labeled virus was incubated with IgG or Fab at 22°C for 30 min to allow complexes to form. The virus-antibody mixture was then added to an excess volume of liposomes that encapsulate SRB and transferred to a 40-µl fluorescence microcuvette. The reaction mixture was incubated at neutral pH at 37°C for 10 min to allow liposomes and the virus to reach a stable baseline. We have observed from our recently reported studies that pH 5.25 irreversibly triggers HA and provides optimal dequenching profiles in fluorescence fusion assays; therefore, fusion of the virus and liposomes was initiated by decreasing the pH to 5.25 by the addition of buffer containing 150 mM NaCl, 10 mM HEPES, 50 mM sodium citrate (pH 3.0), and 0.02% NaN_3 (5, 6, 14). Measurements were collected on a Varian Cary Eclipse spectrophotometer using excitation/emission wavelength pairings of 644/655 nm for DiD and 565/586 nm for SRB, with 2.5-nm slit widths, at 37°C.

Once the target lipid becomes perturbed by insertion of the fusion peptide, leakage of SRB from the hydrophilic compartment of the liposome relieves fluorescence quenching. Lipid mixing occurs as the virus and liposome fuse, and DiD dye diffuses through a larger membrane, where fluorescence dequenching is monitored. Fluorescence dequenching of SRB and DiD was normalized by using the formula $[F_{(t)} - F_{(0)}]/[F_{(max)} - F_{(0)}]$, where $F_{(0)}$ is the fluorescence reading prior to acidification and $F_{(max)}$ is the fluorescence reading after complete dequenching by the addition of Triton X-100 detergent to a final concentration of 1%.

2.2.9 Negative-stain electron microscopy of influenza virus

The HA concentration in spin-purified X31 influenza virus was determined by Western blot analysis. X31 influenza virus at 100 µg/ml (HA) was adsorbed onto glow-discharged C-Flat, 300-mesh, Cu grids (Electron Microscopy Sciences) and stained by using methylamine tungstate (Nano-W; Nanoprobes). Grids were imaged on a Tecnai T12 electron microscope operating at 120 keV and equipped with a 4k-by-4k charge-coupled-device (CCD) camera at a magnification of ×42,000, corresponding to a pixel size of 2.60 Å per pixel.

2.2.10 Negative-stain electron microscopy of the Fab:BHA complex

The ability of Fab to stabilize prefusion BHA under fusion-activating conditions was assessed by performing reference-free 2D classification of the Fab:BHA complex under neutral and acidic pH conditions using the EMAN 2.1 image processing suite (25). In short, a 3-µl aliquot of the Fab:BHA complex at pH 7.4, or with the pH adjusted to 5.25 for 10 min, was applied to glow-discharged C-Flat, 300-mesh, Cu grids (Electron Microscopy Sciences) and stained by using Nano-W. Data were collected by using a Tecnai T12 transmission electron microscope operating at 120 keV. Images were taken by using a Gatan 4k-by-4k CCD camera at a magnification of either ×67,000 or ×52,000 and a defocus range of −3 to −1 µm, corresponding to a pixel size of 1.60 Å or 2.07 Å per pixel, respectively. Particles were selected by using interactive particle picking from ~100 micrographs. Particle stacks of ~8,000 particles were created and subjected to reference-free 2D classification and clustering to generate 50 2D classes. Representative class averages for each sample were chosen for clarity.

2.2.11 Cryo-EM and tomography processing

Purified virus, 10-nm colloidal gold beads (Electron Microscopy Sciences), and purified IgG were combined at the desired ratios of Ab to HA. The combined solution was incubated at room temperature for 5 min prior to addition to glow-discharged holey carbon-coated grids (C-flat, 200 mesh; Electron Microscopy Sciences) and plunge- frozen in liquid ethane by using a Vitrobot Mark IV specimen preparation unit (FEI Co.).

Vitrified grids were imaged at 200 keV in an FEI Tecnai F20 transmission electron microscope equipped with a 4k-by-4k CCD camera at a nominal magnification of ×50,000 (and binned by a factor of 2, yielding a pixel size of 4.4 Å per pixel) or a Gatan K2 Summit direct detector in counting mode at a calibrated magnification of ×11,500, corresponding to a pixel size of 3.2 Å per pixel. Images were acquired at a 3-µm defocus, and specimens were tilted in 2° increments from 58° to −58° by using the Leginon software package (26). The total electron dose for the entire tilt series was estimated to be ~80 electrons/Å^2. The K2 image frames were aligned prior to tomographic reconstruction (27). Tomograms were reconstructed by using the weighted back-projection method in the IMOD software package (28) and denoised as previously described (5).

2.3 Results

2.3.1 Binding affinities of IgG and Fab for soluble bromelain-released HA

The affinity of bromelain-released HA (BHA) for HC19 and FI6v3 (IgG and the respective Fab) was determined by using biolayer interferometry (BLI) (Fig. 2.2). For BLI data collection, assays using anti-human Fab-CH1 biosensors were used to capture both IgG and isolated Fabs in our study. Anti-human Fc biosensors capturing IgG were also tested, yielding rates of association (k_{on}) similar to those for isolated Fab; however, rates of dissociation (k_{dis}) for IgG could not be accurately determined. We chose to use the anti-human Fab-CH1 biosensors as the common means of capturing both Fab and IgG in order to make the experiments and observed binding kinetics as comparable as possible.

BHA binds HC19 IgG and isolated Fab with nanomolar affinities (3.25 nM and 1.13 nM, respectively). The variance in the affinities between HC19 IgG and Fab is attributed to an accelerated k_{dis} for IgG (Fig. 2.2B). k_{on} values were similar for both HC19 IgG and Fab, and no avidity effects were detected for captured IgG when loading densities of 3 μg/ml, 5 μg/ml, and 10 μg/ml were compared. For FI6v3, the k_{on} and k_{dis} of BHA were similar and yielded only a modest difference in the K_D (equilibrium dissociation constant) values (Fig. 2.2B). Overall, BLI shows that digestion of IgG into monovalent Fab does not impact the antibody paratope. The Fabs bind with affinities similar to those of full-length IgG, suggesting that any differences between IgG and Fab in subsequent experiments are due to the effects of bivalent Fab presentation by IgG and not a change in the Fab domain's capacity to bind HA.

2.3.2 Inhibition of HA-mediated membrane disruption and fusion activities by IgG and Fab

Fluorescence spectroscopy was used to monitor HA-mediated fusion between influenza virus and liposomes, and to compare the inhibitory effects of IgG and Fab fragments, targeting two distinct epitopes on HA. DiD (1,1′-dioctadecyl-3,3,3′,3′-tetramethyl-indodicarbocyanine,4-chlorobenzenesulfonate salt)-labeled virus was preincubated with IgG or Fab at the desired Ab/HA ratios prior to the addition of sulforhodamine B (SRB)-encapsulating liposomes. Following the mixing of these components, the solution was acidified to trigger HA activation. The fluorescence assay enables us to monitor two stages of HA activity: (i) fusion peptide insertion into the target liposomal membrane, which leads to leakage and

fluorescence dequenching of the encapsulated SRB dye, and (ii) lipid mixing of the merged membranes that occurs during fusion pore formation, reported by DiD dequenching (5, 6).

Increasing molar fractions of IgG and Fab relative to a constant amount of HA led to the increased inhibition of HA activities. Comparison of fusion peptide disruption of target membranes, monitored by SRB dequenching for HA1 head domain-targeting HC19 IgG and Fab, demonstrated that bivalent IgGs were more potent in their ability to reduce apparent HA activity than were monovalent Fabs, where levels of activity were only modestly diminished relative to those of the control (Fig. 2.3A). At the highest concentration of full-length IgG or Fab, SRB leakage was reduced by ~75% for IgG, compared to only ~20% inhibition for Fabs. A substantially smaller difference between IgG- and Fab-mediated inhibition was observed for the lipid-mixing stage of HA-mediated membrane fusion, which was inhibited to similar extents for both intact IgG and Fab (~85% and 74% for IgG and Fab, respectively) (Fig. 2.3B). Thus, it appears that intact HC19 IgG could effectively inhibit both an early stage of fusion peptide-induced membrane disruption and the later stage of lipid mixing of HA-mediated membrane fusion, while the Fab fragment was effective only in inhibiting lipid mixing, while permitting significant fusion peptide interactions with and disruption of membranes.

For the stem-targeting broadly neutralizing antibody (bnAb) FI6v3, the Fab fragment showed a significantly reduced ability to inhibit fusion peptide-induced membrane disruption, monitored by SRB dequenching, compared to IgG, even at concentrations approaching saturation, ~40% and ~70%, respectively (Fig. 2.3C). Late-stage lipid mixing, as indicated by DiD dequenching, was potently inhibited by intact FI6v3 IgG, while surprisingly, FI6v3 Fab was far less effective in inhibiting membrane fusion, even at concentrations approaching equivalence with the binding sites on HA, 90% versus 50%, respectively (Fig. 2.3D). The presentation of the Fab domains in the context of intact, bivalent IgG thus appears to play a prominent role in the stem-targeted antibody's ability to arrest HA-mediated membrane fusion activity.

2.3.3 Neutralization of influenza virus by bivalent IgG versus monovalent Fab

The inhibitory activity of HC19 and FI6v3 (both IgG and Fab) on influenza virus infection was evaluated by measuring the 50% tissue culture infective dose (TCID50) of X31 influenza virus. We hypothesized that neutralization would follow a profile similar to that for fluorescence fusion assays. A molar

ratio of 1:1 (IgG/HA) was chosen, where HA would not be completely inhibited and a degree of fusion activity would remain. In the case of Fabs, the concentration was selected to include the equivalent number of Fab copies as present in IgG (two Fab copies per IgG copy); thus, the molar concentration of Fab was 2-fold higher than that of IgG.

Both HC19 and FI6v3 intact IgGs displayed strong neutralizing activity against X31 influenza virus, where 70% and >95% neutralizations were achieved, respectively (Fig. 2.4). FI6v3 was more efficient at inhibiting virus infectivity, even at an IgG/HA trimer ratio of only 1:1, suggesting that stem-directed antibodies require an occupancy of only a fraction of the binding sites to achieve potent neutralization. Antibodies such as HC19 that target the RBD may require a higher occupancy of binding sites to achieve levels of neutralization similar to those of FI6v3.

HC19 IgG and Fab exhibited differences in the extents of neutralization that paralleled the trends in the inhibition of HA function observed in fluorescence fusion assays. HC19 IgG neutralized 70% of virus infectivity, compared to only 40% neutralization by an equivalent number of monovalent Fabs. Even larger differences in neutralization between IgG and Fab were observed for the stem-directed antibody FI6v3. More than 95% neutralization efficacy against X31 influenza virus was observed for FI6v3 IgG; however, no significant neutralization by Fab was detected. Overall, bivalent interactions by IgG appear to play a pivotal role in the antibody's ability to effectively neutralize influenza virus and prevent infection of cells.

2.3.4 Imaging of Fab:BHA complexes under neutral and acidic pH using negative-stain EM

Negative-stain transmission electron microscopy (EM) imaging was performed on Fab:BHA complexes at pH 7.5 and 5.25 to assess the impact that Fab binding may have on BHA's ability to undergo the acidic-pH-triggered conformational changes that are required to mediate fusion. Class averages of ~8,000 BHA trimers at pH 7.5 exhibit the characteristic prefusion "peanut-shaped" structure that is observed on the surface of virus particles (Fig. 2.5A). After adjusting the pH to 5.25 for 10 min, BHA aggregates into rosettes commonly observed in solubilized fusion glycoproteins due to the formation of the stable postfusion helical bundle with tightly clustered fusion peptides (29-31).

Imaging of HC19 Fab bound to BHA showed classes of particles where Fab density could be observed projecting from the receptor binding domain on HA1 (Fig. 2.5B). The HC19 Fab:BHA complex at

pH 7.5 displays a prefusion organization for the spike that was similar to that observed with BHA alone. After HC19 Fab and BHA were complexed for 1 h, the pH was adjusted to pH 5.25 for 10 min prior to grid preparation and imaging. Classification of particles shows that the acidified complex retains an organization similar to that of the neutral-pH complex, indicating that the binding of HC19 to BHA stabilizes the trimer in a state that is similar to that of the prefusion form, in which the HA spike remains largely intact (Fig. 2.5B). A modest narrowing of the base of the BHA stem is observed under acidic conditions with HC19 bound, which would be consistent with previous low-resolution imaging of HA-intermediate states on the surface of intact influenza virions, which suggested that the fusion peptide-associated regions were released from the main stem body and otherwise maintained an intact prefusion-like HA spike under activation conditions (32).

For FI6v3 Fab, density in the negative-stain EM images could be observed projecting from the HA2 fusion domain, consistent with the reported Fab-HA structure (13). Under neutral conditions, the BHA trimer remained in its prefusion form. The proposed mechanism of action for stem-directed antibodies is to prevent HA from undergoing critical changes necessary for fusion, and indeed, after exposure to acidic pH, the Fab:BHA complex, at the level of resolution afforded by negative-stain EM, appeared to maintain the prefusion organization (Fig. 2.5C).

2.3.5 Assessment of the ability of nAb to mediate particle aggregation by dynamic light scattering and negative-stain EM

We hypothesized that an epitope's position on the HA spike could impact the ability of IgG to mediate interparticle aggregation. To test for interparticle aggregation, we used dynamic light scattering (DLS) to measure the time-dependent aggregation of influenza virus across various IgG/HA trimer molar ratios. We first examined if antibodies bound to the HC19 epitope at the RBD on the membrane-distal end of HA could mediate the cross-linking of HA on separate virus particles. DLS detected HC19-mediated aggregate formation at IgG/HA ratios of >1:3 (Fig. 2.6A). Over the final 30 min, at this relatively low IgG/HA ratio, a modest 11% ± 1% increase in the average particle radius was detected. This finding indicates that only a fraction of sites needs to be bound for aggregate formation to start to occur. Increasing the concentration of HC19 further promoted aggregation, with an increase in the average measured particle

radius of 88% ± 6% relative to the control at IgG/HA ratios of 2:1. Aggregates showed a high degree of polydispersity, with a particle distribution ranging from 100 nm to 1 μm. Negative-stain imaging further illustrated the IgG-mediated aggregation of virus with increasing concentrations of HC19 (Fig. 2.6B). Interestingly, the particle size appeared to slightly decrease when approaching a 3:1 ratio (averaged radius of ~170 nm). Such a reduction in aggregation may be due to a further coating of the viral surface where Ab competes for available HA molecules (33).

To investigate if aggregation was due to IgG bivalency, parallel experiments using HC19 digested into monovalent Fab fragments were carried out. HC19 Fab binding to HA on the surface of the virus had a negligible impact on the size of scattering populations, with only a 4% ± 2% increase across all ratios, which is likely the result of the bound Fab extending from the tops of HA trimers (Fig. 2.6C). The HC19 Fab data support the conclusion that aggregation by IgG is attributed to bivalent interactions in the intact HC19 antibody.

To test the dependency of the epitope location on the ability of IgG to aggregate the virus, we performed parallel experiments using FI6v3, a stem-directed bnAb. Both FI6v3 IgG and FI6v3 Fab failed to produce an increase in the particle radius as measured by DLS (Fig. 2.7A and C). Negative-stain EM micrographs of FI6v3 bound to X31 influenza virus particles appear monodispersed across a range of IgG concentrations (Fig. 2.7B). These data suggest that the aggregation of influenza virus is dependent not only on bivalent interactions but also on the epitope targeted by IgG.

2.3.6 HC19 IgG cross-linking of HA spikes imaged by cryo-ET

From the negative-stain EM data, we observed an extensive aggregation of influenza virus by HC19 but were unable to resolve the 3-dimensional organization of IgG bound to HA trimers. To overcome this limitation, we used cryo-electron tomography (cryo-ET) to characterize IgG-virus interactions under more native conditions. Cryo-ET has been instrumental in the visualization of enveloped viruses that exhibit a pleomorphic structure and are unsuitable for traditional single-particle techniques, with the resolution being sufficient to distinguish different forms of viral surface glycoproteins alone and in complex with antibody Fabs (3, 5, 6, 34-36).

Tomographic analysis of HC19 associated with X31 virus demonstrated the antibody's ability to cross-link HA spikes within a given particle as well as to aggregate multiple particles by cross-linking HA spikes on separate viruses. Analysis of ~20 tomograms revealed that the cross-linking of adjacent HA on a single virion appeared to be the dominant binding mode at lower concentrations of HC19 (IgG/HA ratio of 1:6), and the observed densities linking HA spikes were consistent with our negative-stain two-dimensional (2D) classification of HC19 bound to BHA (Fig. 2.5 and 2.8A and B). Both the cross-linking of adjacent HA molecules and aggregation of the virus were observed in ~30 tomograms of samples collected at IgG/HA ratios of 1:3. Density for lipid and protein components across the interface of two viruses can be assigned from a radial density plot in which the complete HA density measures ~14 nm across and is consistent with known crystal structures (Fig. 2.8C) (37). The density between the two particles shown in Fig. 2.8C is consistent with 2 Fab layers with a thickness of ~7 nm, with the Fc fragment likely being localized in an adjacent x-y plane at a different z height.

Further increasing the HC19/HA ratio to 1:2 (~15 tomograms) led to extensive aggregation and coating of exposed HA by HC19 (Fig. 2.8D and E). At this HC19/HA ratio, clear imaging of virus bound by saturating amounts of IgG was not possible; due to the larger aggregates, the ice layer was too thick to provide sufficient beam penetration, resulting in poor image contrast.

In contrast to the high levels of HC19-induced influenza virus aggregation that were observed, FI6v3-bound viruses imaged by cryo-ET were largely monodispersed, as sampled across ~10 tomograms. This is consistent with the observations by negative-stain EM and provides support for the hypothesis that the Ab-mediated aggregation of virus is heavily dependent upon the epitope location. The positioning of lobes of extra density that we attribute to antibody bound to an HA spike by the Fab domain is consistent with known cocrystal structures of FI6v3 Fabs bound to isolated HA trimers (13). Imaging of FI6v3-complexed virus at an IgG/HA ratio of 1:2 revealed regions where the organization of HA appears disrupted, with dense arrays of HA spikes that are normally observed on the viral surface no longer being apparent. It appears that the binding of IgG to the HA stem may cause this reorganization of HA by displacing the trimer spikes (Fig. 2.9).

2.4 Discussion

HA-mediated virus entry begins with receptor binding and ends with the merging of virus and host membranes that is driven by the fusion protein carrying out a sequence of dynamic conformational changes. For at least some influenza virus strains, including X31 H3N2 Aichi, this sequence of HA reorganization commences with fusion peptide release, only later to be followed by HA1 receptor binding subunit dissociation and large-scale HA2 fusion subunit refolding to the postfusion state (14, 32, 38). Binding of nAbs to HA is thought to interrupt various steps in the sequence of events that HA must traverse to carry out membrane fusion. From recent studies of whole viruses undergoing fusion, it has been possible to determine that as HA refolds, the viral and host membranes are drawn into tightly localized close apposition through the action of a set of several HA spikes (5, 6, 39, 40). These localized dimples transition to encompass increasingly large areas of virus and host membranes that are in direct contact (6). The formation of these tightly docked virus-target membrane intermediate states requires HA spikes to exhibit a degree of lateral mobility, as the fusion proteins are displaced from the membrane contact zones and instead are observed in partially refolded hairpin configurations at the periphery of membrane contact zones. Crystal structures of Fab bound to soluble antigen have been used to infer the stage at which the antibody is inhibiting the activity of HA; however, to understand the mechanism of inhibition, it is necessary to characterize the direct functional consequences of binding in the context of intact IgG, which can exhibit bivalent interactions and cross-linking of antigen copies on the virus surface. Here we sought to examine how intact, neutralizing antibodies targeting distinct epitopes on HA in the context of whole virus particles could interfere with the fusion protein's function and sequence of events that lead to virus entry.

The receptor binding subunit HA1 is highly immunodominant and often elicits subtype-specific Abs; however, neutralizing Abs with cross-reactivity against various HA subtypes, such as S139/1 and 5J8, have been detected (41, 42). Anti-HA1 Abs often block receptor binding and can prevent virus release from infected cells (43). A correlation between binding affinity and neutralization potency is commonly observed for Abs targeting the RBD, where bivalent interactions are thought to enhance antibody avidity (41, 42, 44). In instances where individual monovalent binding by Fab to HA across subtypes is weak, it has been proposed that bivalent binding by IgG may result in increased avidity, leading to broader antibody specificities and enhanced cross-subtype neutralization (41). The first nAb that we examined, HC19, has

an epitope that overlaps the receptor binding site of HA1. The intraparticle spike cross-linking that we observed by cryo-ET, particularly at lower IgG/HA ratios, is consistent with this antibody exhibiting avid, bivalent binding. The 50% inhibitory concentration (IC_{50}) for HC19 IgG (~10 nM) in previously reported plaque reduction assays was 3 orders of magnitude lower than that observed for the respective Fab fragment, underscoring the greater potency of bivalent IgG (11). While we did not observe as dramatic an effect, we found that HC19 Fab was indeed significantly less effective than IgG in neutralizing virus, and data from fluorescence assays of the inhibition of HA-mediated fusion were in excellent agreement with the infectivity results. These results support the role of antibody bivalency in enhancing the activity of HC19.

Bivalent interactions of such antibodies may also result in the cross-linking of antigenic sites on separate particles, potentially expanding the modes of Ab-mediated neutralization by aggregating virions together. The angle at which the Fab arm binds to the HA spike, as seen in a previously reported crystal structure, is consistent with the Fab arms in intact IgG being able to reach adjacent trimers within a virus particle as well as bridge separate particles (10, 11). The binding angle and the specific epitope position on HA, even for antibodies targeting the HA1 subunit, are key determining factors of an antibody's ability to induce virus aggregation. It has been shown, for example, that HA1-directed nAbs 3F5 and 7B2 also form clusters of aggregated influenza virus particles (16), while nAbs targeting the hinge region of HA1, which is lower on the spike, orient the IgG molecule more in plane with the virus surface and have activity that is less dependent on antibody bivalency and spike cross-linking that could produce virus aggregation (23, 45).

When antibodies such as HC19 that target the receptor binding site produce large particle aggregates, numerous HAs that are not necessarily bound by an antibody are likely inaccessible due to their burial in the aggregates. In our DLS and EM studies, we observed that the degree of aggregation was largely dependent on the IgG concentration and that aggregates began to form rapidly even before the first measurement time point. Aggregates were detected at lower concentrations of HC19 IgG (1:3 ratio of IgG/HA), and the particle radius continued to increase until the Ab approached saturation of binding sites. At a 3:1 IgG/HA ratio, the average particle radius began to decrease, perhaps due to the saturation of the epitopes on the surface of individual virus particles. These data indicate that, in agreement with data from previous studies, aggregation occurs over a relatively narrow range of IgG/HA ratios (46-48).

Once the virus is aggregated into a large bolus, questions regarding the effect on infectivity remain. One possible outcome is the internalization of aggregates through an alternate, clathrin-independent pathway, giving rise to the delivery of a large quantity of virus into cells (49, 50). Previous studies on influenza virus suggest that aggregation may in some instances enhance infection rather than neutralize the virus through the delivery of a higher viral load to permissive cells (51, 52). Alternatively, aggregated virus could be degraded through phagocytosis by the use of Fc effector functions (53, 54). Indeed, the role of Ab-mediated aggregation further complicates mechanisms of neutralization of virus and may depend on the viral system being studied. For example, the IgG-induced aggregation of nonenveloped, icosahedral picornaviruses has been shown to contribute to Ab-mediated neutralization (55, 56). Aggregation of HIV-1 by dimeric IgA (tetravalent Fab presentation) is thought to inhibit movement across mucosal surfaces (57). In the present study, we observed enhanced neutralization by IgG compared to that by Fab at concentrations of IgG where extensive aggregation of influenza virus by the HA1-targeting HC19 nAb occurred. This suggests that the ability of IgG to aggregate virus can increase the efficacy of antibodies in inhibiting influenza virus infection. From our comparison of HC19 IgG and Fab activities with the complementary assays that we employed, we find that particle aggregation and interspike cross-linking modestly enhanced the activity of this nAb relative to the Fab fragment.

Additionally, in a previously unanticipated role, we found that HC19 and likely similar antibodies that bind to the HA1 receptor binding subunit also appear to be able to inhibit later stages of HA's conformational change that are required for lipid mixing. The fusion inhibition data shown in Fig. 2.3 suggest that HC19 may bind to the HA trimer in such a fashion that the fusion peptides can still be released and then bind to and perturb the target membrane; however, lipid mixing was dramatically inhibited, even by Fab alone. We note that these data are consistent with an HA fusion activation pathway where the fusion peptide can be released prior to HA1 dissociation without requiring full HA spike reorganization (14, 38, 58). Another HA1-targeted nAb, HC63, was previously shown to inhibit HA activation; however, in that case, the antibody itself bridges two HA1 subunits of the same trimer, preventing their dissociation (9, 12). For HC19, Fab interacts with a single protomer (10), and hence, we infer that it acts by stabilizing the subunit's conformation and indirectly, the HA1-HA1 “cage” that prevents the full refolding of the HA2 subunit. In support of this model, negative-stain EM analysis of the soluble bromelain-released HA trimer bound by

HC19 Fab and exposed to acidic pH indicated that the trimeric spike overall remained intact. It thus appears that the gross refolding of HA, required for the merging of the two membranes, is prevented when HC19 Fab was bound, although the fusion peptide appears to be deployed and able to disrupt membranes (Fig. 2.3 and 2.5). Alternatively, it is conceivable that with Fab bound to the HC19 epitope at the apex of the spike, the fusion machinery may be sterically blocked from drawing the two membranes into close enough proximity to fuse, despite allowing fusion peptide insertion into the target membrane. In total, the multiple mechanisms by which HC19 perturbs HA function, including blocking receptor binding, cross-linking HA spikes, aggregating particles, and inhibiting the conformational changes leading to membrane merging, are likely responsible for the reduction in infectivity observed in our neutralization assays (Fig. 2.4).

Whereas the effect of antibody bivalency in HC19 was measurable but relatively modest, in the case of FI6v3, IgG and Fab exhibited dramatic differences in their abilities to arrest the fusion process as well as neutralize virus and inhibit infection. We observed that fusion peptide-induced SRB dequenching and lipid mixing were far more potently inhibited by intact FI6v3 IgG than by Fabs. While it was tempting to speculate that differences in binding affinities could be the cause of this variation, BLI measurements of IgG and Fab bound to BHA, in the cases of both HC19 and FI6v3, yielded similar K_Ds, suggesting that these differences are instead due to the ability of IgG to form bivalent interactions. The highest levels of FI6v3 inhibition were observed for a range of IgG/HA ratios similar to those reported previously for other stem-directed antibodies, CR8020 and CR6261 (19). Our data are consistent with results from a single-particle fluorescence microscopy study of fusion inhibition, which suggested that bivalent IgG targeting the stems can disrupt networks of HA spikes that must work together for productive fusion to occur. Previous work showed that fusion requires the engagement of HA with a minimum of 3 to 5 neighboring spikes (5, 39, 40). In addition, in that fluorescence study, the authors deduced that ~60% occupancy by stem-directed antibodies was required to inhibit fusion (19). That level of bound antibody is roughly consistent with ratios of IgG/HA spike (between 0.5:1 and 1:1) where we observed both potent inhibition of HA function and neutralization of virus infectivity. If bivalent IgG is cross-linking adjacent HA spikes on a virion, this would result in tightly bound networks of HA that have constrained lateral mobility. IgG displayed potent neutralizing activity with a 95% reduction in infectivity when bound at an IgG/HA ratio of 1:1. At this same ratio, Fab was unable to inhibit the virus, further suggesting that the ability of IgG to bind bivalently to HA is

critical for FI6v3 and likely other stem-directed antibodies. Indeed, a significant decrease in fusion activity, as measured by fluorescence spectroscopy, materialized only once the Fab/HA ratio was 3:1. We postulate that complete saturation of the available binding sites on the trimeric HA spike may be necessary for Fab to have an inhibitory effect on the fusion protein's function. This may suggest that the three HA2 subunits per trimer are not cooperatively coupled to each other. In terms of using stem-targeting nAbs or engineered binders as entry-inhibiting antiviral agents, the relatively low potency of FI6v3 Fab may hint that high concentrations of inhibitors will be necessary for the compounds to be effective.

Why was FI6v3 IgG so effective when Fab was not? Our recent cryo-electron tomography studies depicting the interplay of HA and membrane remodeling during fusion indicate that shortly after initial contact and HA-induced dimple formation on the target membrane, large spans of the target and virus membranes are drawn into direct apposition (6). HA becomes excluded from these regions and must be laterally displaced to the periphery of the membrane contact zone. IgG bound to two HA spikes and, on a broader scale, cross-linking many spikes into a network, would prevent such displacement from occurring. Additionally, a cross-linked network of HA may act at an even earlier stage to prevent sufficient numbers of activated HA trimers from being recruited to the fusion site in order to produce the proper sequence of membrane docking and remodeling that can lead to fusion.

While bivalent interspike cross-linking by FI6v3 IgG within a given virus particle appears to be critical for its activity, in contrast to HC19, neither FI6v3 IgG nor Fab was able to aggregate virus. Stem-directed Abs such as FI6v3 must diffuse through a dense array of HA spikes on the surface of influenza virus, and the location of this epitope further down the HA stem prevents the Ab from being able to reach across to bridge two epitope sites on separate particles. Previous studies examined the HA distribution on the virus and inferred the accessibility of the HA2 stem epitope to antibodies (59) but did not actually examine whole virus complexed with antibody. Another cryo-electron tomography study previously examined a stem-targeting bnAb, C179, bound to H1N1 influenza virus virions, but focused on the averaged structure of the trimer-antibody complex, which primarily revealed the orientation of one Fab domain projecting from the prefusion trimer (17). In that study, Harris et al. also observed that the distribution of trimers on virions was able to accommodate up to 75% antibody occupancy of HA. We note that for FI6v3, consistent with the findings of the study on C179, we also did not observe significant density for the Fc

domain in an orientation where it would be accessible or extend beyond the HA arrays. We speculate that this may indicate that the Fc-mediated effects associated with stem-targeting nAbs such as FI6v3 may be targeting HA on the surface of infected cells, where the HA density may be lower, rather than on free virus (53, 54).

In conclusion, we observed that the Ab-mediated inhibition of HA function occurs by multiple complementary mechanisms, and is largely dependent on the specific epitope that is targeted and on the bivalent nature of IgG molecules. We have shown that the ability of nAbs to aggregate influenza virus particles enhances the inhibition of HA at an early stage of fusion peptide-induced membrane disruption through the occlusion of infectious virions, even at concentrations well below antigen saturation. Surprisingly, for HC19, binding to HA also inhibited HA function at the lipid-mixing stage of the fusion pathway by preventing the refolding of HA through the stabilization of the trimer under fusion-activating conditions. Epitopes further down the HA stem do not exhibit cross-linking across separate particles, but the findings here support a model of neutralization where bivalent binding to a sufficient amount of antigen is needed to disrupt the cooperative network of HA required for fusion. The epitope that is targeted influences the type of bivalent interactions that can take place between HA and the virus and should be considered when developing a general model of Ab-mediated neutralization.

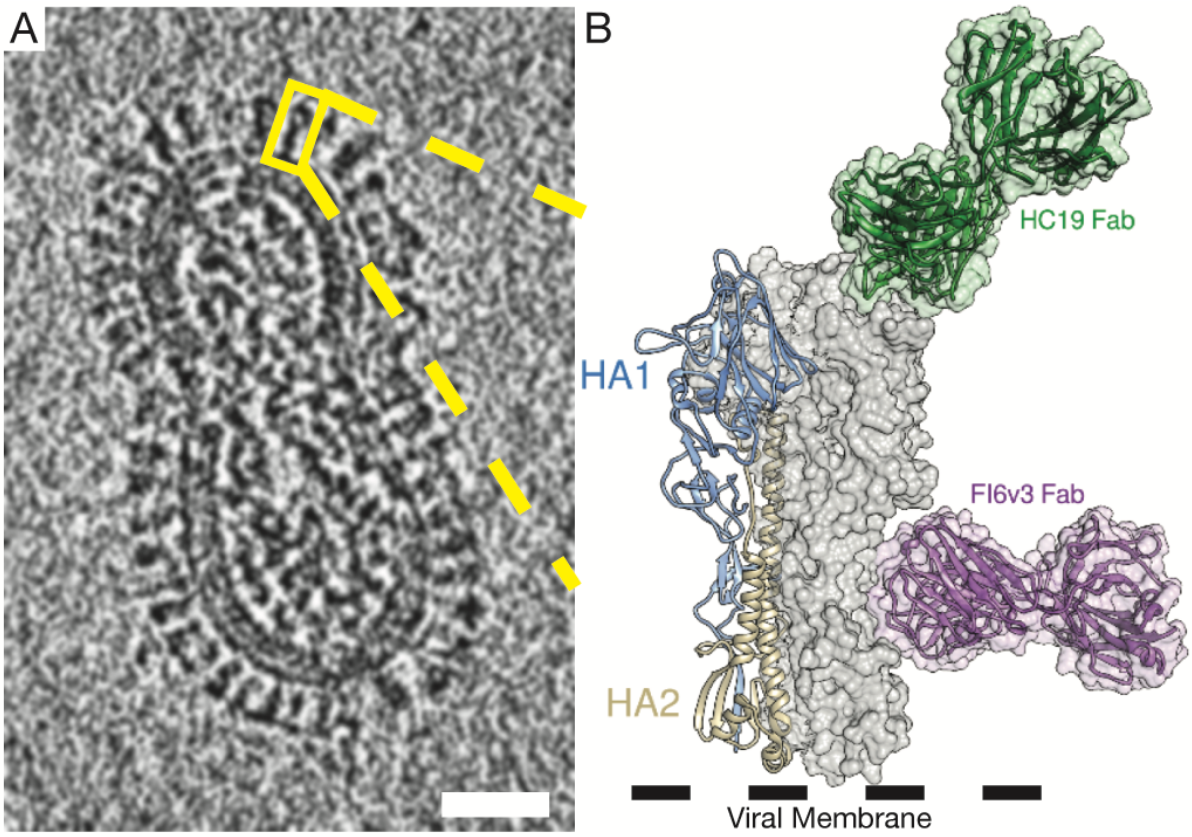

Figure 2.1: Cryo-electron tomography used to visualize the high density of HA on the viral surface. **(A)** An 8.0-nm computational slice through X31 influenza virus imaged by cryo-ET, with an individual HA trimer highlighted (yellow box). **(B)** Structural features of HA modeled in an expanded view of the highlighted trimer in panel A, with a single HA monomer consisting of the receptor binding domain (HA1) and the fusion domain (HA2) shown in a ribbon diagram (PDB accession number 4FNK). Epitopes for HC19 (PDB accession number 2VIR) and FI6v3 (PDB accession number 3ZTJ) are highlighted using the respective crystal structures. Bar = 25 nm.

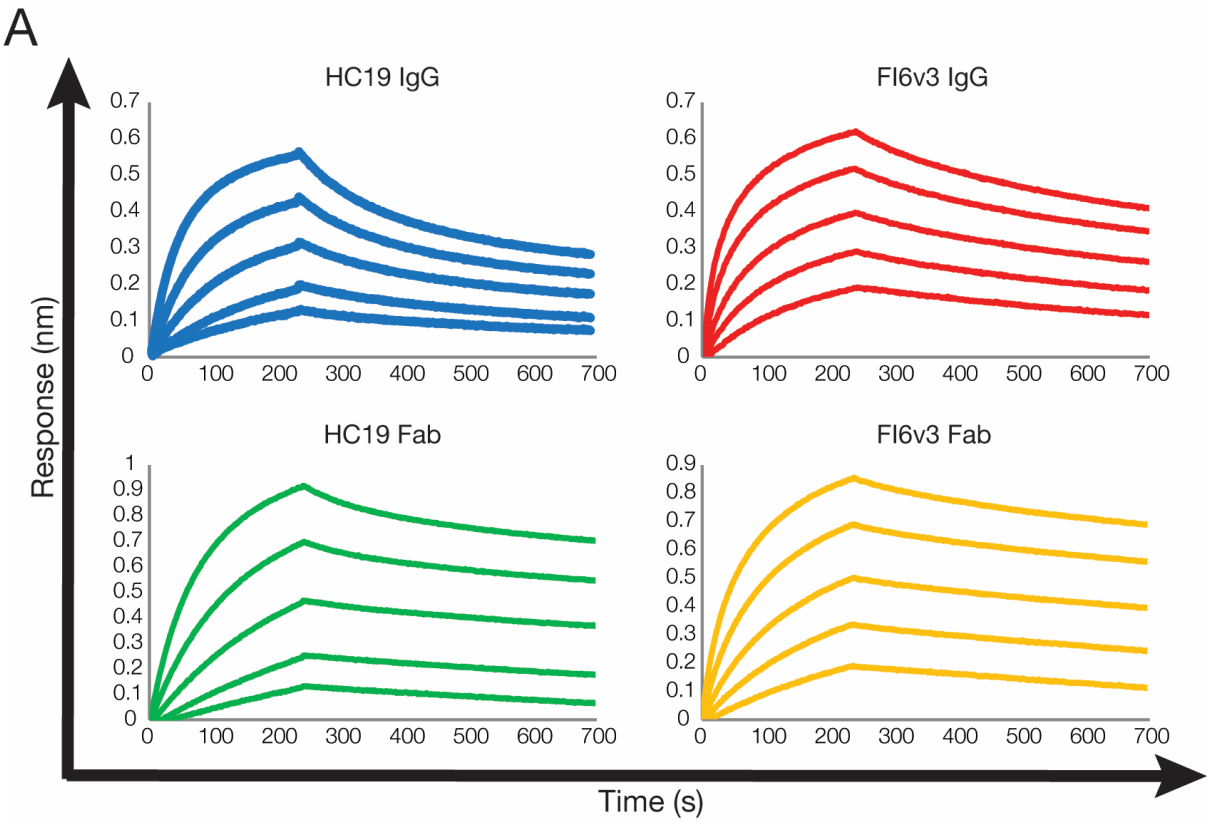

B

	k_a (1/Ms) (10^5)	k_d (1/s) (10^{-4})	K_D nM
HC19 IgG	6.3 +/- 0.3	20.1 +/- 0.3	3.3 +/- 0.7
HC19 Fab	4.5 +/- 0.2	5.1 +/- 0.8	1.1 +/- 0.2

	k_a (1/Ms) (10^4)	k_d (1/s) (10^{-4})	K_D nM
FI6v3 IgG	6 +/- 2	7 +/- 1	12 +/- 3
FIv63 Fab	3.6 +/- 0.5	4.6 +/- 0.3	13 +/- 1

Figure 2.2: Affinities of IgG and Fab measured by using biolayer interferometry. **(A)** Binding sensorgrams show binding of BHA to immobilized HC19 IgG (blue), HC19 Fab (green), FI6v3 IgG (red), and FI6v3 Fab (orange). **(B)** Association and dissociation constants yield similar K_Ds between HC19 IgG and Fab and between FI6v3 IgG and Fab. Values shown are the averages and standard deviations of data from experiments repeated in triplicates.

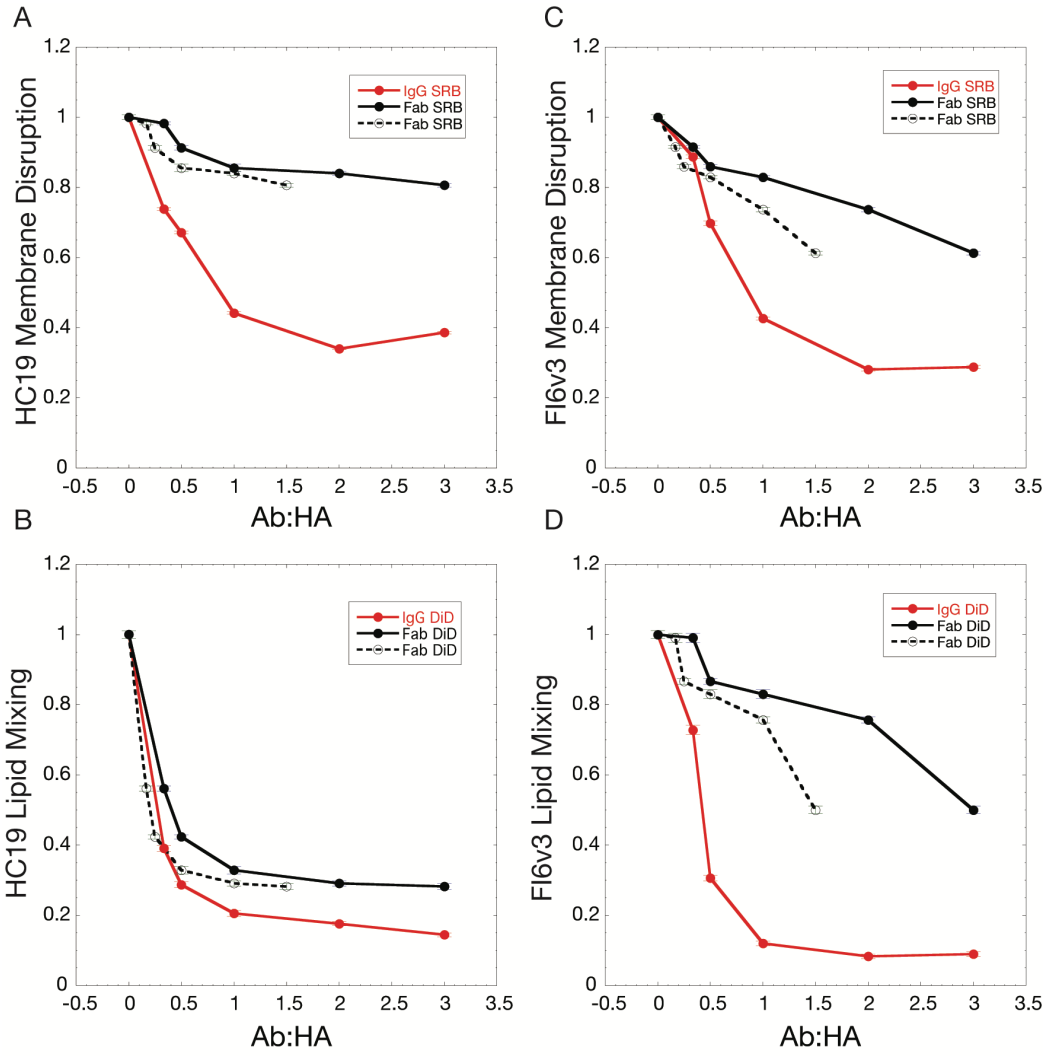

Figure 2.3: Fluorescence fusion assay monitors antibody-mediated inhibition of HA function by tracking dequenching of the fluorescent dyes SRB, indicating membrane disruption, and DiD, indicating lipid mixing. Plotted are the inhibitory effects of IgG and Fab. The dashed line is a normalized version of the Fab inhibition data and represents inhibition at an equivalent number of Fab arms compared to IgG (1 Fab = 0.5 IgG). **(A)** HC19 inhibition of membrane disruption is enhanced through bivalent interactions between IgG and HA on X31 virus, even at subsaturating concentrations, where aggregation was observed by DLS. Fab binding has little impact on membrane disruption inhibition. **(B)** Extents of inhibition of lipid mixing by IgG and Fab are similar, suggesting that bivalency may not play a large role in fusion inhibition for HC19. **(C)** Membrane disruption is more potently inhibited by FI6v3 IgG than by monovalent Fab. **(D)** Inhibition of lipid mixing by FI6v3 IgG is greater than that by Fab, suggesting that cross-linking of neighboring trimers is important for HA inhibition.

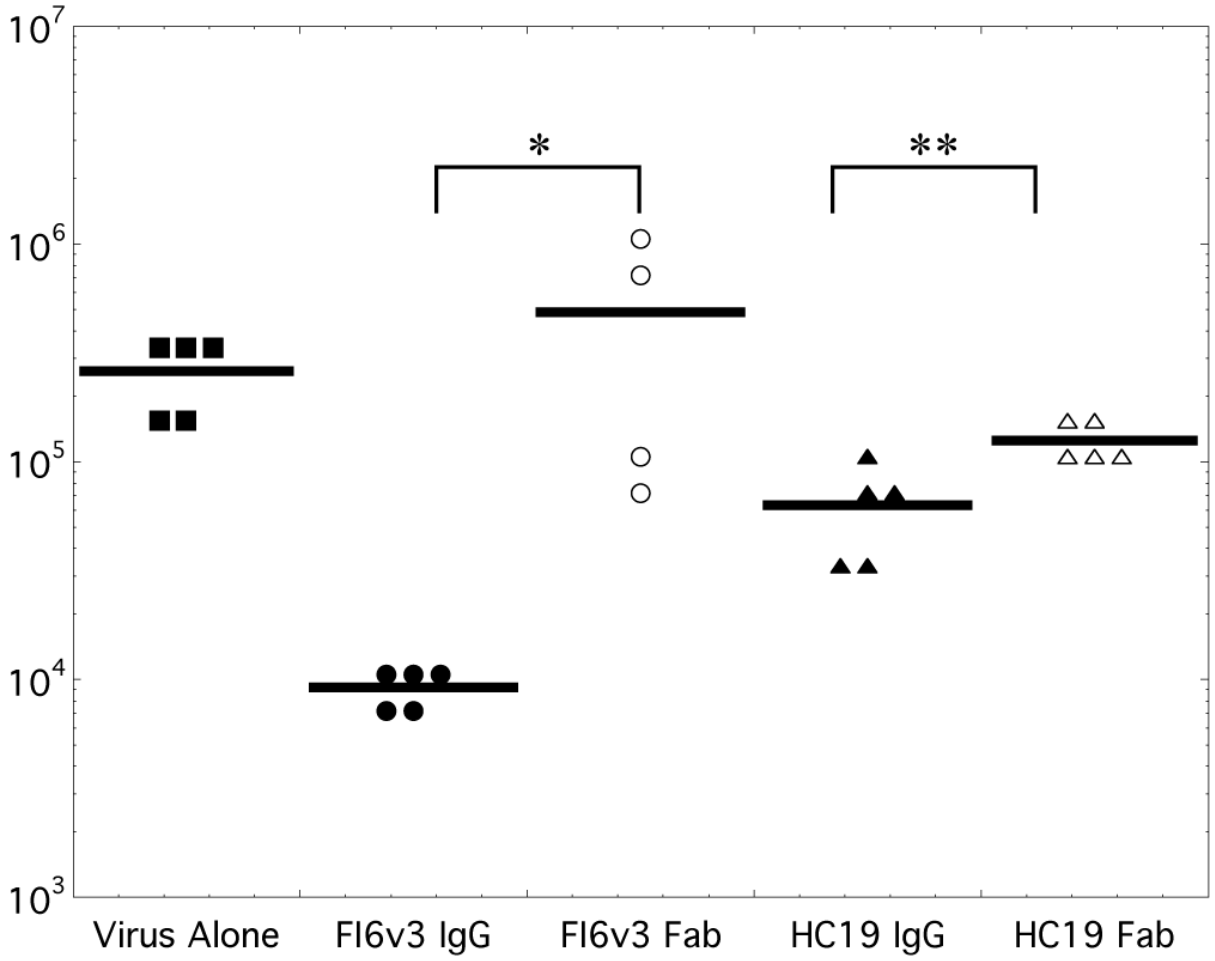

Figure 2.4: Neutralization assay measuring TCID50. Antibody-mediated neutralization of influenza virus was evaluated by measuring the TCID50 of influenza virus. IgGs for both FI6v3 and HC19 displayed stronger neutralization than did the respective Fabs. While HC19 Fab could neutralize virus to some degree, FI6v3 Fab did not exhibit a significant ability to neutralize the virus (*, $P > 0.05$; **, $P < 0.01$).

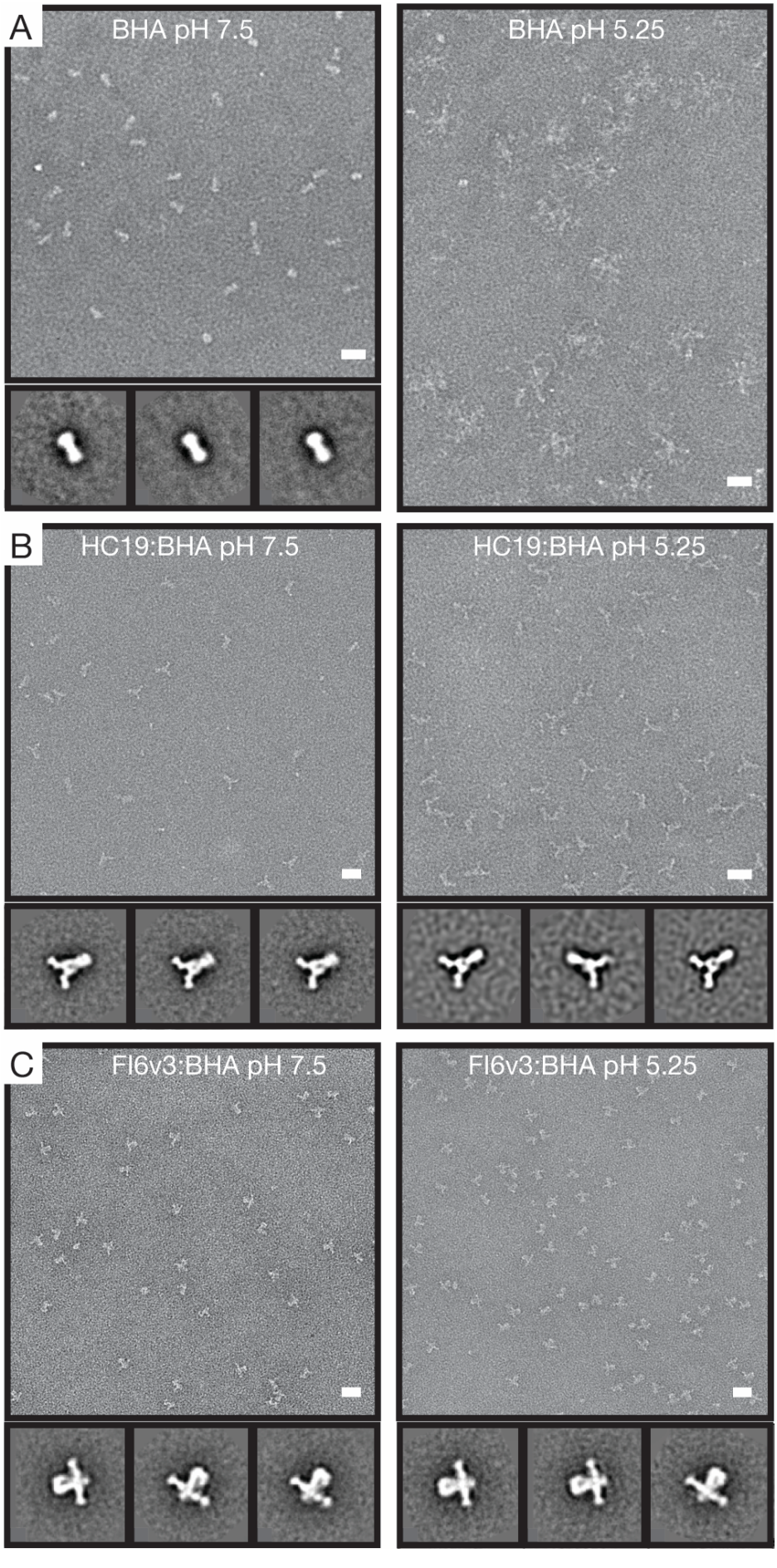
A
BHA pH 7.5
BHA pH 5.25
B
HC19:BHA pH 7.5
HC19:BHA pH 5.25
C
FI6v3:BHA pH 7.5
FI6v3:BHA pH 5.25

Figure 2.5: Negative-stain EM and 2D classification of Fab:BHA complexes under neutral and acidic conditions reveal structural similarities. **(A)** Electron micrographs and representative class averages of BHA at pH 7.5 and BHA that has been acidified for 10 min at pH 5.25. In response to acidic pH, BHA refolds into a postfusion conformation, forming small aggregates (rosettes) that are not amenable to 2D classification. **(B)** BHA bound by HC19 Fab at pH 7.5 maintains the prefusion form of the BHA trimer. After acidification for 10 min at pH 5.25, HC19 Fab appears to stabilize the BHA timer in a structure similar to that at neutral pH. **(C)** Both BHA bound by FI6v3 Fab at pH 7.5 and the Fab:BHA complex acidified for 10 min at pH 5.25 stabilize the BHA trimer and prevent refolding into a postfusion form. Bar = 20 nm.

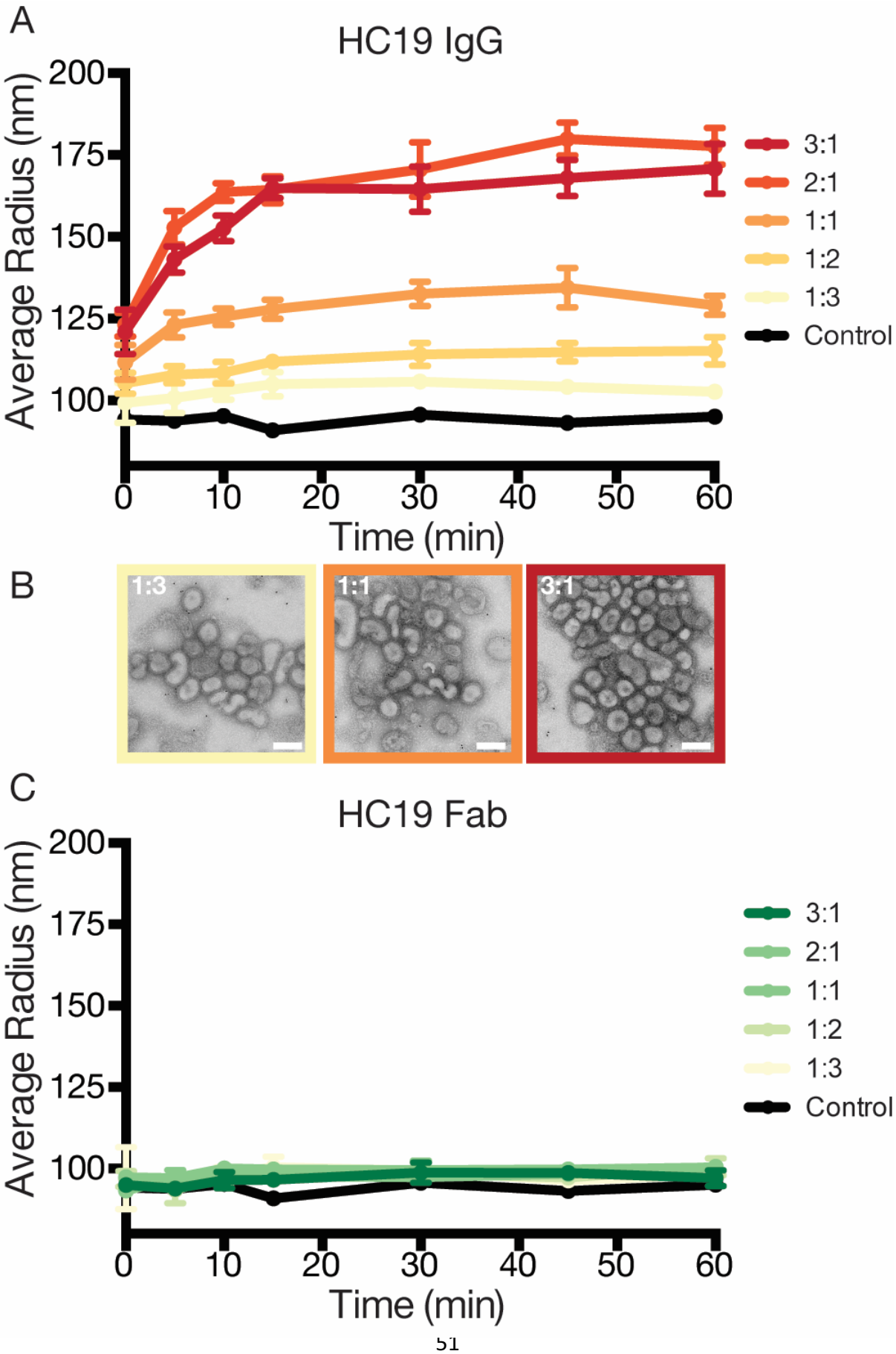
A
HC19 IgG
Average Radius (nm)
200
175
150
125
100
0
10
20
30
40
50
60
Time (min)
3:1
2:1
1:1
1:2
1:3
Control
B
1:3
1:1
3:1
C
HC19 Fab
Average Radius (nm)
200
175
150
125
100
0
10
20
30
40
50
60
Time (min)
3:1
2:1
1:1
1:2
1:3
Control

Figure 2.6: Dynamic light scattering monitors the time- and concentration-dependent aggregation of influenza virus X31 by HC19 IgG. **(A)** As the ratio of IgG/HA increases, HC19 aggregates virus particles, with peak aggregation occurring at 2:1 ratios. **(B)** Negative-stain micrographs further illustrate the extent of aggregation as the ratio of IgG/HA increases. **(C)** Digestion of IgG into monovalent Fab arms fails to aggregate influenza virus X31, emphasizing the complex binding that occurs between bivalent IgG and HA presented on the virus surface. Bar = 200 nm.

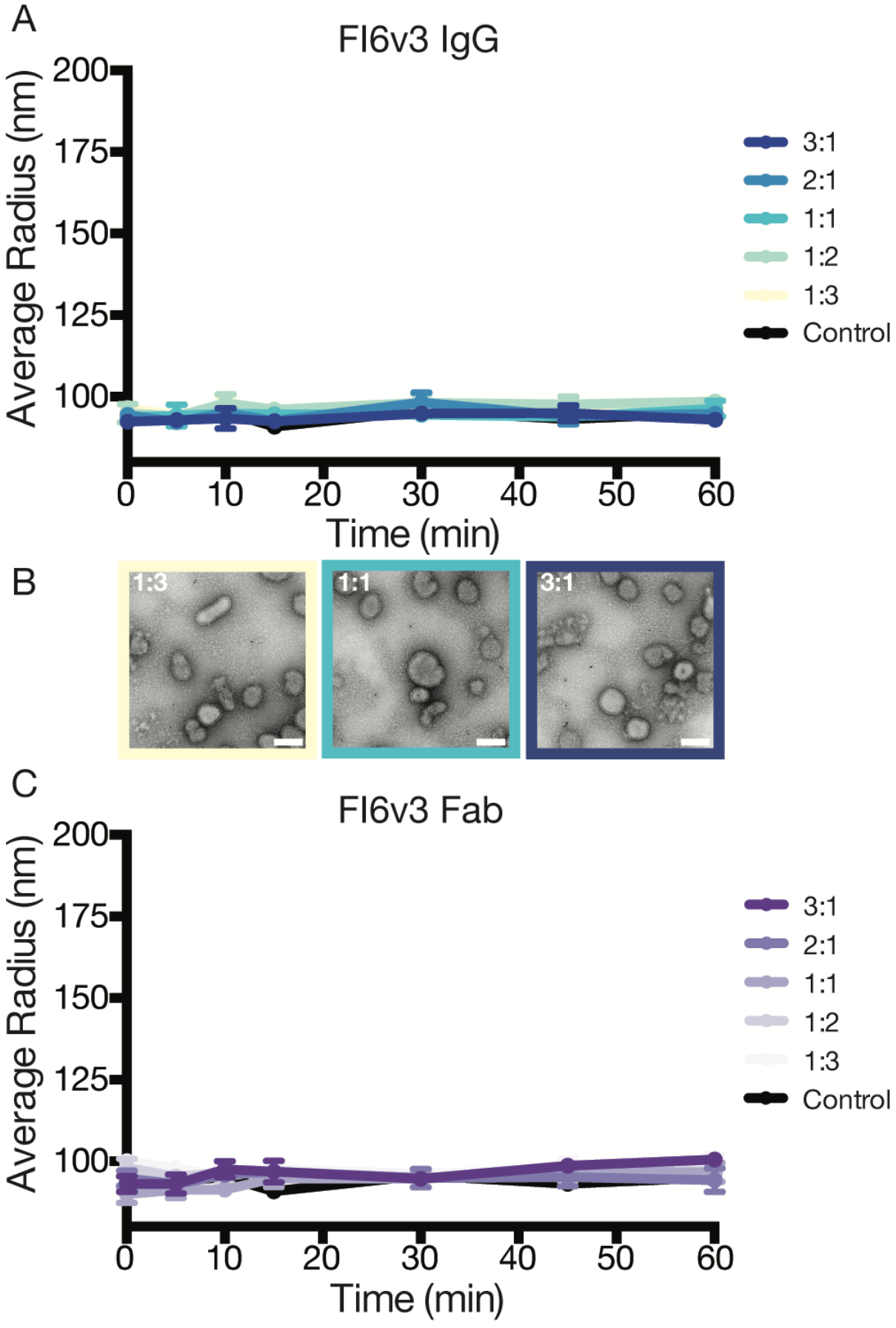
A
Fl6v3 IgG
Average Radius (nm)
200
175
150
125
100
0
10
20
30
40
50
60
Time (min)
3:1
2:1
1:1
1:2
1:3
Control
B
1:3
1:1
3:1
C
Fl6v3 Fab
Average Radius (nm)
200
175
150
125
100
0
10
20
30
40
50
60
Time (min)
3:1
2:1
1:1
1:2
1:3
Control

Figure 2.7: Dynamic light scattering does not detect aggregate formation of influenza virus X31 in the presence of IgG or Fab from stem-directed antibody FI6v3. **(A)** IgG incubated with influenza virus X31 at various ratios had no effect on particle radius in solution. **(B)** Negative-stain micrographs of influenza virus across various ratios of IgG/HA appear monodispersed, demonstrating the inability of FI6v3 to form bivalent interactions across multiple virus particles. **(C)** Similar to IgG, FI6v3 Fab fails to aggregate influenza virus X31. Bar = 200 nm.

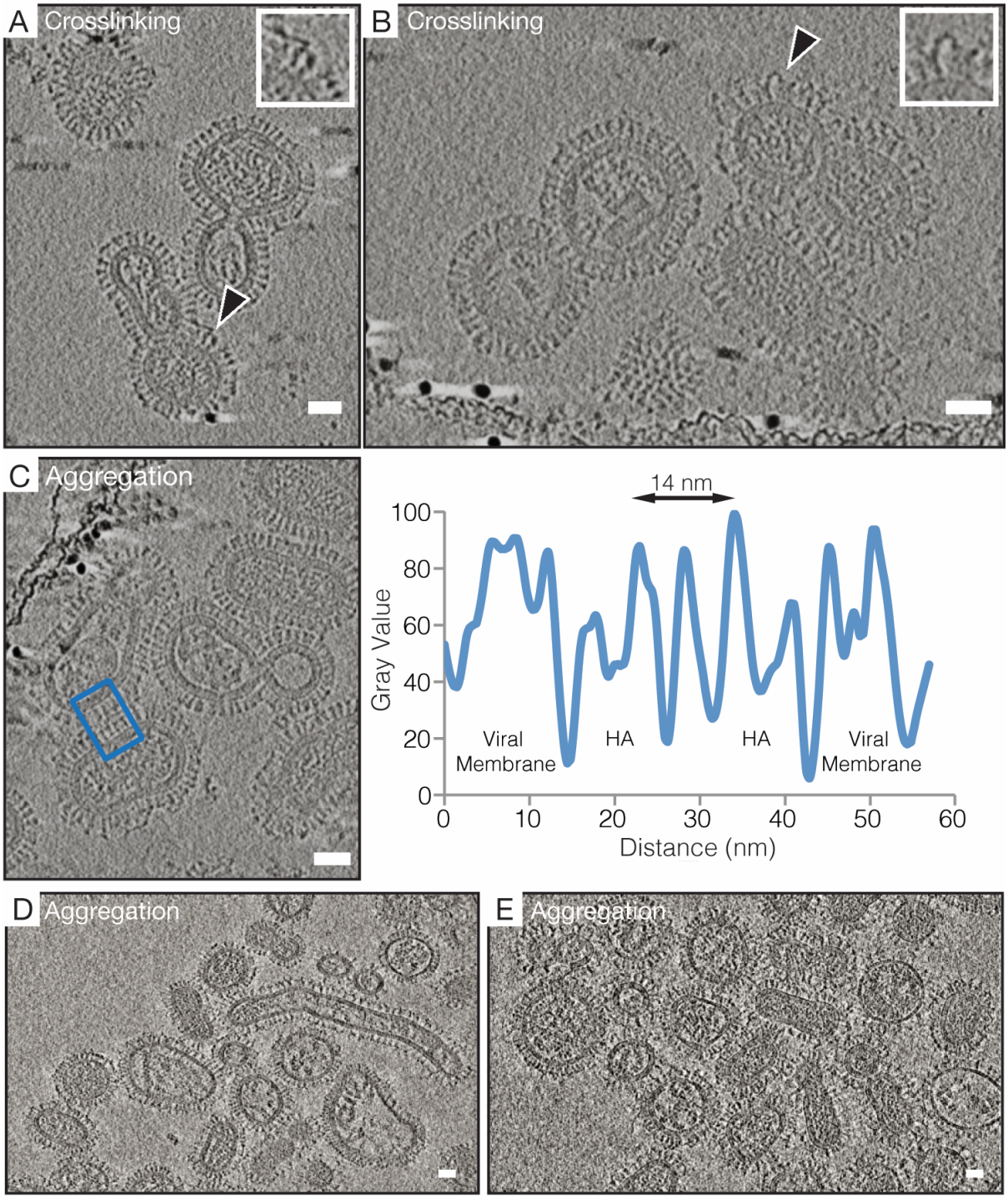
A Crosslinking
B Crosslinking
C Aggregation
14 nm
Gray Value
100
80
60
40
20
0
Viral Membrane
HA
HA
Viral Membrane
0
10
20
30
40
50
60
Distance (nm)
D Aggregation
E Aggregation

Figure 2.8: HC19 IgG-mediated cross-linking of HA on the surface of intact X31 influenza occurs between adjacent antigens on single particles and between antigens on separate particles, causing aggregation to occur. **(A and B)** A 4.4-nm-thick computational slice through HC19 IgG-complexed virus at a ratio of 1:6 (IgG/HA). Black arrowheads point toward IgG-cross-linked HA trimers on the surface of individual particles, and expanded views of these interactions are shown in the insets. **(C)** A 4.4-nm-thick computational slice through HC19 IgG-complexed virus at a ratio of 1:3 (IgG/HA). The radial density average at the interface between two virus particles was measured so that the distribution of lipid and protein components could be assigned. The blue box indicates the measured area used for the radial density plot. **(D and E)** Computational slices (8.0 nm thick) through HC19 IgG-complexed virus at a ratio of 1:2 (IgG/HA) illustrating extensive aggregation that occurs. Bar = 25 nm.

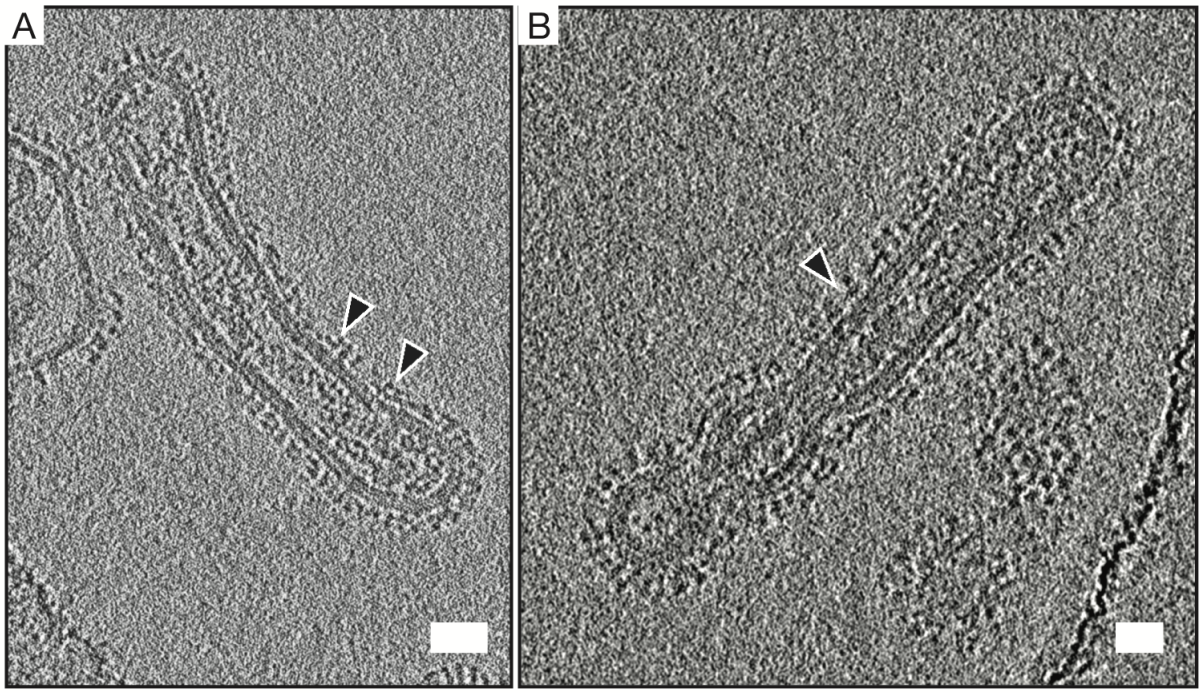

Figure 2.9: FI6v3 bound to X31 may disrupt the dense network of HA on the surface of the virus. Shown is a 6.4-nm-thick computational slice of FI6v3 bound to X31 at a ratio of 1:2 (IgG/HA). Black arrowheads point toward FI6v3 IgG-bound HA. Additional density ~6 nm above the viral membrane corresponds to FI6v3 bound to the stem region of HA2. FI6v3 fails to aggregate X31 due to the epitope's location further down the HA stem. The IgG-virus mixture was incubated for 30 min prior to vitrification. Bar = 25 nm.

References

1. Inglis SC, Carroll AR, Lamb RA, Mahy BW. 1976. Polypeptides specified by the influenza virus genome I. Evidence for eight distinct gene products specified by fowl plague virus. Virology 74:489-503.
2. Ruigrok RW, Andree PJ, Hooft van Huysduynen RA, Mellema JE. 1984. Characterization of three highly purified influenza virus strains by electron microscopy. J Gen Virol 65 (Pt 4):799-802.
3. Harris A, Cardone G, Winkler DC, Heymann JB, Brecher M, White JM, Steven AC. 2006. Influenza virus pleiomorphy characterized by cryoelectron tomography. Proc Natl Acad Sci U S A 103:19123-7.
4. Skehel JJ, Wiley DC. 2000. Receptor Binding and Membrane Fusion in Virus Entry: The Influenza Hamagglutinin. Annual Review of Biochemistry:531-569.
5. Lee KK. 2010. Architecture of a nascent viral fusion pore. The EMBO Journal 29:1299-1311.
6. Gui L, Ebner JL, Mileant A, Williams JA, Lee KK. 2016. Visualization and Sequencing of Membrane Remodeling Leading to Influenza Virus Fusion. J Virol 90:6948-62.
7. Chlanda P, Zimmerberg J. 2016. Protein-lipid interactions critical to replication of the influenza A virus. FEBS Lett 590:1940-54.
8. Lee PS, Wilson IA. 2015. Structural characterization of viral epitopes recognized by broadly cross-reactive antibodies. Curr Top Microbiol Immunol 386:323-41.
9. Barbey-Martin C, Gigant B, Bizebard T, Calder LJ, Wharton SA, Skehel JJ, Knossow M. 2002. An antibody that prevents the hemagglutinin low pH fusogenic transition. Virology 294:70-4.
10. Bizebard T, Daniels R, Kahn R, Golinelli-Pimpaneau B, Skehel JJ, Knossow M. 1994. Refined three-dimensional structure of the Fab fragment of a murine IgG1, lambda antibody. Acta Crystallographica Section D, Biological Crystallography 50:768-777.
11. Fleury D, Barrere B, Bizebard T, Daniels RS, Skehel JJ, Knossow M. 1999. A complex of influenza hemagglutinin with a neutralizing antibody that binds outside the virus receptor binding site. Nat Struct Biol 6:530-4.
12. Knossow M, Gaudier M, Douglas A, Barrere B, Bizebard T, Barbey C, Gigant B, Skehel JJ. 2002. Mechanism of neutralization of influenza virus infectivity by antibodies. Virology 302:294-8.
13. Corti D, Voss J, Gamblin SJ, Codoni G, Macagno A, Jarrossay D, Vachieri SG, Pinna D, Minola A, Vanzetta F, Silacci C, Fernandez-Rodriguez BM, Agatic G, Bianchi S, Giacchetto-Sasselli I, Calder L, Sallusto F, Collins P, Haire LF, Temperton N, Langedijk JP, Skehel JJ, Lanzavecchia A. 2011. A neutralizing antibody selected from plasma cells that binds to group 1 and group 2 influenza A hemagglutinins. Science 333:850-6.
14. Garcia NK, Guttman M, Ebner JL, Lee KK. 2015. Dynamic changes during acid-induced activation of influenza hemagglutinin. Structure 23:665-76.
15. Calder LJ, Rosenthal PB. 2016. Cryomicroscopy provides structural snapshots of influenza virus membrane fusion. Nat Struct Mol Biol 23:853-8.
16. Tran EE, Podolsky KA, Bartesaghi A, Kuybeda O, Grandinetti G, Wohlbold TJ, Tan GS, Nachbagauer R, Palese P, Krammer F, Subramaniam S. 2016. Cryo-electron Microscopy Structures of Chimeric Hemagglutinin Displayed on a Universal Influenza Vaccine Candidate. MBio 7:e00257.
17. Harris AK, Meyerson JR, Matsuoka Y, Kuybeda O, Moran A, Bliss D, Das SR, Yewdell JW, Sapiro G, Subbarao K, Subramaniam S. 2013. Structure and accessibility of HA trimers on intact 2009 H1N1 pandemic influenza virus to stem region-specific neutralizing antibodies. Proc Natl Acad Sci U S A 110:4592-7.

18. Klasse P. 2014. Neutralization of Virus Infectivity by Antibodies: Old Problems in New Perspectives. Advances in Biology.

19. Otterstrom JJ, Brandenburg B, Koldijk MH, Juraszek J, Tang C, Mashaghi S, Kwaks T, Goudsmit J, Vogels R, Friesen RHE, Van Oijen AM. 2014. Relating influenza virus membrane fusion kinetics to stoichiometry of neutralizing antibodies at the single-particle level. Proceedings of the National Academy of Sciences of the United States of America 111:E5143-E5148.

20. Taylor H, Armstrong S, Dimmock N. 1987. Quantitative relationships between an influenza virus and neutralizing antibody. Virology:288-298.

21. Schneider CA, Rasband WS, Eliceiri KW. 2012. NIH Image to ImageJ: 25 years of image analysis. Nat Methods 9:671-5.

22. Cassidy JT, Nordby GL. 1975. Human serum immunoglobulin concentrations: prevalence of immunoglobulin deficiencies. J Allergy Clin Immunol 55:35-48.

23. Edwards MJ, Dimmock NJ. 2000. Two influenza A virus-specific Fabs neutralize by inhibiting virus attachment to target cells, while neutralization by their IgGs is complex and occurs simultaneously through fusion inhibition and attachment inhibition. Virology 278:423-35.

24. Edwards MJ, Dimmock NJ. 2001. A haemagglutinin (HA1)-specific FAb neutralizes influenza A virus by inhibiting fusion activity. J Gen Virol 82:1387-95.

25. Tang G, Peng L, Baldwin PR, Mann DS, Jiang W, Rees I, Ludtke SJ. 2007. EMAN2: an extensible image processing suite for electron microscopy. J Struct Biol 157:38-46.

26. Suloway C, Shi J, Cheng A, Pulokas J, Carragher B, Potter CS, Zheng SQ, Agard DA, Jensen GJ. 2009. Fully automated, sequential tilt-series acquisition with Leginon. J Struct Biol 167:11-8.

27. Li X, Mooney P, Zheng S, Booth CR, Braunfeld MB, Gubbens S, Agard DA, Cheng Y. 2013. Electron counting and beam-induced motion correction enable near-atomic-resolution single-particle cryo-EM. Nat Methods 10:584-90.

28. Kremer JR, Mastronarde DN, McIntosh JR. 1996. Computer visualization of three-dimensional image data using IMOD. J Struct Biol 116:71-6.

29. Laver WG, Valentine RC. 1969. Morphology of the isolated hemagglutinin and neuraminidase subunits of influenza virus. Virology 38:105-19.

30. McCraw DM, Gallagher JR, Harris AK. 2016. Characterization of Influenza Vaccine Hemagglutinin Complexes by Cryo-Electron Microscopy and Image Analyses Reveals Structural Polymorphisms. Clin Vaccine Immunol 23:483-95.

31. Skehel JJ, Bayley PM, Brown EB, Martin SR, Waterfield MD, White JM, Wilson IA, Wiley DC. 1982. Changes in the conformation of influenza virus hemagglutinin at the pH optimum of virus-mediated membrane fusion. Proc Natl Acad Sci U S A 79:968-72.

32. Fontana J, Cardone G, Heymann JB, Winkler DC, Steven AC. 2012. Structural changes in Influenza virus at low pH characterized by cryo-electron tomography. J Virol 86:2919-29.

33. Outlaw MC, Dimmock NJ. 1991. Insights into neutralization of animal viruses gained from study of influenza virus. Epidemiol Infect 106:205-20.

34. Ortiz JO, Brandt F, Matias VR, Sennels L, Rappsilber J, Scheres SH, Eibauer M, Hartl FU, Baumeister W. 2010. Structure of hibernating ribosomes studied by cryoelectron tomography in vitro and in situ. J Cell Biol 190:613-21.

35. Liljeroos L, Huiskonen JT, Ora A, Susi P, Butcher SJ. 2011. Electron cryotomography of measles virus reveals how matrix protein coats the ribonucleocapsid within intact virions. Proc Natl Acad Sci U S A 108:18085-90.

36. Chang JT, Schmid MF, Rixon FJ, Chiu W. 2007. Electron cryotomography reveals the portal in the herpesvirus capsid. J Virol 81:2065-8.

37. Wilson IA, Skehel JJ, Wiley DC. 1981. Structure of the haemagglutinin membrane glycoprotein of influenza virus at 3 A resolution. Nature 289:366-73.

38. White JM, Wilson IA. 1987. Anti-peptide antibodies detect steps in a protein conformational change: low-pH activation of the influenza virus hemagglutinin. J Cell Biol 105:2887-96.

39. Ivanovic T, Choi JL, Whelan SP, van Oijen AM, Harrison SC. 2013. Influenza-virus membrane fusion by cooperative fold-back of stochastically induced hemagglutinin intermediates. Elife 2:e00333.

40. Danieli T, Pelletier SL, Henis YI, White JM. 1996. Membrane fusion mediated by the influenza virus hemagglutinin requires the concerted action of at least three hemagglutinin trimers. J Cell Biol 133:559-69.

41. Lee PS, Yoshida R, Ekiert DC, Sakai N, Suzuki Y, Takada A, Wilson IA. 2012. Heterosubtypic antibody recognition of the influenza virus hemagglutinin receptor binding site enhanced by avidity. Proc Natl Acad Sci U S A 109:17040-5.

42. Hong M, Lee PS, Hoffman RM, Zhu X, Krause JC, Laursen NS, Yoon SI, Song L, Tussey L, Crowe JE, Jr., Ward AB, Wilson IA. 2013. Antibody recognition of the pandemic H1N1 Influenza virus hemagglutinin receptor binding site. J Virol 87:12471-80.

43. Brandenburg B, Koudstaal W, Goudsmit J, Klaren V, Tang C, Bujny MV, Korse HJ, Kwaks T, Otterstrom JJ, Juraszek J, van Oijen AM, Vogels R, Friesen RH. 2013. Mechanisms of hemagglutinin targeted influenza virus neutralization. PLoS One 8:e80034.

44. Ekiert DC, Kashyap AK, Steel J, Rubrum A, Bhabha G, Khayat R, Lee JH, Dillon MA, O'Neil RE, Faynboym AM, Horowitz M, Horowitz L, Ward AB, Palese P, Webby R, Lerner RA, Bhatt RR, Wilson IA. 2012. Cross-neutralization of influenza A viruses mediated by a single antibody loop. Nature 489:526-32.

45. N. A-MF. 2007. Structure of the sialic acid binding site in influenza A virus: Hemagglutinin. Journal of Biological Sciences 1:113-122.

46. Lafferty KJ. 1963. The Interaction between Virus and Antibody. III. Examination of Virus-Antibody Complexes with the Electron Microscope. Virology 21:91-99.

47. Dimmock NJ, Hardy SA. 2004. Valency of antibody binding to virions and its determination by surface plasmon resonance. Rev Med Virol 14:123-35.

48. Almeida J, Cinader B, Howatson A. 1963. The Structure of Antigen-Antibody Complexes. A Study by Electron Microscopy. J Exp Med 118:327-40.

49. Rossman JS, Leser GP, Lamb RA. 2012. Filamentous influenza virus enters cells via macropinocytosis. J Virol 86:10950-60.

50. de Vries E, Tscherne DM, Wienholts MJ, Cobos-Jimenez V, Scholte F, Garcia-Sastre A, Rottier PJ, de Haan CA. 2011. Dissection of the influenza A virus endocytic routes reveals macropinocytosis as an alternative entry pathway. PLoS Pathog 7:e1001329.

51. Wallis C, Melnick JL. 1967. Virus aggregation as the cause of the non-neutralizable persistant fraction. Journal of Virology 1:478-488.

52. Madel B. 1978. Neutralization of animal viruses. Advances in Virus Research 23:205-268.

53. Mullarkey CE, Bailey MJ, Golubeva DA, Tan GS, Nachbagauer R, He W, Novakowski KE, Bowdish DM, Miller MS, Palese P. 2016. Broadly Neutralizing Hemagglutinin Stalk-Specific Antibodies Induce Potent Phagocytosis of Immune Complexes by Neutrophils in an Fc-Dependent Manner. MBio 7.

54. DiLillo DJ, Tan GS, Palese P, Ravetch JV. 2014. Broadly neutralizing hemagglutinin stalk-specific antibodies require FcgammaR interactions for protection against influenza virus in vivo. Nat Med 20:143-51.

55. Thomas AA, Vrijsen R, Boeyé A. 1986. Relationship between poliovirus neutralization and aggregation. Journal of Virology 59:479-485.

56. Smith TJ, Mosser AG, Baker TA. 1995. Structural studies of the mechanisms of antibody-mediated neutralization of human rhinovirus. Virology 6:233-242.

57. Stieh DJ, King DF, Klein K, Liu P, Shen X, Hwang KK, Ferrari G, Montefiori DC, Haynes B, Pitisuttithum P, Kaewkungwal J, Nitayaphan S, Rerks-Ngarm S, Michael NL, Robb ML, Kim JH, Denny TN, Tomaras GD, Shattock RJ. 2014. Aggregate complexes of HIV-1 induced by multimeric antibodies. Retrovirology 11.

58. White JM, Delos SE, Brecher M, Schornberg K. 2008. Structures and mechanisms of viral membrane fusion proteins: multiple variations on a common theme. Crit Rev Biochem Mol Biol 43:189-219.

59. Wasilewski S, Calder LJ, Grant T, Rosenthal P. 2012. Distribution of surface glycoproteins on influenza A virus determined by electron cryotomography. Vaccine 30:7368-7373.

Chapter 3. Infant-derived neutralizing antibody targets HIV-1 envelope at conserved glycans using significant variable light chain contacts

*The following chapter was conducted in collaboration with the lab of Julie Overbaugh at Fred Hutchinson Cancer Research Institute, Seattle, WA

3.1 Introduction

An effective vaccine against HIV-1 will require elicitation of broadly neutralizing antibodies (bnAbs) capable of blocking entry of a range of antigenically diverse HIV-1 isolates. The entry of HIV-1 into host immune cells is facilitated by the HIV-1 envelope glycoprotein (Env), which is a heavily glycosylated trimer composed of three identical copies of non-covalently associated heterodimers. Each heterodimer consists of a receptor binding domain, gp120, which recognizes CD4 receptors on the surface of T-cells, and a fusion subunit, gp41, that mediates fusion of the viral and host membrane (1-4). Furthermore, Env is the sole virally encoded antigen on the surface of the virus and the major target of neutralizing antibodies.

Once infected with HIV-1, a majority of individuals develop antibodies capable of binding Env; however, only a fraction of those antibodies is able to block viral entry and often only target the infecting strain (5-7). Immune pressure generated by this early response drives the evolution of HIV-1, which results in the emergence of resistant HIV-1 isolates (8-10). Studies of chronically infected adults have revealed that a subset of individuals are able to develop broadly neutralizing antibodies (bnAbs) that potently neutralize a range of HIV-1 isolates, and successful isolation of such antibodies has inspired efforts towards characterizing the interactions between Env and bnAbs (11-13). Improved methods in single-particle cryo-electron microscopy have resulted in numerous high resolution structures that have identified neutralization sensitive epitopes targeted by bnAbs, namely the V1/V2 apex, V3-glycan, CD4 binding site, gp120-gp41 interface, and the membrane-proximal external region (14-19). Identifying these sites of vulnerability provide optimism that a suitable immunogen can be designed to elicit a similar response; however, eliciting a bnAb response by immunization is complicated by the unusual properties of adult-derived HIV-1 bnAbs that reflect long-term affinity maturation including extensive somatic hypermutation (SHM) and rare

insertions and deletions (indels). Both SHM and indels are suggested to be important for neutralization breadth (20-23).

Until recently, the ability of HIV-1 infected infants to elicit a neutralizing antibody response against the virus has been unknown. It has now been observed that antibody responses generated in HIV-1-infected infants potently neutralize a diverse panel of HIV-1 isolates and target similar epitopes on the Env glycoprotein as in adults (24, 25). BF520.1 is a bnAb isolated from a HIV-1 infected infant that contributed to plasma breadth within the first year of infection (26). The infant's unique ability to generate a rapid response may suggest that bnAbs responsible for breadth have distinct features relative to adult HIV-1-specific bnAbs such as lower somatic hypermutation. Indeed, BF520.1 developed rapidly, exhibited low levels of SHM (6%) and neutralized 58% of isolates tested. While adult HIV-1 bnAbs have been extensively characterized, high resolution information of the interactions between infant bnAbs and the epitope targeted on Env is not known (24).

This chapter is focused on the providing the first structural study of infant derived HIV-1 bnAb, BF520.1, in complex with a soluble envelope construct. Single-particle electron microscopy supports studies suggesting that infant-derived antibodies target similar epitopes as adult-derived bnAbs. BF520.1, in particular, targets the V3-glycan supersite, which is a highly immunogenic epitope commonly targeted by bnAbs in adults. While many functional studies focus on the contribution of the variable heavy chain (VH) on heterologous neutralization, we find that light chain variable loops, namely CDRL1 plays a significant role in broad neutralization by BF520.1. While the CDRH3 loop may contribute to binding, the lack of mutations suggests a minor role in neutralization. Overall, the identification of a rapidly developed, infant bnAb with low SHM is encouraging for vaccine development and immunization strategies that aim to elicit bnAbs without the requirement for a long-term maturation pathway.

3.2 Materials and Methods

3.2.1 SOSIP production and purification

The most promising native-like (NL) structures have been obtained by engineering trimer-stabilizing mutations, termed SOSIP, into truncated Env sequences (1). BG505.SOSIP.T332N trimers were synthesized using a previously established protocol (2). In brief, following production in 293F cells, soluble

envelope oligomers were separated from the extracellular milieu using Galanthus nivalis lectin (Vector Labs). This mixture was then subjected to DEAE cation exchange chromatography, and trimer was resolved from aberrantly disulfide-bonded dimer and gp140 monomer, using hydrophobic interaction chromatography and preparative-grade size-exclusion chromatography. Purity was assessed by SDS-PAGE, BN-PAGE, and dynamic light scattering, and found to be >95% native-like trimer. Presence of native-like SOSIP trimer was further confirmed by negative-stain electron microscopy.

3.2.2 Fab preparation

Fab fragments were generated from 2.0 mg of IgG antibody using a papain digestion kit (Pierce). The Fab fragments were separated from Fc fragments and undigested IgG by gravity flow using a Protein A column (Pierce). Purity and size of Fab fragments was confirmed by SDS-PAGE.

3.2.3 Negative-stain electron microscopy epitope mapping

A 3-ml aliquot of BG505.W6.C2.T332N-BF520.1 complex, diluted to 20 μg/ml in PBS, was applied for 60 s to glow discharged C-Flat, 300 mesh, Cu grids (Electron Microscopy Sciences) and stained for an additional 60 s using Nano-W (Nanoprobes). Data were collected using a FEI Tecnai T12 transmission electron microscope operating at 120 keV. Images were taken using a Gatan 4 k × 4 k charge-coupled device (CCD) at a magnification of 52,000× and defocus range of 0.5–3.0 μm corresponding to a pixel size of 2.07 Å. Single-particle reconstruction was performed using EMAN2.1 image processing suite (3). In short, particles were selected using interactive particle picking from 392 micrographs. A 2× binned, phase-flipped, CTF-corrected stack of 35,914 particles were created and subjected to reference free 2D classification and clustering to generate 200 2D classes. Classes containing free BF520.1-Fab or sub-stoichiometric populations were omitted, and the remaining 26,013 particles were reclassified to generate 150 2D classes. Again, classes containing sub-stoichiometric and free BF520.1-Fab populations were removed, and a 2× binned particle stack containing 18,325 particles was used for 3D refinement using the coordinates from the PDB: 5ACO cryo-EM structure of BG505 SOSIP.664 HIV-1 Env trimer bound by PGT128 Fab (4). The model was low-pass filtered to 60 Å and used as an initial model for refinement with C3 symmetry imposed. Notably, the 5ACO coordinates only include the Fv and not the constant region of the PGT128 Fab; thus, the density we observe for the complete Fab emerged in the course of the reconstruction. The BG505

SOSIP-664 HIV-1 trimer (PDB: 4ZMJ) (5) and PGT128-Fab crystal structure (PDB: 3TV3) (6) were docked into the negative-stained 3D map using UCSF Chimera package from the Computer Graphics Laboratory, University of California, San Francisco (7).

3.2.4 Sample preparation for cryo-electron microscopy

Purified BG505.SOSIP.T332N trimers were mixed with 4-fold molar excess BF520.1 Fab and diluted to 0.4 mg/mL in PBS or PBS supplemented with 70 μM n-Dodecyl--D-Maltoside (DDM). The mixture incubated for 1 h at room temperature prior to vitrification. A 3.0 μL aliquot was applied at 4ºC and 100% humidity to glow-discharged C-Flat 1.2/1.3 4C holey carbon-coated grids (Electron Microscopy Sciences), blotted, and immediately plunge frozen in liquid ethane using a Vitrobot Mark IV specimen preparation unit (FEI Co.).

3.2.5 Cryo-EM data collection

Vitrified grids were imaged using an FEI Titan Krios operating at 300 keV and equipped with a Gatan K2 summit direct detector device. Micrographs were collected at 130,000×, corresponding to a pixel size of 0.55 Å/pixel in super resolution mode. Each image received a dose rate of ~ 8 e^-/pix/s with 200 ms exposure per frame and an estimated defocus ranging from 1.0 - 3.5 μm. Data were collected in three separate sessions, resulting in a total of 3454 images using EPU (908 micrographs) (FEI) software and Leginon (2546 micrographs) automated data collection software (8).

3.2.6 Cryo-EM data processing

Frame alignment and CTF estimation were carried out independently for data collected using EPU and data collected using Leginon software. Frame alignment and dose-weighting were completed using MotionCor2 (9), and CTF estimation was performed using CTFFIND4 (10). Relion 2.1 (11) was utilized for further processing and 3D refinement. Approximately 1,000 particles were manually selected and subjected to 2D classification to build templates for automated particle picking. A total of 559,022 particles was selected and binned to 8.8 Å/pixel for expeditious processing. The binned particle stack was subjected to 2D classification where 116,972 were selected for 3D refinement. This particle stack was re-extracted as a 4× binned stack (pixel size 2.2 Å/pix). Approximately 32,000 particles were chosen for 3D classification and

a subset of ~9,000 particles was selected to build a low-resolution 3D model, resulting in a 9.02 Å map. This model was low-pass filtered to 60 Å, and refinement was performed on the full stack of 116,972 particles in Relion 2.1 with C3 symmetry imposed. Map sharpening and post processing in Relion yielded a 4.8 Å structure using the "gold-standard" FSC cutoff of 0.143.

3.2.7 Model Building

The atomic model was generated by first fitting the BG505.SOSIP.T332N trimer from the BG505:PGT128 cryo-EM structure (PDB ID: 5ACO) with glycans temporarily removed into the generated 4.8 Å map using the fitmap command in UCSF Chimera (7). Overall, docking of the BG505 structure showed a good quality fit, resulting in a correlation score of 0.8602. No further modification to the protein structure was performed. Both glycans at positions N332 and N301 were manually placed into their corresponding densities in the 4.8 Å map.

The BF520.1 variable heavy and light chains were submitted as a single polypeptide sequence to MUlti-Sources ThreadER (MUSTER) Online to predict the structure of BF520.1(12). The structure template used for structure determination was a single chain variant of anti-gp120 antibody, b12 (PDB ID:3JUY) (13). Using Chimera's fitmap command, the BG505.SOSIP.T332N trimer and the BF520.1 variable domain were sequentially docked into the 4.8 Å map.

3.3 Results

3.3.1 Epitope specificity of BF520.1

During the course of our study, collaborators determined that infant cross-clade bnAb, BF520.1, exhibits a similar neutralization profile to the PGT-class of bnAbs, which are adult-derived antibodies targeting the N332 glycan in variable loop 3 region (V3) (Figure 1) (14-16). This observation prompted examination on the effect of the N332 glycan on BF520.1 neutralization that revealed that removal of the N332 glycan disrupted the neutralization for two viruses tested (93- and 5-fold increase in IC_{50}) (Figure 2A and B). A similar observation was detected for a prototype N332-directed bnAb, PGT128 (32-and 17-fold increase IC_{50}). Addition of the N332 glycan to an infant, clade A heterologous virus BG505.W6.C2 resulted in increased neutralization sensitivity (17-fold decrease IC_{50}) (17). These data suggest that BF520.1 likely

targets a similar site on Env as N332-dependent adult nAbs such as 2G12 and the PGT class of adult bnAbs (6, 15, 18, 19).

Single-particle negative-stain electron microscopy (EM) analysis of Fab from the BF520.1 bnAb complexed with BG505.SOSIP.T332N trimers, which encodes N332 and is structurally similar to Env on virus particles, confirmed that the antibody targets the base of the V3 loop (Figure 2C) (1). BF520.1 and PGT128 appear to dock to the trimer at the base of V3 with an overlapping footprint and to be oriented relative to the trimer with a similar angle of approach (4, 6). The BF520.1 Fab, however, is slightly twisted and docked more closely to the gp120 core than PGT128 (Figure 3.3).

3.3.2 Increasing heterologous neutralization by the maturing BF520.1 heavy chain

The ontogeny of BF520.1 was determined by collaborators using next generation sequencing (NGS) of the infant's B cell repertoire on an available post-infection sample. Using two replicates of the NGS data, the most probable routes of development for the BF520.1 variable heavy chain (VK) and variable light chain (VK) were selected, and lineage intermediates were synthesized for further study. The synthesized antibodies were tested for HIV neutralizing activity against a panel of heterologous viruses that were selected from both the original virus panel used to describe infant plasma neutralization breadth (20) and the standardized "global panel" (21) based on their ability to be neutralized by the mature BF520.1 antibody with an IC_{50} <20 μg ml^{-1} (16). The inferred naïve mAb derived by pairing the inferred naïve VH and VK did not demonstrate neutralizing activity against any virus tested (Figure 3.4A). To identify the VH substitutions that were important for neutralization breadth, the naïve VH and VH lineage intermediates (Int1-6_{VH}) were paired with the mature VK and tested for neutralizing activity. In contrast to the lack of neutralization by the naïve mAb, the naïve VH paired with the mature VK (naïve$_{VH}$mature$_{VK}$) demonstrated cross-clade tier 2 neutralizing activity (Figure 3.4A). The Int1$_{VH}$mature$_{VK}$ mAb had comparable activity to the naïve$_{VH}$mature$_{VK}$ mAb, suggesting that the CDRH2 G57D substitution in this Int1$_{VH}$ did not confer increased neutralizing activity (Figure 3.4 A and B). Increased neutralization breadth was observed for Int2$_{VH,}$ specifically by a Y32N substitution, and further cross-clade breadth and potency was observed in Int3$_{VH}$ with FR2 M34I and CDRH3 F114L substitutions (Figure 3.4 A and B). Addition of N52A in the CDRH2 of Int4$_{VH}$, gained breadth and potency comparable to the mature mAb BF520.1 (Figure 3.4 A and B). Overall, these data demonstrate

increasing heterologous neutralizing activity along the maturation pathway, and show that the heavy chain CDRH1 Y32N and CDHR2 N52A substitutions are important for the neutralization breadth of the mature BF520.1.

3.3.3 Contribution of kappa light chain maturation towards HIV neutralization breadth

Given the surprising finding that the naïve VH paired with the mature VK ($naïve_{VH}mature_{VK}$) demonstrated cross-clade tier 2 HIV neutralizing activity and the naïve mAb did not (Figure 3.4 A), collaborators examined the evolution of VK in relation to neutralization breadth. In contrast to the heterologous neutralizing activity seen for the $naïve_{VH}mature_{VK}$ mAb, the $mature_{VH}naïve_{VK}$ mAb neutralized only tier 1A SF162 variant, but not tier 2 viruses, suggesting that maturation in VK is necessary for BF520.1 heterologous neutralization breadth (Figure 3.5 A).

To identify which mutations in VK contributed to increased neutralizing activity, VK lineage intermediates ($Int1\text{-}7_{VK}$) were paired with the mature VH and tested for cross-clade tier 2 neutralizing activity. Overall, VK lineage intermediates demonstrated increasing breadth with maturation (Figure 3.5 A and B). A dramatic jump in neutralization breadth was demonstrated by $Int2_{VK}$, which contains CDRL1 S30A and FR3 S67F substitutions. A further increase in potency and breadth was also observed by substitutions in $Int3_{VK}$ (CDRL1 S28N and CDRL2 T53S). Importantly, $Int5_{VK}$ (CDRL1 S31Y and CDRL2 G50E) neutralized all viruses that were neutralized by BF520.1 and $Int6_{VK}$ (FR2 L33F) reached comparable potency as the mature antibody (Figure 3.5 A and B). In contrast to CDRL1, the BF520.1 VK does not contain CDRL3 mutations based on the inferred naïve sequence, which suggest that kappa chain mutations in and around the CDRL1 are important for BF520.1 heterologous neutralization breadth.

3.3.4 Cryo-EM structure of the BG505.SOSIP trimer in complex with BF520.1 Fab

Single particle cryo-electron microscopy was used to gain structural insight into the interaction of BF520.1 Fab and BG505.SOSIP trimer, which is a clade A transmitted envelope variant from a Kenyan infant, who was in the same cohort as BF520 (17, 22). The resulting 4.8 Å map (Figure 3.6 and Figure 3.7) revealed features consistent with the resolution estimate including helices, beta-sheet structure as well as bulky densities for glycans that protrude from glycosylation sites, including N332 and N301, which are critical features for BF520.1 activity (Figure 3.7).

The positioning of the CDRH loops in our structural model indicates that they make multiple contacts with both protein and N-linked glycans (Figure 3.6 B). The CDRH1 loop is in close proximity to the base of the gp120 V3-loop, with N32 oriented towards the conserved GDIR sequence, consistent with increased neutralization observed when asparagine is introduced at position 32 on the CDRH1 loop (Y32N substitution). Adjacent residues of CDRH1 as well as the CDRH2 loop are located proximal to the N301 glycan. It is unclear if residue 52 (N52A substitution) in CDRH2 mediates direct contact between either the GDIR sequence or N301 glycan; however, it is plausible that substitution for alanine could influence loop positioning such that residues H54 and S55 would interact with the N301 glycan. The relative orientation of the CDRH3 loop suggests it may interact with the V3 GDIR sequence as well as the N332 glycan, though given variability in CDRH3 positioning between homology models, the contacts are less certain for this loop.

The structure of the Env trimer in complex with BF520.1 supports a role for the BF520.1 VK in neutralization through extensive contacts between the CDRL1 loop and the N332 glycan. Based upon the BF520.1 homology model, N28, A30, and Y31, which were implicated in nAb breadth are positioned directly adjacent to the N332 glycan (Figure 3.6 C), although we cannot unambiguously identify the position of specific residues. L33F and G50E mutations contributed to increased potency, but from the structure, it is unclear whether these residues could directly contact the N332 glycan or protein surface (23, 24); they may instead alter local paratope structure in a more indirect fashion. The position of CDRL3 loop suggests it likely does not interact with the BG505 trimer or key glycans, which may explain why it does not contain mutations that contribute to BF520.1 breadth.

3.4 Discussion

The V3 loop region is centered around the conserved N332 glycan, contains highly immunogenic features, and plays an essential role in HIV-1 infectivity. Indeed, antibodies against the V3-region are induced in majority of human subjects following HIV infection or after vaccination with HIV gp120 vaccines, and many are capable of blocking entry (25-27). V3 targeting bnAbs isolated from additional HIV-1 infected donors can adopt a variety of Env-binding orientations and display a diverse set of interactions with surrounding glycans, including glycans at positions N301, and combinations of glycans at N137/N156/N301, and N386/N392 (18, 28). Common features for V3-targeting bnAbs are high degrees of somatic

hypermutation (SHM), and long CDRH3 loops that are suggested to penetrate the gp120 glycan shield to contact conserved peptide sequences at the base of V3, namely the ^{324}GDIR^{327} sequence (4, 6, 29).

While adult-derived bnAbs have been extensively characterized, bnAbs derived from HIV-1 infants have only recently been studied. BF520.1, which was isolated from an HIV-1 infected infant, developed more rapidly than adult V3-bnAbs, and achieved broad and potent capability with as little as 3.0% SHM (2.4% VH and 3.7% VK SHM). This is in contrast to known adult V3-glycan bnAbs, which required rare mutation events to occur (30, 31) and/or higher levels of SHM (32) compared to BF520.1 (33). Here, we have shown that BF520.1 targets the V3 region of HIV-1 Env similar to known adult bnAb PGT128. Initial epitope mapping revealed a similar binding orientation as PGT128, although slightly more twisted and more closely bound to the Env surface. Neutralization of HIV-1 isolates and related mutants lacking N332 further support a critical role of the N332 glycan in the epitope targeted by BF520.1.

Mutations important for increasing BF520.1 functional activity were primarily found in the heavy chain CDRH2 and light chain CDRL1, with little-to-no contribution from the CDRH3 and CDRL3. The cryo-EM structural model indicated that CDRH2 and CDRL1 residues appear to contribute to the BF520.1 paratope by mediating contacts with the conserved V3-glycan site, namely the archetypal features of V3-targeting bnAbs: GDIR sequence and glycans at position 301 and 332 (34). The Y32N substitution offered increased neutralization potency and the relative orientation of N32 in our structural model suggests interactions with the GDIR motif. The interactions of the alanine substitution at position 54 could not be confidently determined, but the exchange of a charged asparagine for alanine may affect the CDRL2 loop positioning and allow interactions between adjacent residues and the N301 glycan. In contrast to the position of CDRL3, located too distant to make meaningful contacts with the trimer, the structure suggests that CDRH3 may interact with both the V3 GDIR sequence and N332 glycan. This mode of binding by CDRH3 has been observed for the PGT-class of antibodies, namely PGT128.

The crystal structure of PGT128 in complex with gp120 identified the GDIR motif and glycans at positions N332 and N301 as the primary contacts defining the PGT128 epitope (35). The CDRH3 loop, which is highly mutated in PGT128, is suggested to penetrate the glycan shield in order to contact both the GDIR motif and N332 glycan. Our structural model similarly indicates potential CDRH3 contacts against

the GDIR motif and N332 glycan; however, it is unclear if the lack of mutations during maturation suggest a minor role in neutralization breadth or if the naïve CDRH3 sequence is optimally suited for binding.

With few exceptions (31), functional studies have largely focused on the contribution of VH to heterologous neutralizing activity (30, 32), despite previous structural studies showing that adult-derived V3-glycan bnAb light chains contact the N332 glycan and conserved GDIR motif (36, 37). For PGT128, less certainty exists about the contribution of the light chain, which is recessed relative to the heavy chain and has been suggested to either allow contacts with high mannose glycans at N137/N156, or to avoid making contacts altogether (35). In contrast, the slight rotation of BF520.1 relative to PGT128 places the CDRL1 loop in closer proximity to the N332 glycan. Each of the three substitutions in CDRL1 (N28, A30 and Y31) are situated to make meaningful contacts with N332, which supports increasing breadth and potency along the VK maturation pathway. Significant CDRL contacts are not unique to BF520.1 and have been observed in other V3 targeted antibody lineages such as PGT122, PGT124 and BG18 (37-39). For each of the three, the central feature of the epitope is contacts between CDRH3 and glycan N332, but it should be noted that the binding angle of these antibodies are substantially higher, which allows light chain contacts with additional glycans and the V1 loop region towards the trimer apex (37, 38). The PGT122 CDRL1 and L3 loops bind the GDIR motif while CDRL3 binds the N137 glycan in the V1 (39). The primary glycan targeted by PGT124 is the N332 glycan, which makes contacts using both CDRL2 and a long HCDR3 (37). In contrast, the BG18 light chain only contacts V1 (38). While each of these antibodies bind to their epitope, in part, using CDRL contacts, the major determinant of neutralization breadth has been focused on the extensively maturated CDRH loops, leaving the contribution of light chain development largely unexplored. Our data, combined with the molecular interactions described for several V3 targeted bnAbs further underscores the diversity in which different antibody lineages target a similar epitope and highlights the importance of considering both the heavy and light chain in the development of HIV-specific bnAbs.

			V3 glycan	Outer domain glycan	V3 glycans	CD4bs		V1/V2 glycans			gp120-gp41 interface	MPER	
		BF520 Plasma	**BF520.1**	**2G12**	**PGT121**	**b12**	**VRC01**	**PG16**	**PGT145**	**PGT151**	**4E10**	**2F5**	**10E8**
Clade A	398F1	527	0.47	>20	<0.02	2.4	0.44	>20	>20	<0.02	>20	4.76	0.81
Clade B	TRO11	175	4.92	2.75	0.03	>20	3.08	16	0.37	>20	6.74	>20	0.08
	X2278	183	1.19	2.14	<0.02	>20	0.63	<0.02	<0.02	2.21	>20	16.0	1.37
CRF07_BC	BJOX002000	159	0.62	>20	<0.02	>20	>20	<0.02	>20	<0.02	16.8	>20	1.37
	CH119	122	5.48	>20	<0.02	>20	7.15	10.3	2.94	>20	>20	>20	3.84
	CE1176	118	4.59	>20	<0.02	>20	17.8	<0.02	>20	<0.02	>20	>20	0.99
Clade C	CE0217	107	2.49	>20	<0.02	>20	1.68	<0.02	0.29	>20	12.9	>20	2.09
	25710	120	>20	>20	<0.02	>20	5.37	<0.02	<0.02	>20	4.98	>20	0.09
Clade G	X1632	116	>20	>20	>20	>20	0.35	0.26	2.24	>20	15.7	8.76	2.29
CRF01_AE	CNE55	113	>20	>20	>20	>20	2.2	17.3	<0.02	>20	>20	6.29	0.28
	CNE8	>100	>20	>20	>20	>20	3.86	3.16	1.29	>20	10.6	4.46	1.01
AC recomb	246F3	>100	>20	>20	>20	>20	1.44	<0.02	>20	8.56	>20	5.58	1.91
% Breadth		83	58	17	67	8	92	92	67	42	50	50	100
geometric mean IC_{50} (μg ml^{-1}) viruses neutralized			1.95	2.43	0.02	2.4	2.13	0.24	0.23	0.17	10.3	6.86	0.82
geometric mean IC_{50} (μg ml^{-1}) all viruses			5.14	14.1	0.35	16.8	2.57	0.35	1.01	2.76	14.4	11.7	0.82

Plasma IC_{50}

- IC_{50} >1000
- 500 ≤ IC_{50} < 1000
- 200 ≤ IC_{50} < 500
- 100 ≤ IC_{50} < 200
- IC_{50} < 100

mAb IC_{50} (μg ml^{-1})

- IC_{50} < 0.2
- 0.2 ≤ IC_{50} < 2
- 2 ≤ IC_{50} < 10
- 10 ≤ IC_{50} < 20
- IC_{50} >20

Figure 3.1: Neutralization by BF520.1 against a global panel of tier 2 viruses reveal similarities to adult bnAbs targeting V3 glycans. mAb IC_{50} values are an average of two to three independent experiments performed in duplicate. First-generation bnAbs are indicated in gray. This work was performed and kindly provided by Cassie Simonich at Fred Hutchinson Cancer Research Center, Seattle, WA. Figured adapted from (16).

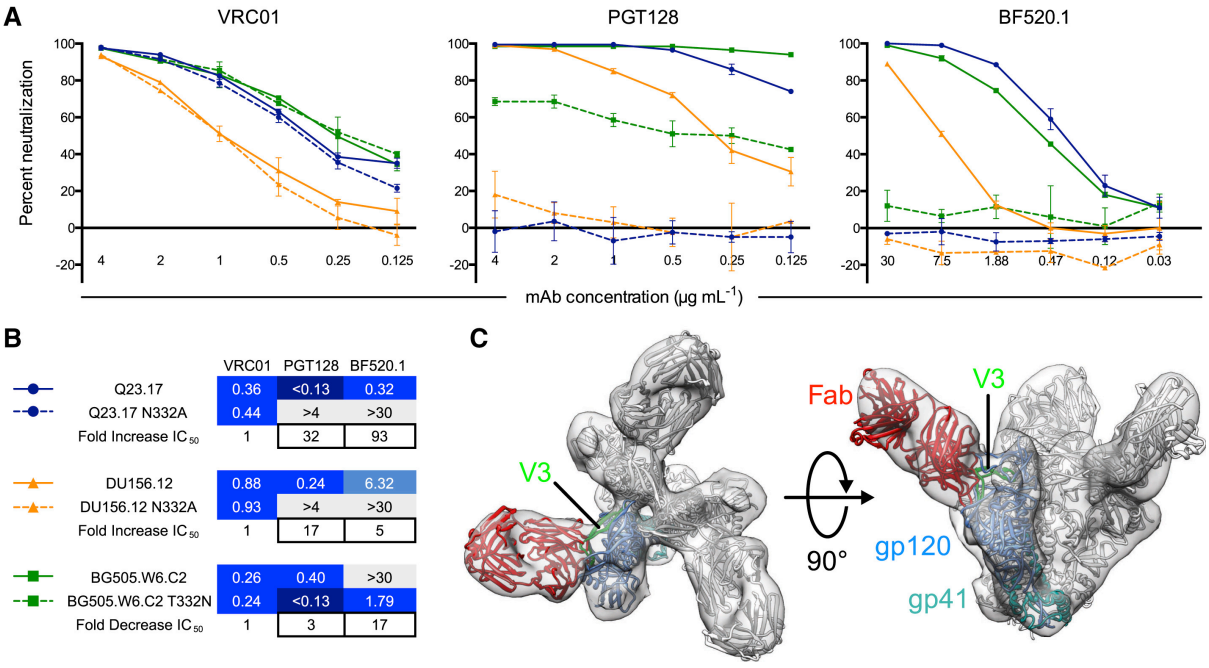

Figure 3.2 N332 glycan is important for binding and neutralization by BF520.1. **(A and B)** mAb neutralization of Q23.17 and DU156.12 wild-type viruses and relative mutant viruses lacking the N332 glycan, as well as BG505.W6.C2 and a mutant virus with N332 (T332N) suggest a role of glycans in binding by BF520.1. PGT128 and VRC01 are positive and negative controls, respectively. Viruses lacking N332 are indicated by dashed lines. **(C)** Negative-stain EM of the BG505.SOSIP.T332N trimer in complex with BF520.1 Fab indicates that the V3 region of HIV-1 Env is targeted by BF520.1. Neutralization data (Panel A and B) were performed and kindly provided by Cassie Simonich at Fred Hutchinson Cancer Research Center, Seattle, WA. Figure adapted from (16).

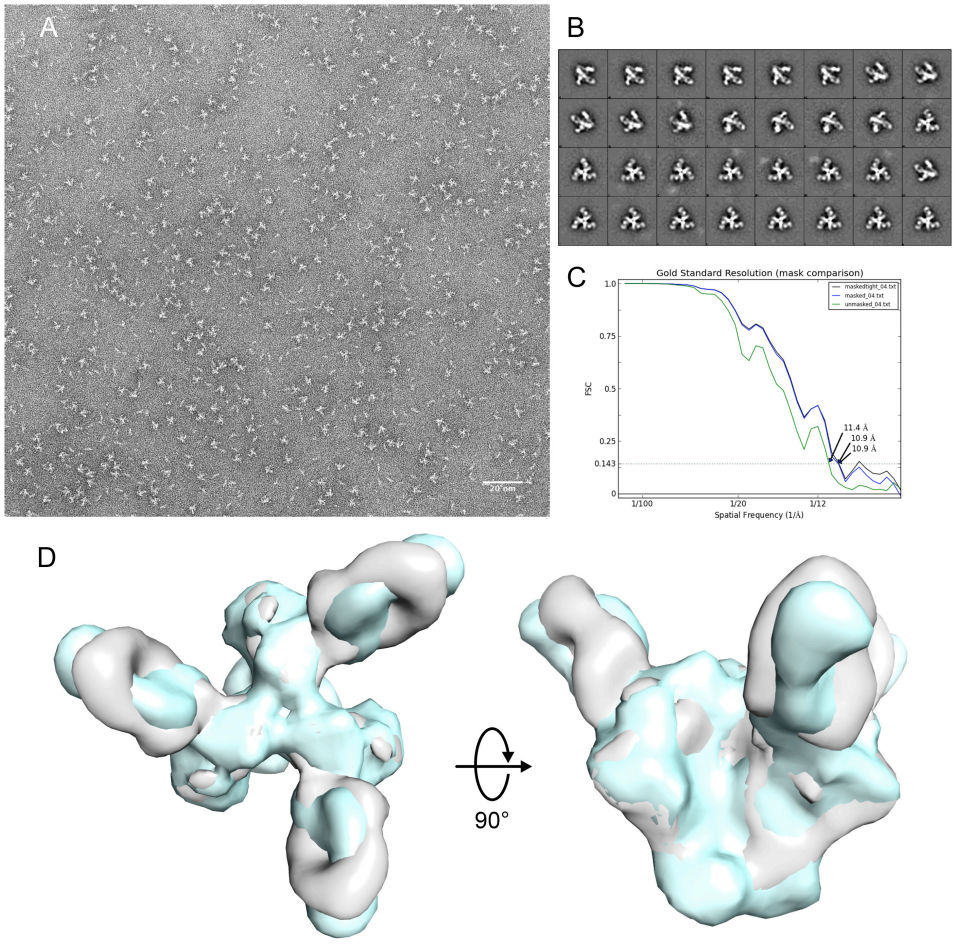

Figure 3.3: EM of BF520.1 Fab Complexed with BG505.SOSIP.T332N related to Figure 3.2 **(A)** Negative-stain image of BG505:BF520.1-Fab complex (scale bar = 20 nm). **(B)** Reference free 2D class averages showing both top and side views of BG505 SOSIP:BF520.1-Fab complex. **(C)** Fourier-shell correlation (FSC) curve for the BF520.1-BG505 SOSIP trimer negative-stain EM reconstruction obtained by 'gold standard' refinement in EMAN2.1. **(D)** Surface rendering of BG505 SOSIP:BF520.1-Fab negative-stain EM map, lowpass-filtered to 20 Å compared with BG505 SOSIP:PGT128 cryo-EM map (cyan; emd_3121), also low-pass filtered to 20 Å. While epitopes for both antibodies are similar, BF520.1 appears to bind at a slightly different angle of approach relative to PGT128.

A

Tier	Clade		VH / VK	BF520.1 lineage heavy chain intermediates								
			VH	naïve $_{VH}$	naïve $_{VH}$	Int1 $_{VH}$	Int2 $_{VH}$	Int3 $_{VH}$	Int4 $_{VH}$	Int5 $_{VH}$	Int6 $_{VH}$	mature $_{VH}$
			VK	naïve $_{VK}$	mature $_{VK}$							
1A	B	SF162		>20	0.7	0.6	<0.6	<0.6	<0.6	<0.6	<0.6	<0.6
1B		Q23.17		>20	1.1	2.2	0.9	<0.6	<0.6	<0.6	<0.6	<0.6
2	A	BG505.W6M.C2_T332		>20	>20	>20	7.0	3.1	1.7	1.0	1.3	1.1
		398F1		>20	5.5	4.9	3.7	1.3	0.6	<0.6	<0.6	<0.6
	B	X2278		>20	19.5	>20	3.8	2.3	1.2	0.7	0.9	1.0
		TRO.11		>20	>20	>20	>20	>20	6.5	4.8	7.9	5.9
	BC	BJOX002000		>20	>20	>20	15.8	3.4	1.0	0.8	1.3	0.9
		CH119		>20	>20	>20	>20	14.7	6.1	3.7	6.1	6.0
	C	CE1176		>20	17.0	17.9	13.5	8.7	6.1	5.6	7.0	5.1
		QC406.F3		>20	<0.6	0.7	<0.6	<0.6	<0.6	<0.6	<0.6	<0.6
		CE0217		>20	>20	>20	>20	12.3	2.1	2.1	4.4	2.8
		DU156.12		>20	>20	>20	16.9	9.8	2.0	1.8	2.3	2.2
		DU422.1		>20	5.7	12.9	3.2	4.4	2.2	1.4	2.9	2.6
		SIV		>20	>20	>20	>20	>20	>20	>20	>20	>20

B

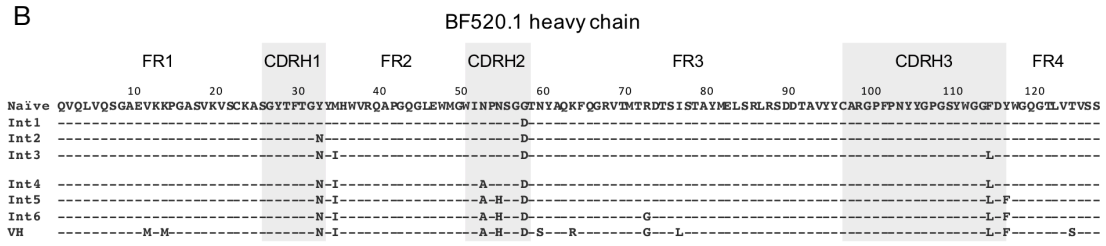

Figure 3.4: Neutralization of panel viruses by BF520.1 inferred VH lineage intermediates. **(A)** The top rows of the table (VH and VK) show the origin of the antibody chain sequence used indicated by Int#$_{VH}$. These were paired with the indicated kappa chain; in most cases, the mature kappa chain (mature$_{VK}$). The panel of viruses are shown to the left with the tier, clade and name indicated. IC_{50} values (μg ml^{-1}) represent an average of two to three independent experiments performed in duplicate. IC_{50} values are color-coded with darker shades, indicating more potent neutralization. Grey indicates that 50% neutralization was not achieved at the highest mAb concentration tested. **(B)** Amino acid alignment of BF520.1 naïve, inferred lineage intermediates, and mature heavy chain sequences. Data was collected and kindly provided by Cassie Simonich at Fred Hutchinson Cancer Research Center, Seattle, WA. Unpublished data.

A

BF520.1 lineage kappa chain intermediates

Tier	Clade	VH / VK	naïve VH / naïve VK	mature VH / naïve VK	Int1 VK	Int2 VK	Int3 VK	Int4 VK	Int5 VK	Int6 VK	Int7 VK	mature VK
1A	B	SF162	>20	1.1	0.9	<0.6	<0.6	<0.6	<0.6	<0.6	<0.6	<0.6
1B	A	Q23.17	>20	>20	>20	1.0	<0.6	0.7	0.7	<0.6	<0.6	<0.6
2	A	BG505.W6M.C2_T332	>20	>20	>20	18.7	3.2	2.2	1.6	1.0	1.3	1.1
		398F1	>20	>20	>20	10.3	1.7	1.5	1.0	0.7	<0.6	<0.6
	B	X2278	>20	>20	>20	11.7	2.5	1.4	1.1	0.9	0.9	1.0
		TRO.11	>20	>20	>20	>20	>20	>20	14.6	7.0	8.0	5.9
	BC	BJOX002000	>20	>20	>20	>20	5.7	3.5	1.6	0.8	1.1	0.9
		CH119	>20	>20	>20	>20	>20	18.3	8.8	5.2	4.5	6.0
	C	CE1176	>20	>20	>20	15.0	8.2	6.9	6.3	5.3	5.6	5.1
		QC406.F3	>20	>20	>20	1.1	<0.6	<0.6	<0.6	<0.6	<0.6	<0.6
		CE0217	>20	>20	>20	>20	>20	>20	6.4	3.1	4.7	2.8
		DU156.12	>20	>20	>20	>20	>20	15.7	3.7	0.9	2.1	2.2
		DU422.1	>20	>20	>20	11.0	5.1	5.4	5.2	3.9	4.3	2.6
		SIV	>20	>20	>20	>20	>20	>20	>20	>20	>20	>20

B

BF520.1 light chain

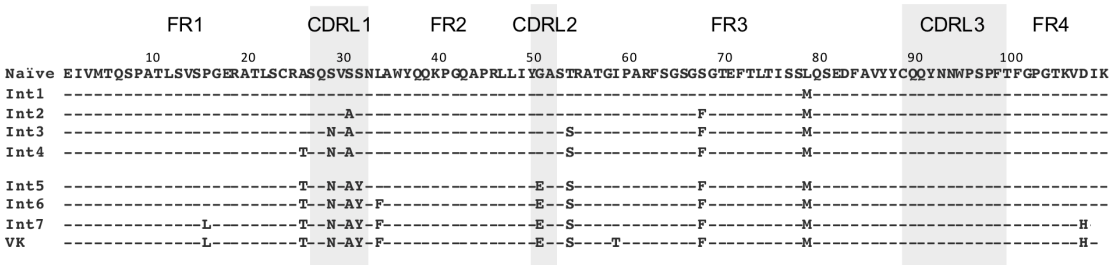

Figure 3.5: Neutralization of panel viruses by BF520.1 inferred VK lineage intermediates. **(A)** Layout is as described for Figure 3.3. **(B)** Amino acid alignment of BF520.1 naïve, inferred lineage intermediates and mature kappa chain sequences. Data was collected and kindly provided by Cassie Simonich at Fred Hutchinson Cancer Research Center, Seattle, WA. Unpublished data.

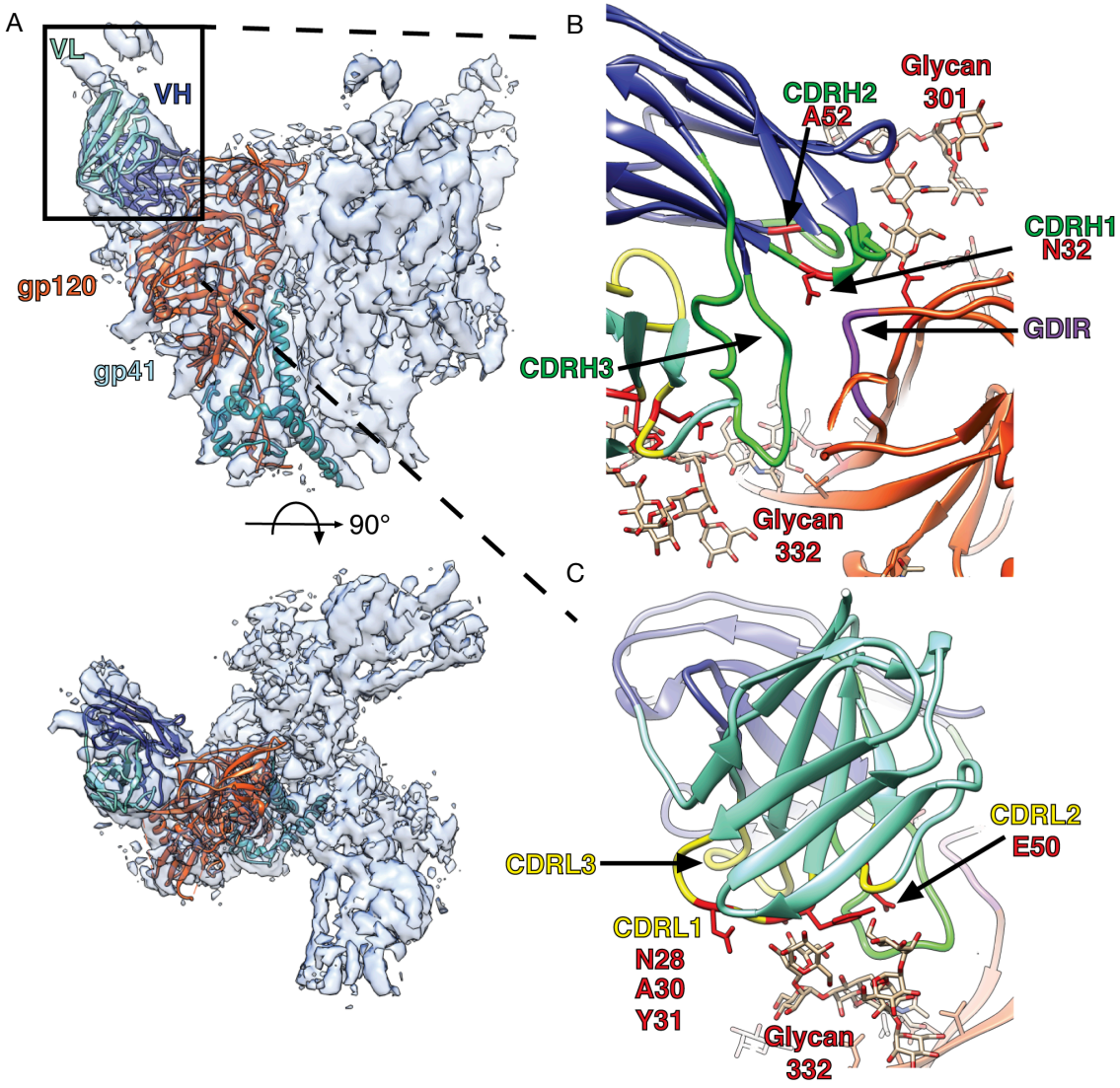

Figure 3.6: Cryo-EM reconstruction and model of the BG505.SOSIP.T332N trimer in complex with BF520.1 Fab. **(A)** Side (above) and top (below) views of the cryo-EM reconstruction and structural model. A single monomer consisting of gp120 (orange) and gp41 (dark cyan), and the BF520.1-Fv variable heavy chain (dark blue) and variable light chain (aquamarine) are highlighted. Glycans removed for clarity. The BG505.SOSIP trimer structure 5ACO.pdb docked into the new EM density map with a correlation score of 0.8602 (4). A global search yielded a preferred placement of the BF520.1 Fv model into the Fab density with a correlation score of 0.8513 (Supplementary Figure 5g). **(B)** Expanded view of the VH domain and gp120. Shown are the conserved gp120 GDIR sequence (purple), glycans N332 and N301, and CDRH

loops (green). Mutations that confer potent neutralization (red) are indicated. **(C)** Expanded view of the VL domain and the N332 glycan. CDRL loops (yellow) and mutations that conferred potent neutralization (red) are highlighted.

A

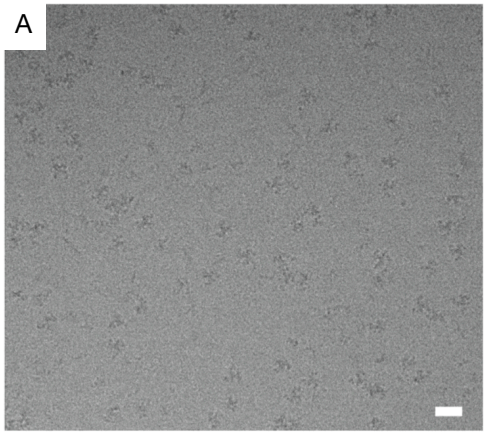

B

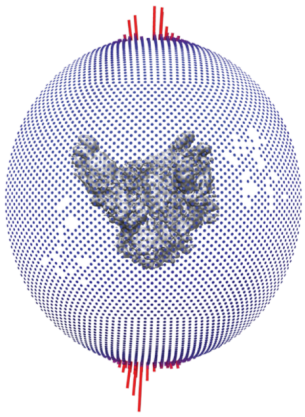

C

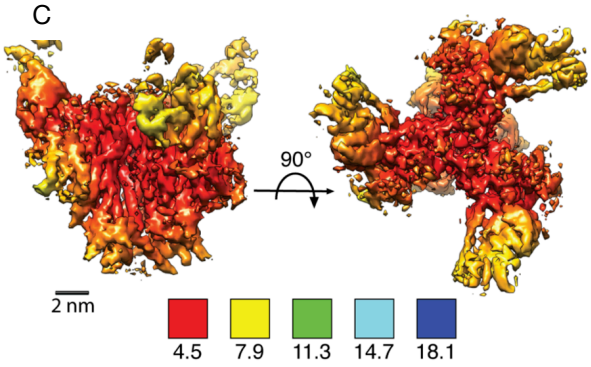

D

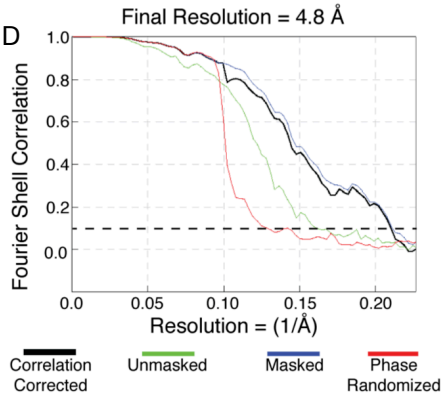

E

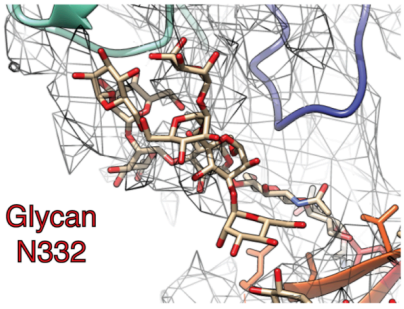

F

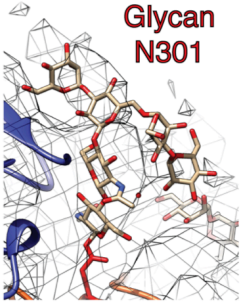

G

Fit	Molecule	Correlation
1	**BF520.1**	**0.8513**
2	BF520.1	0.6995
3	BF520.1	0.6991
4	BF520.1	0.6732

H

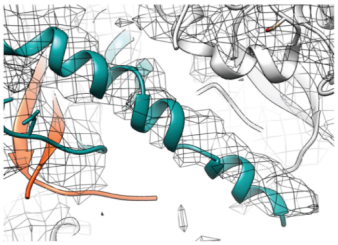

I

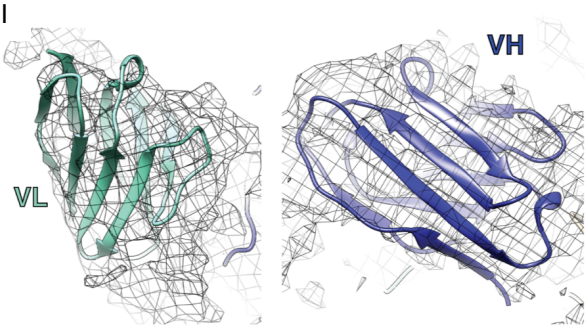

J

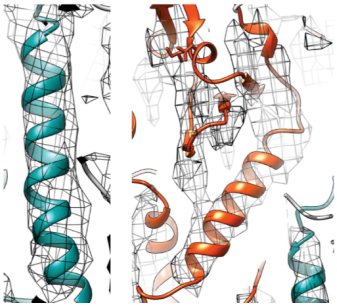

Figure 3.7: Data collection and refinement of BG505.SOSIP.T332N in complex with BF520.1 Fab. **(A)** A sample, frame aligned, micrograph illustrating particle density and distribution. **(B)** Angular distribution plot generated in Relion/2.1. **(C)** Local resolution analysis of the 4.8 Å cryo-EM reconstruction. The color key shown below indicates local resolution in Å. **(D)** Fourier-shell correlation curves for correlation corrected (black), unmasked (green), masked (blue) and phase randomized (red). Dashed line represents the "gold-standard" FSC cutoff of 0.143. **(E and F)** Densities corresponding to N332 and N301 glycans and positioning of glycans into the cryo-EM density. **(G)** Correlation scores of the top fits for the BF520.1 Fab structure into the cryo-EM map. Scores were generated by Chimera UCSF fitmap command utilizing a global search. **(H)** Positioning of gp41 HR2 α-helix into the cryo-EM density. **(I)** Best fit of BF520.1 homology model determined in **(H)**. Shown are the variable light chain (left) and variable heavy chain (right). **(J)** Positioning of the g41 HR1 α-helix (left) and the gp120 α1 helix into the cryo-EM density.

References

1. Sanders RW, Derking R, Cupo A, Julien JP, Yasmeen A, de Val N, Kim HJ, Blattner C, de la Pena AT, Korzun J, Golabek M, de Los Reyes K, Ketas TJ, van Gils MJ, King CR, Wilson IA, Ward AB, Klasse PJ, Moore JP. 2013. A next-generation cleaved, soluble HIV-1 Env trimer, BG505 SOSIP.664 gp140, expresses multiple epitopes for broadly neutralizing but not non-neutralizing antibodies. PLoS Pathog 9:e1003618.

2. Verkerke HP, Williams JA, Guttman M, Simonich CA, Liang Y, Filipavicius M, Hu SL, Overbaugh J, Lee KK. 2016. Epitope-Independent Purification of Native-Like Envelope Trimers from Diverse HIV-1 Isolates. J Virol 90:9471-82.

3. Tang G, Peng L, Baldwin PR, Mann DS, Jiang W, Rees I, Ludtke SJ. 2007. EMAN2: an extensible image processing suite for electron microscopy. J Struct Biol 157:38-46.

4. Lee JH, de Val N, Lyumkis D, Ward AB. 2015. Model Building and Refinement of a Natively Glycosylated HIV-1 Env Protein by High-Resolution Cryoelectron Microscopy. Structure 23:1943-1951.

5. Kwon YD, Pancera M, Acharya P, Georgiev IS, Crooks ET, Gorman J, Joyce MG, Guttman M, Ma X, Narpala S, Soto C, Terry DS, Yang Y, Zhou T, Ahlsen G, Bailer RT, Chambers M, Chuang GY, Doria-Rose NA, Druz A, Hallen MA, Harned A, Kirys T, Louder MK, O'Dell S, Ofek G, Osawa K, Prabhakaran M, Sastry M, Stewart-Jones GB, Stuckey J, Thomas PV, Tittley T, Williams C, Zhang B, Zhao H, Zhou Z, Donald BR, Lee LK, Zolla-Pazner S, Baxa U, Schon A, Freire E, Shapiro L, Lee KK, Arthos J, Munro JB, Blanchard SC, Mothes W, Binley JM, et al. 2015. Crystal structure, conformational fixation and entry-related interactions of mature ligand-free HIV-1 Env. Nat Struct Mol Biol 22:522-31.

6. Pejchal R, Doores KJ, Walker LM, Khayat R, Huang PS, Wang SK, Stanfield RL, Julien JP, Ramos A, Crispin M, Depetris R, Katpally U, Marozsan A, Cupo A, Maloveste S, Liu Y, McBride R, Ito Y, Sanders RW, Ogohara C, Paulson JC, Feizi T, Scanlan CN, Wong CH, Moore JP, Olson WC, Ward AB, Poignard P, Schief WR, Burton DR, Wilson IA. 2011. A potent and broad neutralizing antibody recognizes and penetrates the HIV glycan shield. Science 334:1097-103.

7. Pettersen EF, Goddard TD, Huang CC, Couch GS, Greenblatt DM, Meng EC, Ferrin TE. 2004. UCSF Chimera--a visualization system for exploratory research and analysis. J Comput Chem 25:1605-12.

8. Suloway C, Shi J, Cheng A, Pulokas J, Carragher B, Potter CS, Zheng SQ, Agard DA, Jensen GJ. 2009. Fully automated, sequential tilt-series acquisition with Leginon. J Struct Biol 167:11-8.

9. Zheng SQ, Palovcak E, Armache JP, Verba KA, Cheng Y, Agard DA. 2017. MotionCor2: anisotropic correction of beam-induced motion for improved cryo-electron microscopy. Nat Methods 14:331-332.

10. Rohou A, Grigorieff N. 2015. CTFFIND4: Fast and accurate defocus estimation from electron micrographs. J Struct Biol 192:216-21.

11. Scheres SH. 2012. RELION: implementation of a Bayesian approach to cryo-EM structure determination. J Struct Biol 180:519-30.

12. Wu S, Zhang Y. 2008. MUSTER: Improving protein sequence profile-profile alignments by using multiple sources of structure information. Proteins 72:547-56.

13. Clark KR, Walsh ST. 2009. Crystal structure of a 3B3 variant--a broadly neutralizing HIV-1 scFv antibody. Protein Sci 18:2429-41.

14. Goo L, Jalalian-Lechak Z, Richardson BA, Overbaugh J. 2012. A combination of broadly neutralizing HIV-1 monoclonal antibodies targeting distinct epitopes effectively neutralizes variants found in early infection. J Virol 86:10857-61.

15. Walker LM, Huber M, Doores KJ, Falkowska E, Pejchal R, Julien JP, Wang SK, Ramos A, Chan-Hui PY, Moyle M, Mitcham JL, Hammond PW, Olsen OA, Phung P, Fling S, Wong CH, Phogat S,

Wrin T, Simek MD, Principal Investigators PG, Koff WC, Wilson IA, Burton DR, Poignard P. 2011. Broad neutralization coverage of HIV by multiple highly potent antibodies. Nature 477:466-70.

16. Simonich CA, Williams KL, Verkerke HP, Williams JA, Nduati R, Lee KK, Overbaugh J. 2016. HIV-1 Neutralizing Antibodies with Limited Hypermutation from an Infant. Cell 166:77-87.

17. Wu X, Parast AB, Richardson BA, Nduati R, John-Stewart G, Mbori-Ngacha D, Rainwater SM, Overbaugh J. 2006. Neutralization escape variants of human immunodeficiency virus type 1 are transmitted from mother to infant. J Virol 80:835-44.

18. Kong L, Lee JH, Doores KJ, Murin CD, Julien JP, McBride R, Liu Y, Marozsan A, Cupo A, Klasse PJ, Hoffenberg S, Caulfield M, King CR, Hua Y, Le KM, Khayat R, Deller MC, Clayton T, Tien H, Feizi T, Sanders RW, Paulson JC, Moore JP, Stanfield RL, Burton DR, Ward AB, Wilson IA. 2013. Supersite of immune vulnerability on the glycosylated face of HIV-1 envelope glycoprotein gp120. Nat Struct Mol Biol 20:796-803.

19. Mouquet H, Scharf L, Euler Z, Liu Y, Eden C, Scheid JF, Halper-Stromberg A, Gnanapragasam PN, Spencer DI, Seaman MS, Schuitemaker H, Feizi T, Nussenzweig MC, Bjorkman PJ. 2012. Complex-type N-glycan recognition by potent broadly neutralizing HIV antibodies. Proc Natl Acad Sci U S A 109:E3268-77.

20. Goo L, Chohan V, Nduati R, Overbaugh J. 2014. Early development of broadly neutralizing antibodies in HIV-1-infected infants. Nat Med 20:655-8.

21. deCamp A, Hraber P, Bailer RT, Seaman MS, Ochsenbauer C, Kappes J, Gottardo R, Edlefsen P, Self S, Tang H, Greene K, Gao H, Daniell X, Sarzotti-Kelsoe M, Gorny MK, Zolla-Pazner S, LaBranche CC, Mascola JR, Korber BT, Montefiori DC. 2014. Global panel of HIV-1 Env reference strains for standardized assessments of vaccine-elicited neutralizing antibodies. J Virol 88:2489-507.

22. Nduati R, John G, Mbori-Ngacha D, Richardson B, Overbaugh J, Mwatha A, Ndinya-Achola J, Bwayo J, Onyango FE, Hughes J, Kreiss J. 2000. Effect of breastfeeding and formula feeding on transmission of HIV-1: a randomized clinical trial. JAMA 283:1167-74.

23. Klein F, Diskin R, Scheid JF, Gaebler C, Mouquet H, Georgiev IS, Pancera M, Zhou T, Incesu RB, Fu BZ, Gnanapragasam PN, Oliveira TY, Seaman MS, Kwong PD, Bjorkman PJ, Nussenzweig MC. 2013. Somatic mutations of the immunoglobulin framework are generally required for broad and potent HIV-1 neutralization. Cell 153:126-38.

24. Ovchinnikov V, Louveau JE, Barton JP, Karplus M, Chakraborty AK. 2018. Role of framework mutations and antibody flexibility in the evolution of broadly neutralizing antibodies. Elife 7.

25. Carrow EW, Vujcic LK, Glass WL, Seamon KB, Rastogi SC, Hendry RM, Boulos R, Nzila N, Quinnan GV, Jr. 1991. High prevalence of antibodies to the gp120 V3 region principal neutralizing determinant of HIV-1MN in sera from Africa and the Americas. AIDS Res Hum Retroviruses 7:831-8.

26. Gottardo R, Bailer RT, Korber BT, Gnanakaran S, Phillips J, Shen X, Tomaras GD, Turk E, Imholte G, Eckler L, Wenschuh H, Zerweck J, Greene K, Gao H, Berman PW, Francis D, Sinangil F, Lee C, Nitayaphan S, Rerks-Ngarm S, Kaewkungwal J, Pitisuttithum P, Tartaglia J, Robb ML, Michael NL, Kim JH, Zolla-Pazner S, Haynes BF, Mascola JR, Self S, Gilbert P, Montefiori DC. 2013. Plasma IgG to linear epitopes in the V2 and V3 regions of HIV-1 gp120 correlate with a reduced risk of infection in the RV144 vaccine efficacy trial. PLoS One 8:e75665.

27. Zolla-Pazner S, Edlefsen PT, Rolland M, Kong XP, deCamp A, Gottardo R, Williams C, Tovanabutra S, Sharpe-Cohen S, Mullins JI, deSouza MS, Karasavvas N, Nitayaphan S, Rerks-Ngarm S, Pitisuttihum P, Kaewkungwal J, O'Connell RJ, Robb ML, Michael NL, Kim JH, Gilbert P. 2014. Vaccine-induced Human Antibodies Specific for the Third Variable Region of HIV-1 gp120 Impose Immune Pressure on Infecting Viruses. EBioMedicine 1:37-45.

28. Pancera M, Zhou T, Druz A, Georgiev IS, Soto C, Gorman J, Huang J, Acharya P, Chuang GY, Ofek G, Stewart-Jones GB, Stuckey J, Bailer RT, Joyce MG, Louder MK, Tumba N, Yang Y, Zhang

B, Cohen MS, Haynes BF, Mascola JR, Morris L, Munro JB, Blanchard SC, Mothes W, Connors M, Kwong PD. 2014. Structure and immune recognition of trimeric pre-fusion HIV-1 Env. Nature 514:455-61.

29. Sok D, Pauthner M, Briney B, Lee JH, Saye-Francisco KL, Hsueh J, Ramos A, Le KM, Jones M, Jardine JG, Bastidas R, Sarkar A, Liang CH, Shivatare SS, Wu CY, Schief WR, Wong CH, Wilson IA, Ward AB, Zhu J, Poignard P, Burton DR. 2016. A Prominent Site of Antibody Vulnerability on HIV Envelope Incorporates a Motif Associated with CCR5 Binding and Its Camouflaging Glycans. Immunity 45:31-45.

30. Bonsignori M, Kreider EF, Fera D, Meyerhoff RR, Bradley T, Wiehe K, Alam SM, Aussedat B, Walkowicz WE, Hwang KK, Saunders KO, Zhang R, Gladden MA, Monroe A, Kumar A, Xia SM, Cooper M, Louder MK, McKee K, Bailer RT, Pier BW, Jette CA, Kelsoe G, Williams WB, Morris L, Kappes J, Wagh K, Kamanga G, Cohen MS, Hraber PT, Montefiori DC, Trama A, Liao HX, Kepler TB, Moody MA, Gao F, Danishefsky SJ, Mascola JR, Shaw GM, Hahn BH, Harrison SC, Korber BT, Haynes BF. 2017. Staged induction of HIV-1 glycan-dependent broadly neutralizing antibodies. Sci Transl Med 9.

31. Sok D, Laserson U, Laserson J, Liu Y, Vigneault F, Julien JP, Briney B, Ramos A, Saye KF, Le K, Mahan A, Wang S, Kardar M, Yaari G, Walker LM, Simen BB, St John EP, Chan-Hui PY, Swiderek K, Kleinstein SH, Alter G, Seaman MS, Chakraborty AK, Koller D, Wilson IA, Church GM, Burton DR, Poignard P. 2013. The effects of somatic hypermutation on neutralization and binding in the PGT121 family of broadly neutralizing HIV antibodies. PLoS Pathog 9:e1003754.

32. MacLeod DT, Choi NM, Briney B, Garces F, Ver LS, Landais E, Murrell B, Wrin T, Kilembe W, Liang CH, Ramos A, Bian CB, Wickramasinghe L, Kong L, Eren K, Wu CY, Wong CH, Investigators IPC, The IAHIVRN, Kosakovsky Pond SL, Wilson IA, Burton DR, Poignard P. 2016. Early Antibody Lineage Diversification and Independent Limb Maturation Lead to Broad HIV-1 Neutralization Targeting the Env High-Mannose Patch. Immunity 44:1215-26.

33. Wiehe K, Bradley T, Meyerhoff RR, Hart C, Williams WB, Easterhoff D, Faison WJ, Kepler TB, Saunders KO, Alam SM, Bonsignori M, Haynes BF. 2018. Functional Relevance of Improbable Antibody Mutations for HIV Broadly Neutralizing Antibody Development. Cell Host Microbe 23:759-765 e6.

34. Crispin M, Ward AB, Wilson IA. 2018. Structure and Immune Recognition of the HIV Glycan Shield. https://doiorg/101146/annurev-biophys-060414-034156 doi:10.1146/annurev-biophys-060414-034156.

35. Kong L, Torrents de la Pena A, Deller MC, Garces F, Sliepen K, Hua Y, Stanfield RL, Sanders RW, Wilson IA. 2015. Complete epitopes for vaccine design derived from a crystal structure of the broadly neutralizing antibodies PGT128 and 8ANC195 in complex with an HIV-1 Env trimer. Acta Crystallogr D Biol Crystallogr 71:2099-108.

36. Freund NT, Wang H, Scharf L, Nogueira L, Horwitz JA, Bar-On Y, Golijanin J, Sievers SA, Sok D, Cai H, Cesar Lorenzi JC, Halper-Stromberg A, Toth I, Piechocka-Trocha A, Gristick HB, van Gils MJ, Sanders RW, Wang LX, Seaman MS, Burton DR, Gazumyan A, Walker BD, West AP, Jr., Bjorkman PJ, Nussenzweig MC. 2017. Coexistence of potent HIV-1 broadly neutralizing antibodies and antibody-sensitive viruses in a viremic controller. Sci Transl Med 9.

37. Garces F, Sok D, Kong L, McBride R, Kim HJ, Saye-Francisco KF, Julien JP, Hua Y, Cupo A, Moore JP, Paulson JC, Ward AB, Burton DR, Wilson IA. 2014. Structural evolution of glycan recognition by a family of potent HIV antibodies. Cell 159:69-79.

38. Barnes CO, Gristick HB, Freund NT, Escolano A, Lyubimov AY, Hartweger H, West AP, Jr., Cohen AE, Nussenzweig MC, Bjorkman PJ. 2018. Structural characterization of a highly-potent V3-glycan broadly neutralizing antibody bound to natively-glycosylated HIV-1 envelope. Nat Commun 9:1251.

39. Julien JP, Sok D, Khayat R, Lee JH, Doores KJ, Walker LM, Ramos A, Diwanji DC, Pejchal R, Cupo A, Katpally U, Depetris RS, Stanfield RL, McBride R, Marozsan AJ, Paulson JC, Sanders RW, Moore JP, Burton DR, Poignard P, Ward AB, Wilson IA. 2013. Broadly neutralizing antibody

PGT121 allosterically modulates CD4 binding via recognition of the HIV-1 gp120 V3 base and multiple surrounding glycans. PLoS Pathog 9:e1003342.

Chapter 4. Evolution of an infant-derived HIV-1 neutralizing antibody suggests early targeting of a conserved glycan

*The following chapter was conducted in collaboration with the lab of Julie Overbaugh at Fred Hutchinson Cancer Research Institute, Seattle, WA.

4.1 Introduction

The HIV-1 Envelope glycoprotein (Env) mediates entry into host immune cells through a series of receptor-driven conformational changes that lead to fusion of the viral and host membranes. Env is a heavily glycosylated trimer that is composed of three identical copies of non-covalently associated heterodimers. Each heterodimer consists of a receptor binding domain, gp120, which recognizes CD4 receptors on the surface of T-cells, and a fusion subunit, gp41, that mediates fusion (1-4). As the sole virally encoded antigen on the surface of HIV-1, Env is also the major target of neutralizing antibodies.

Once infected with HIV-1, an immune response is raised against the Env glycoprotein. A fraction of the antibodies generated by the initial response can block entry of the virus; in most cases, they are only capable of neutralizing the infecting virus strain (5-7). What soon follows is the rapid evolution of HIV-1 and proliferation of neutralization escape variants that leaves the immune system to battle immense antigenic diversity (8-10). In a subset of individuals, however, the neutralizing antibody response expands and develops broadly neutralizing antibodies (bnAbs) capable of neutralizing a diverse range of HIV-1 isolates (11-13). Improvements in the isolation of such antibodies and methods to determine their germline sequences have given rise to optimism that a more complete understanding of the characteristics and evolution of naturally occurring bnAbs may provide insight for the design of vaccine immunogens and immunization strategies that are capable of eliciting a similarly broad response.

Extensive research and available structures of various bnAbs in complex with soluble Env constructs has brought to light neutralizing epitopes that are commonly targeted in chronically infected individuals. These include the V1/V2 apex, CD4 binding site, gp120/gp41 interface and the V3-glycan region Figure (4.1) (13-19). Despite significant progress in characterizing the development of bnAbs in adults, the unusual properties of these antibodies present a set of challenges in eliciting a similar response by immunization (20-23). One such challenge is that most adult bnAbs take years to develop because of

continuous viral escape and antibody maturation often resulting in extensive somatic hypermutation (SHM) (21, 23-30). Additionally, many inferred germline precursors of bnAbs lack detectable binding to recombinant HIV envelope, and thus require the design of germline-targeting immunogens to help guide a broad and potent antibody response through vaccination (20, 22-24, 31, 32).

Recent studies have revealed that infants and children develop bnAb responses at least as, if not more, commonly than adults, and that they do so rapidly within 1-2 years post-infection (33-35). Initial characterization of an HIV-1 infected infant exhibiting a cross-clade neutralizing antibody response led to the isolation of BF520.1 that, in contrast to most bnAbs from HIV-1 infected adults, has limited SHM (VH=6.6%, VK=5% nt) (36). In the previous chapter, a functional and structural approach was used to identify key determinants of neutralization by BF520.1 by focusing on VH and VK development during lineage maturation. The data revealed that the BF520.1 epitope is largely focused on the N332 glycan and several potential contacts between CDRH loops and GDIR sequence, as well as N301 glycan. Furthermore, maturation of the variable kappa chain (VK), specifically in the CDRL1 loop, had an early and dramatic contribution to neutralization breadth through extensive interaction with the N332 glycan.

Here, we begin to explore the evolutionary pathway of the BF520.1 antibody lineage to identify the effect of early somatic mutations on neutralization of HIV-1 and how they impact epitope recognition. $Int2_{VH}Int2_{VK}$ and $Int4_{VH}Int4_{VK}$ are both early antibody lineage intermediates that bridge antibody development from a weakly neutralizing Ab ($Int2_{VH}Int2_{VK}$) to an intermediate exhibiting heterologous breadth ($Int4_{VH}Int4_{VK}$) that is similar to breadth achieved by mature BF520.1. Epitope mapping by negative-stain electron microscopy was consistent with $Int4_{VH}Int4_{VK}$ recognizing the BF520.1 epitope with no detectable change in angle of approach. Ongoing single-particle cryo-EM analysis will provide higher resolution detail to illustrate how antibody-Env contacts evolved over the course of affinity maturation. $Int2_{VH}Int2_{VK}$ possessed tier 1A neutralizing activity following just two amino acid substitutions in VH and three in VK relative to the inferred unmutated common ancestor (germline) sequence, but in contrast to $Int4_{VH}Int4_{VK}$ and BF5201, it bound relatively weakly to SOSIP trimer. We infer that the early mutations in VK, as early as $Int2_{VH}Int2_{VK}$, may anchor early intermediates toward the N332 glycan, allowing further focusing of mutations that increase affinity. A better understanding of the immunologic basis for generating bnAbs and

their development during maturation holds promise of strategies to guide immunogen design aimed at focusing the immune response towards eliciting advantageous antibodies.

4.2 Materials and Methods

4.2.1 SOSIP production and purification

The most promising native-like (NL) structures have been obtained by engineering trimer-stabilizing mutations, termed SOSIP, into truncated Env sequences (37). BG505.SOSIP.T332N trimers were synthesized using a previously established protocol (38). In brief, following production in 293F cells, soluble envelope oligomers were separated from the extracellular milieu using Galanthus nivalis lectin (Vector Labs). This mixture was then subjected to DEAE cation exchange chromatography, and trimer was resolved from aberrantly disulfide-bonded dimer and gp140 monomer, using hydrophobic interaction chromatography and preparative-grade size-exclusion chromatography. Purity was assessed by SDSPAGE, BN-PAGE, and dynamic light scattering, and found to be >95% native-like trimer. Presence of native-like SOSIP trimer was further confirmed by negative-stain electron microscopy.

4.2.2 Fab purification

Fab fragments were generated from 2.0 mg of IgG antibody using a papain digestion kit (Pierce), and separated from Fc fragments and undigested IgG by gravity flow using a Protein A column (Pierce). Purity and size of Fab fragments were confirmed by SDS-PAGE.

4.2.3 Biolayer interferometry

Binding kinetics of BF520.1, $Int4_{VH}Int4_{VK}$, and $Int2_{VH}Int2_{VK}$ Fabs with BG505.SOSIP.T332N were determined by using BLI on an Octet Red system (FortèBio). Hydrated anti-human Fab-CH1 biosensors were immobilized for 4 min with purified IgG or Fab diluted to 10 µg/ml in phosphate-buffered saline (PBS) (pH 7.4) supplemented with 1% BSA, 0.03% Tween 20, and 0.02% NaN_3. After reaching a stable baseline, antibody-immobilized tips were moved to wells containing a 2-fold dilution series of BG505.SOSIP.T332N to monitor association for 4 min. Tips were moved back to wells containing buffer to monitor dissociation for 4 min. Kinetic data were analyzed by using FortèBio Data Analysis 7.0 software. Average measurements

from reference wells were subtracted, and data were processed by Savitzky-Golay filtering prior to fitting using a 1:1 binding model. Reported values are averages of data from experiments repeated in triplicate.

4.2.4 Negative-stain electron microscopy

Negative-stain EM was used to observe binding of $Int2_{VH}Int2_{VK}$ and $Int4_{VH}Int4_{VK}$ to BG505.SOSIP.T332N, and to generate epitope maps to compare binding orientations with the previously solved mature epitope (36). A 3-µl aliquot of the Fab:SOSIP trimer complex was applied to glow-discharged C-Flat, 300-mesh, Cu grids (Electron Microscopy Sciences) and stained by using Nano-W. Data were collected by using a Tecnai T12 transmission electron microscope operating at 120 keV. Images were taken by using a Gatan 4k-by-4k CCD camera at a magnification of 67,000 and a defocus range of −3 to −1 µm, corresponding to a pixel size of 1.6 Å/pixel. Particles were selected by using interactive particle picking from ~120 micrographs using EMAN2.1 image processing suite (39). Particle stacks of ~8,000 particles were created and subjected to reference-free 2D classification and clustering to generate 100 2D classes. Representative class averages for each sample were chosen for clarity. The BF520.1 negative-stain map was lowpass filtered to 60 Å and used as an initial model for refinement of the $Int4_{VH}Int4_{VK}$:SOSIP complex.

4.2.5 Sample preparation for cryo-electron microscopy

Purified BG505.SOSIP.T332N trimers were mixed with 4-fold molar excess $Int4_{VH}Int4_{VK}$ Fab and diluted to 0.47 mg/mL in PBS supplemented with 60 µM n-Dodecyl-β-D-Maltoside (DDM). The mixture incubated for 2 hours at room temperature prior to vitrification. A 3.0 µL aliquot was applied at 4ºC and 100% humidity to glow-discharged C-Flat 1.2/1.3 4C holey carbon-coated grids (Electron Microscopy Sciences), blotted, and immediately plunge frozen in liquid ethane by using a Vitrobot Mark IV specimen preparation unit (FEI Co.).

4.2.6 Cryo-EM data collection

Vitrified grids were imaged using an FEI Titan Krios operating at 300 keV and equipped with a Gatan K2 summit direct detector device. Micrographs were collected at 105,000×, corresponding to a pixel size of 1.35 Å/pixel in counting mode. Each image received a dose rate of ~ 8 e^-/pix/s with 200 ms exposure

per frame, and an estimated defocus ranging from 1.0 - 3.5 µm. Data were collected in three separate sessions, resulting in a total of 4044 images using Leginon (40) automated data collection software.

4.3 Results

4.3.1 Cross-clade neutralization with limited SHM in lineage intermediates

To define the minimal combination of changes in VH and VK that are needed for breadth, intermediates were paired together using percentage SHM to assign probable pairings. Tier 1A neutralizing activity was observed following just two amino acid substitutions in VH ($Int2_{VH}$) and three in VK ($Int2_{Vk}$) with the additions of the VH Y32N and VK S30A being important for the neutralizing activity. Cross-clade heterologous neutralization was achieved with the addition of the VH M34I and VK S28N in the $Int3_{VH}Int3_{Vk}$ mAb, which had a total of four VH and five VK amino acid substitutions or 1.3% and 1.8% SHM at the nucleotide level in VH and VK, respectively. $Int4_{VH}$ paired with $Int4_{VK}$ neutralized the majority of the viruses (9/13; 69%) that are neutralized by mature BF520.1 with only 1.8 VH and 2.1% VK SHM. Further increased neutralization was conferred by single additional substitutions in both VH and VK: N52A ($Int4_{VH}$) and A25T ($Int4_{VK}$). The breadth of BF520.1 was reached with 1.8% VH and 3.4% VK SHM (2.5% overall SHM) for $Int4_{VH}Int5_{VK}$. Finally, the $Int5_{VH}Int6_{VK}$ mAb reached the breadth and potency of mature BF520.1 with only 2.4% VH and 3.7% VK SHM (3.0% overall SHM) (Figure. 4.2). $Int2_{VH}Int2_{VK}$ and $Int4_{VH}Int4_{VK}$ represent two key points along the developmental pathway of BF520.1. The earliest lineage time-point where neutralization occurred was Tier 1A neutralization by $Int2_{VH}Int2_{VK}$ and represents an early intermediate that closely resembles the germline antibody. A later intermediate, $Int4_{VH}Int4_{VK}$, neutralized the majority of viruses neutralized by BF520.1. Although later lineage intermediates had comparable breadth and potency as mature BF520.1, $Int4_{VH}Int4_{VK}$ represents a clear transition in development from limited neutralization to heterologous breadth. Therefore, intermediates $Int2_{VH}Int2_{VK}$ $Int4_{VH}Int4_{VK}$ were chosen for further characterization.

4.3.2 Binding affinities of lineage intermediates for BG505.SOSIP

The affinity of $Int2_{VH}Int2_{VK}$, $Int4_{VH}Int4_{VK}$ and BF520.1 for BG505.SOSIP.T332N was determined by using biolayer interferometry (BLI). We chose to focus on antibody binding to the heterologous BG505.SOSIP trimer based on the neutralization data, showing that BG505.T332N HIV-1 virus was

resistant to neutralization by $Int2_{VH}Int2_{VK}$ while being potently neutralized by $Int4_{VH}int4_{VK}$ and BF520.1. This suggests that mutations occurring after $Invt2_{VH}Int2_{VK}$ may be critical for heterologous neutralization. BF520.1 and lineage intermediate $Int4_{VH}Int4_{VK}$ both bind BG505.SOSIP.T332N with reasonably high affinity; however, the affinity of BF520.1 was approximately ~2.5-fold higher with a measured KD of 37.8 nM versus 92.8 nM for $Int4_{VH}Int4_{VK}$, respectively (Figure 4.3). Although the k_{on} of $Int4_{VH}Int4_{VK}$ was ~2-fold faster than BF520.1, the difference in k_{dis} is responsible for the difference in affinity (Figure 4.3). $Int2_{VH}Int2_{VK}$ had a lower affinity for BG505.SOSIP.T332N compared to both $Int4_{VH}Int4_{VK}$ and mature BF520.1, largely due to the ~10-fold faster off-rate. Nevertheless, $Int2_{VH}Int2_{VK}$ is, in fact, capable of binding Env, although interactions may be more transient than later lineage intermediates. We note that global fitting was only performed using two binding curves; however, triplicate measurements exhibited a low standard deviation (Figure 4.3). Overall, BLI data suggests that the BF520.1 lineage establishes productive contacts towards the V3 epitope at an early stage in maturation, and further development is largely focused on strengthening contacts that result in higher affinity.

4.3.3 Imaging of intermediates bound to Env using negative-stain EM

Negative-stain transmission electron microscopy (EM) imaging was performed on lineage intermediates $Int4_{VH}Int4_{VK}$ and $Int2_{VH}Int2_{VK}$ that were complexed with heterologous Env construct BG505.SOSIP.T332N. With these low-resolution structures, we sought to determine whether any changes in angle of approach by early intermediates take place over the course of affinity maturation as has been observed for adult-derived V1/V2 apex targeting bnAb, PCT64 (41). Imaging of $Int4_{VH}Int4_{VK}$ Fab bound to BG505.SOSIP.T332N trimer showed 2D classes of particles where Fab density could be observed projecting from the V3-glycan region of gp120 (Figure 4.4). Generating a 3-dimensional map revealed that $Int4_{VH}Int4_{VK}$ approaches the epitope in a similar manner and angle compared to the mature BF520.1 (Figure 4.4) (36). At the current resolution, we cannot detect any variation in interactions. The low binding affinity of $Int2_{VH}Int2_{VK}$ manifested itself in low levels of epitope saturation and a large population of unbound BG505.SOSIP.T332N trimers during negative-stain imaging. It is likely that imaging of $Int2_{VH}Int2_{VK}$ bound to BG505.SOSIP.T332N will require glutaraldehyde fixation of the protein complex (42, 43). Therefore,

without a sufficient quantity of $Int2_{VH}Int2_{VK}$ bound to SOSIP trimer, we were unable to generate an epitope map for comparison to $Int4_{VH}Int4_{VK}$ and BF520.1 (Figure 4.5).

4.4 Discussion

It is widely viewed that an effective vaccine against HIV-1 must elicit a broad and potent antibody response to overcome the enormous global diversity among circulating strains (44, 45). Upon initial infection with HIV-1, many individuals develop a neutralizing response against the autologous virus, and passive administration of neutralizing antibodies has shown protection in animal models as well as reduced HIV-1 viremia in chronically infected adults (46-51). Moreover, a subset of individuals develops broadly neutralizing antibodies capable of neutralizing a diverse set of HIV-1 isolates, providing hope that such antibodies could be elicited through vaccination (11, 52-54). Despite significant efforts and the wealth of data generated by numerous investigators, bnAbs have not been elicited by vaccination, and a preventative vaccine against HIV-1 has yet to be developed.

bnAbs targeting the V3-glycan region exhibit some of the most broad and potent neutralization profiles to date. The V3-glycan region is centered around the N332 glycan and plays a critical role in HIV-1 entry and infection. Structural characterization of bnAbs targeting V3 has revealed that the N332 glycan is a central feature in the V3 epitope, though antibodies may bind with a variety of orientations and angles of approach (15, 55, 56). As a result, interactions with additional glycans, as well as regions of V1/V2 are observed, depending on the specific bnAb and its orientation relative to Env.

A pervasive challenge in many adult-derived V3-targeting bnAbs is the extensive SHM, particularly in the CDRH3 loop, that comes from several years of maturation in response to virus evolution. It is now known that in several cases, infants possess a unique ability to elicit a neutralizing response against HIV-1 more rapidly than observed in adults. BF520.1 is currently the best described infant bnAb and has only 6.6% SHM while exhibiting 59% neutralization against a global HIV-1 panel. How does BF520.1 develop this capacity to neutralize with fairly minimal SHM? By tracing back to early stage antibody development, we sought, in part, to address this question.

As described in the previous chapter, next generation sequencing by our collaborating labs identified an inferred germline precursor and the likely developmental route towards the mature BF520.1

bnAb. Cassie Simonich and Laura Noges synthesized intermediates using percentage SHM to assign probable VH and VK pairings and tested the neutralizing ability of the paired intermediates from the inferred germline precursor to mature BF520.1. Following just two VH and three VK substitutions, $Int2_{VH}Int2_{VK}$ was able to neutralize a Tier 1A virus, and was unable to neutralize the heterologous BG505 isolate used for structural characterization of mature BF520.1. Interestingly, $Int4_{VH}Int4_{VK}$ neutralized the majority of viruses that are neutralized by BF520.1 and did so with extremely low levels of SHM (1.8% VH and 2.1% VK). Therefore, we chose these two lineage intermediates to study further to characterize the impact of early mutations on binding and recognition of the heterologous BG505.SOSIP epitope. We observed a pattern of increased affinity and a shift towards heterologous breadth between intermediates $Int2_{VH}Int2_{VK}$ and $Int4_{VH}Int4_{VK}$. The developmental pathway of VK obtains mutations that appear to be focused on CDRL1 and VK-framework regions. Specifically, during progression towards $Int4_{VH}Int4_{VK}$, the only variable loop containing substitutions is CDRL1, which was previously shown to extensively interact with the N332 glycan.

Germline antibodies have been described as conformationally dynamic, and it is commonly thought that over the course of affinity maturation, the paratope becomes more rigid as the antibody focuses towards its epitope (57-59). Several studies have challenged this held belief with observations that greater plasticity can be observed in the mature antibody (60, 61). Nevertheless, mutations in the antibody framework region can play a key role in antibody development. Indeed, framework mutations surrounding CDRL1 in the BF520.1 lineage were shown in the previous chapter to increase neutralization potency. Our current data is unable to describe the effect of framework mutations on paratope stability and must be further explored using additional methodologies such as Hydrogen/Deuterium-exchange Mass Spectrometry (HDX-MS) (62). As previously reported, the presence of the N332 glycan is critical for BF520.1 binding and neutralization, and is the major feature of the targeted epitope (36). We speculate that contacts between the CDRL1 loop and N332 glycan are established at an early stage of maturation and may become stabilized by framework mutations around CDRL1, providing an anchor for the developmental pathway of BF520.1 (Figure 4.6). However, high resolution structures of the BF520.1 lineage intermediates in complex with SOSIP trimer, and a thorough analysis of interactions between the Ab lineage and SOSIPs lacking N332 will be required to either support or refute these claims. To this end, single particle cryo-EM data has been collected for the $Int4_{VH}Int4_{VK}$ intermediate complexed to BG505.SOSIP trimer and is currently

being processed and analyzed. Furthermore, a recent study of the evolution of V2-apex bnAb PC69 suggests that maturation in the angle of binding and alterations in glycan contact are additional evolutionary mechanisms conferring breadth. Between the early and late antibody, the authors observed a steepening of binding angle to accommodate glycan contacts. Epitope mapping of the $Int4_{VH}Int4_{VK}$ intermediate revealed an identical angle of approach to the mature BF520.1 further supporting our notion that the epitope was established at an early stage of maturation. Overall, our data suggests that the rapid development of BF520.1 is in part due to the ability of affinity maturation to establish CDRL1 contacts towards the N332 glycan at an early stage of development, allowing focusing of CDRH contacts with the conserved GDIR sequence. Furthermore, because focused binding to a conserved epitope on Env is established early during development, the BF520.1 lineage pathway may be considered an attractive template for vaccine design.

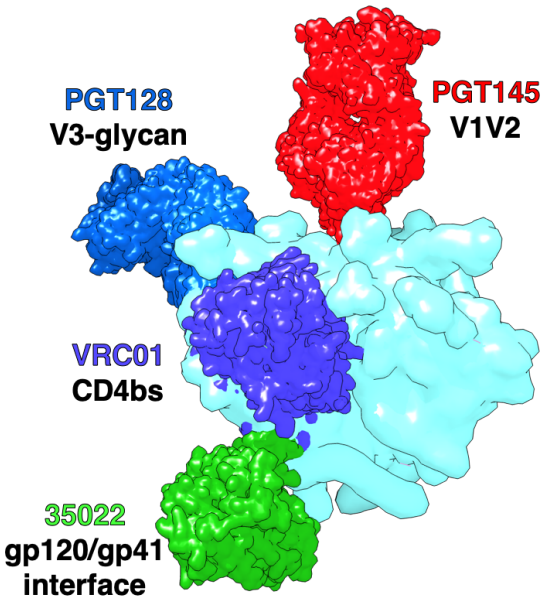

Figure 4.1: High resolution structures have revealed commonly targeted epitopes of adult-derived, broadly neutralizing antibodies. These epitopes include the V1/V2 apex region (red), V3-glycan region (blue), CD4 binding site (purple) and the gp120/gp41 interface (green). Shown for each epitope are prototype bnAbs that have been structurally characterized in HIV-1 infected adults.

A

BF520.1 lineage paired intermediates

Tier	Clade		VH naïve	Int1	Int2	Int3	Int3	Int4	Int4	Int4	Int5	Int6	mature
				0.5	0.8	1.3	1.3	1.8	1.8	1.8	2.4	2.6	6.5 % SHM
			VK naïve	Int1	Int2	Int3	Int4	Int4	Int5	Int6	Int6	Int7	mature
				0.3	1.2	1.8	2.1	2.1	3.4	3.7	3.7	4.3	4.6 % SHM
1A	B	SF162	>20	>20	1.7	<0.6	<0.6	<0.6	<0.6	<0.6	<0.6	<0.6	<0.6
1B		Q23.17	>20	>20	>20	2.1	1.2	<0.6	<0.6	<0.6	<0.6	0.7	<0.6
2	A	BG505.W6M.C2_T332	>20	>20	>20	>20	>20	6.2	2.1	1.4	1.0	1.6	1.1
		398F1	>20	>20	>20	>20	>20	2.0	1.2	<0.6	<0.6	0.8	<0.6
	B	X2278	>20	>20	>20	>20	>20	2.2	1.3	0.7	0.7	0.9	1.0
		TRO.11	>20	>20	>20	>20	>20	>20	18.9	10.3	6.0	6.7	5.9
	BC	BJOX002000	>20	>20	>20	>20	>20	11.9	1.6	0.8	0.7	0.9	0.9
		CH119	>20	>20	>20	>20	>20	>20	8.2	4.4	3.0	5.7	6.0
	C	CE1176	>20	>20	>20	>20	>20	7.5	3.7	4.0	4.1	7.4	5.1
		QC406.F3	>20	>20	>20	3.1	1.1	<0.6	<0.6	<0.6	<0.6	<0.6	<0.6
		CE0217	>20	>20	>20	>20	>20	>20	15.0	5.4	3.7	4.9	2.8
		DU156.12	>20	>20	>20	>20	>20	>20	4.1	2.2	2.0	2.2	2.2
		DU422.1	>20	>20	>20	10.3	8.2	2.8	2.9	2.3	1.5	4.1	2.6
		SIV	>20	>20	>20	>20	>20	>20	>20	>20	>20	>20	>20

B

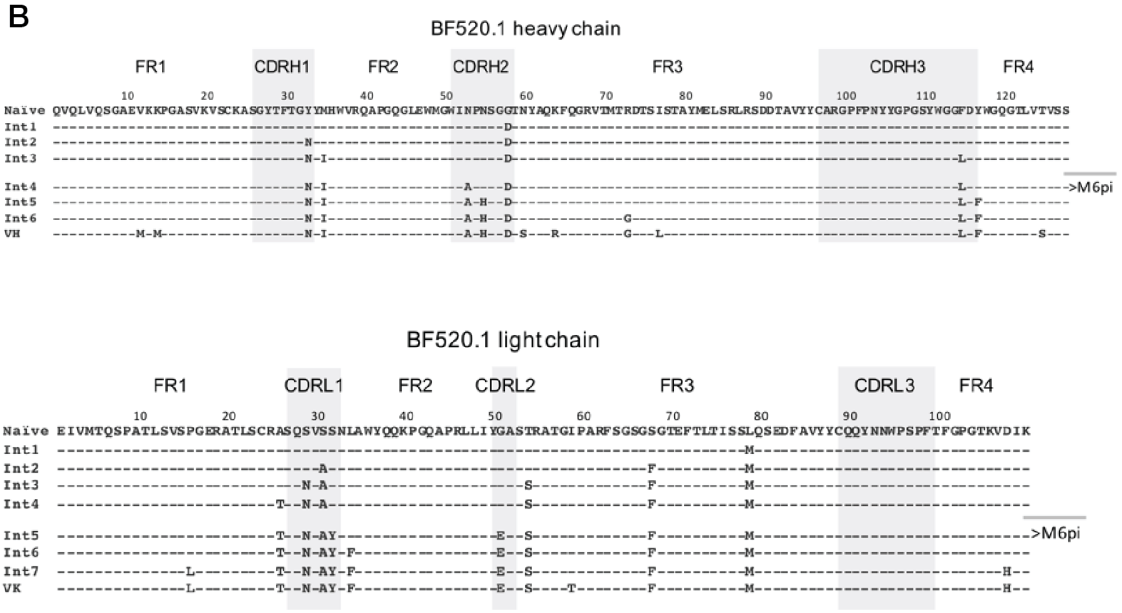

Figure 4.2: Neutralization of a panel of HIV-1 viruses by paired lineage intermediates. **(A)** BF520.1 lineage maturation obtains broad neutralization at an early stage of development. The top rows indicate the intermediate tested with %SHM shown below. The panel viruses are shown to the left with the tier, clade and name indicated. IC_{50} values (μg ml^{-1}) represent an average of two to three independent experiments performed in duplicate. IC_{50} values are color-coded with darker shades indicating more potent neutralization. Grey indicates that 50% neutralization was not achieved at the highest mAb concentration tested. **(B)** Amino acid alignment of BF520.1 naïve, rationally inferred lineage intermediates, and mature heavy and light chain sequences. Experiments were performed and kindly provided by Cassie Simonich and Laura Noges at Fred Hutchinson Cancer Research Center, Seattle, WA.

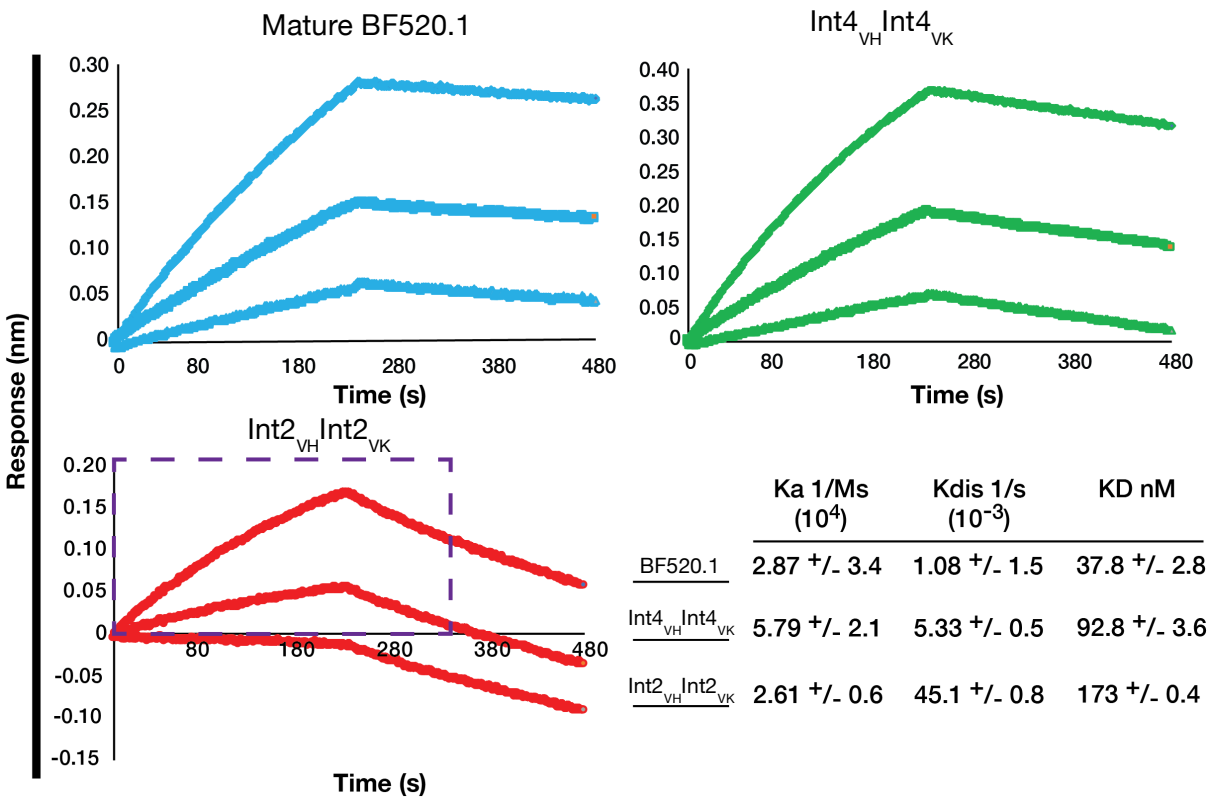

	Ka 1/Ms (10^4)	Kdis 1/s (10^{-3})	KD nM
BF520.1	2.87 +/- 3.4	1.08 +/- 1.5	37.8 +/- 2.8
$Int4_{VH}Int4_{VK}$	5.79 +/- 2.1	5.33 +/- 0.5	92.8 +/- 3.6
$Int2_{VH}Int2_{VK}$	2.61 +/- 0.6	45.1 +/- 0.8	173 +/- 0.4

Figure 4.3: Affinities of paired lineage intermediates measured by biolayer interferometry. Binding affinity increases over the course of antibody maturation and is attributed to a decrease in k_{dis}. Binding curves were globally fit using a 1:1 binding model. For $Int2_{VH}Int2_{VK}$, two binding curves could be fit by truncating the time of dissociation prior to falling below zero (dashed line). Values shown are the averages and standard deviations of data from experiments repeated in triplicate.

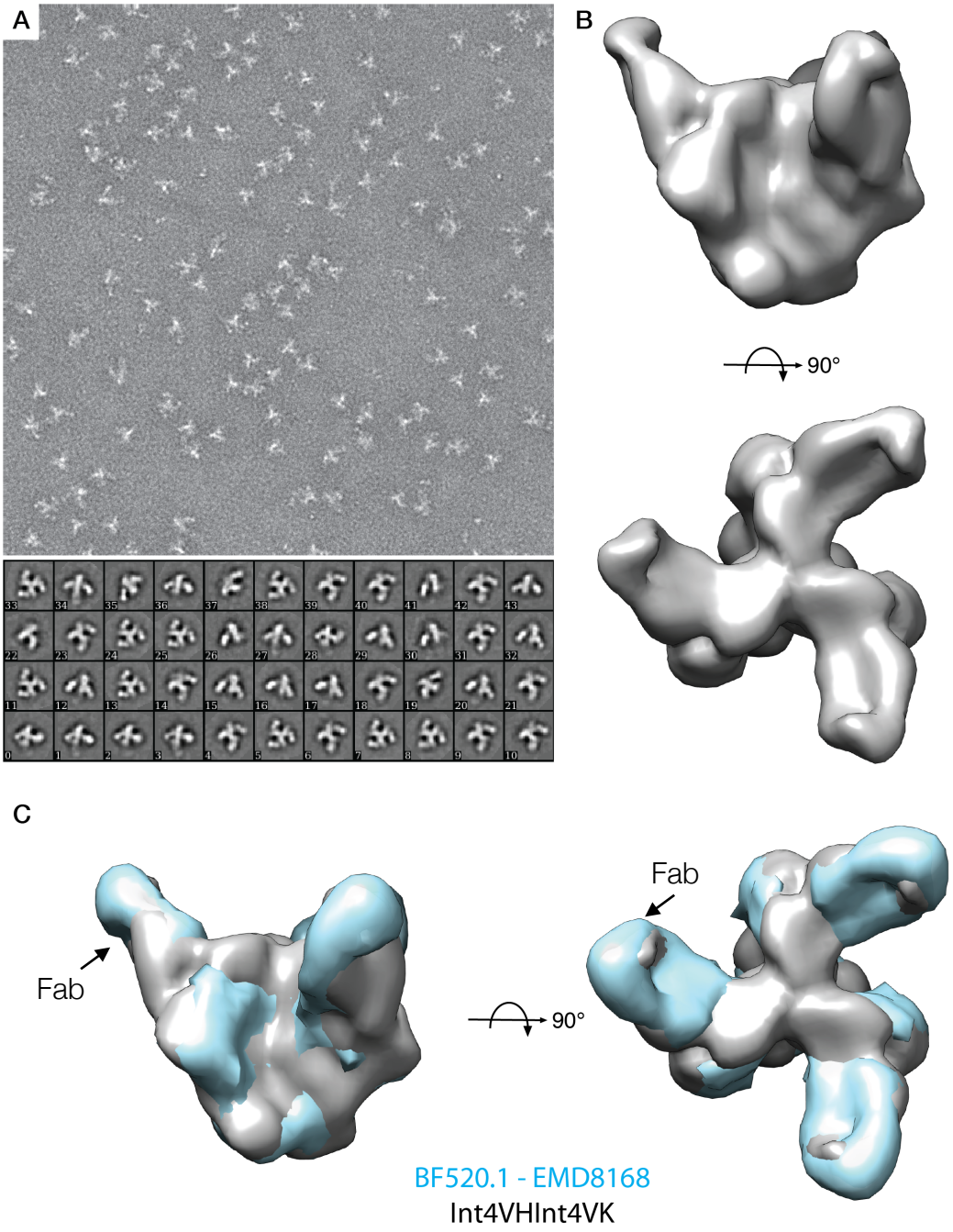

Figure 4.4: Negative-stain reconstruction of $Int4_{VH}Int4_{VK}$:BG505.SOSIP.T332N reveals similar angle of approach as BF520.1. **(A)** Representative negative-stain electron micrograph of $Int4_{VH}Int4_{VK}$ in complex with BG505.SOSIP.T332N, illustrating particle dispersity and orientation of specimen across the carbon support film. Below are 2D class averages composed of ~5,000 particles used for 3D refinement. **(B)** Epitope map reveals that $Int4_{VH}Int4_{VK}$ targets the V3 region. **(C)** Map comparison with BF520.1 (EMD 8168) reveals a similar binding orientation and angle of approach.

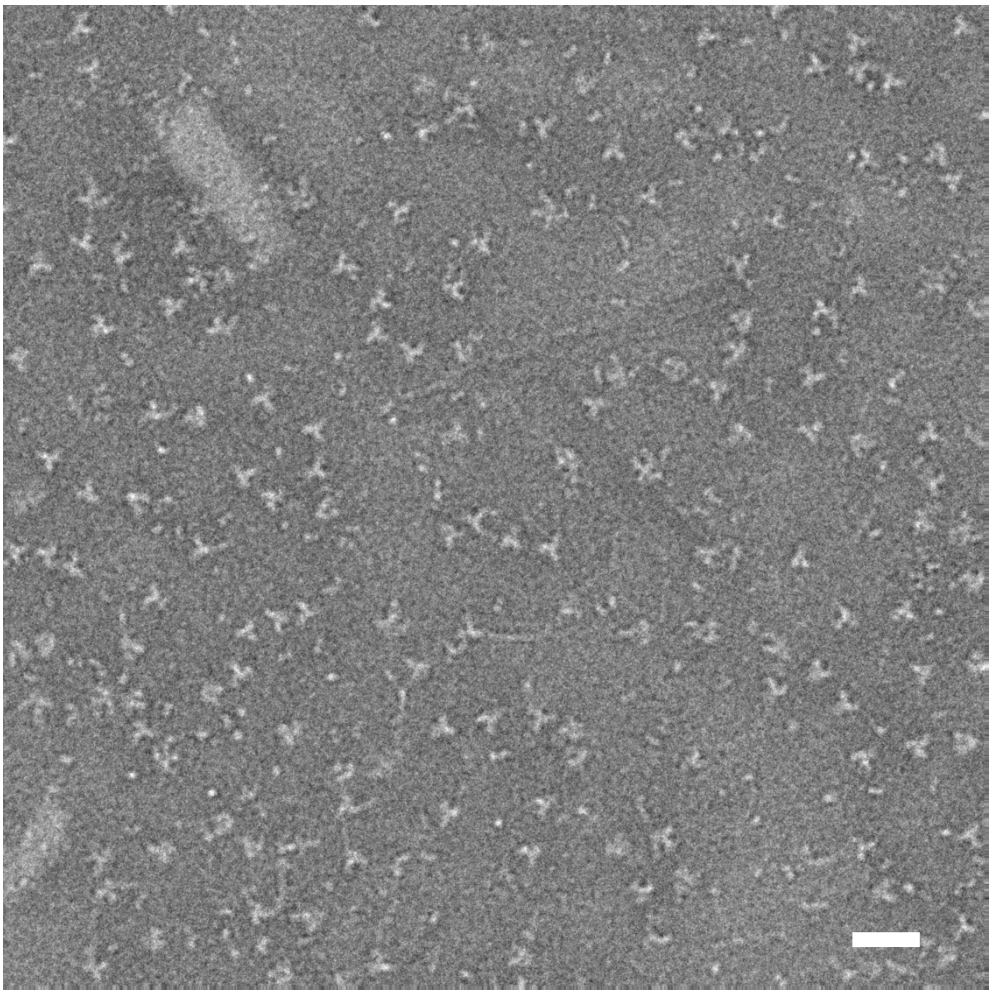

Figure 4.5: $Int2_{VH}Int2_{VK}$ does not saturate binding sites by negative-stain EM. Raw micrograph of $Int2_{VH}Int2_{VK}$ Fab in complex with BG505.SOSIP.T332N trimer. The majority of the particles are unliganded BG505.SOSIP trimer with a small population of Fab bound to trimer. Few instances of binding saturation were observed and we were unable to generate a 3-dimensional map.

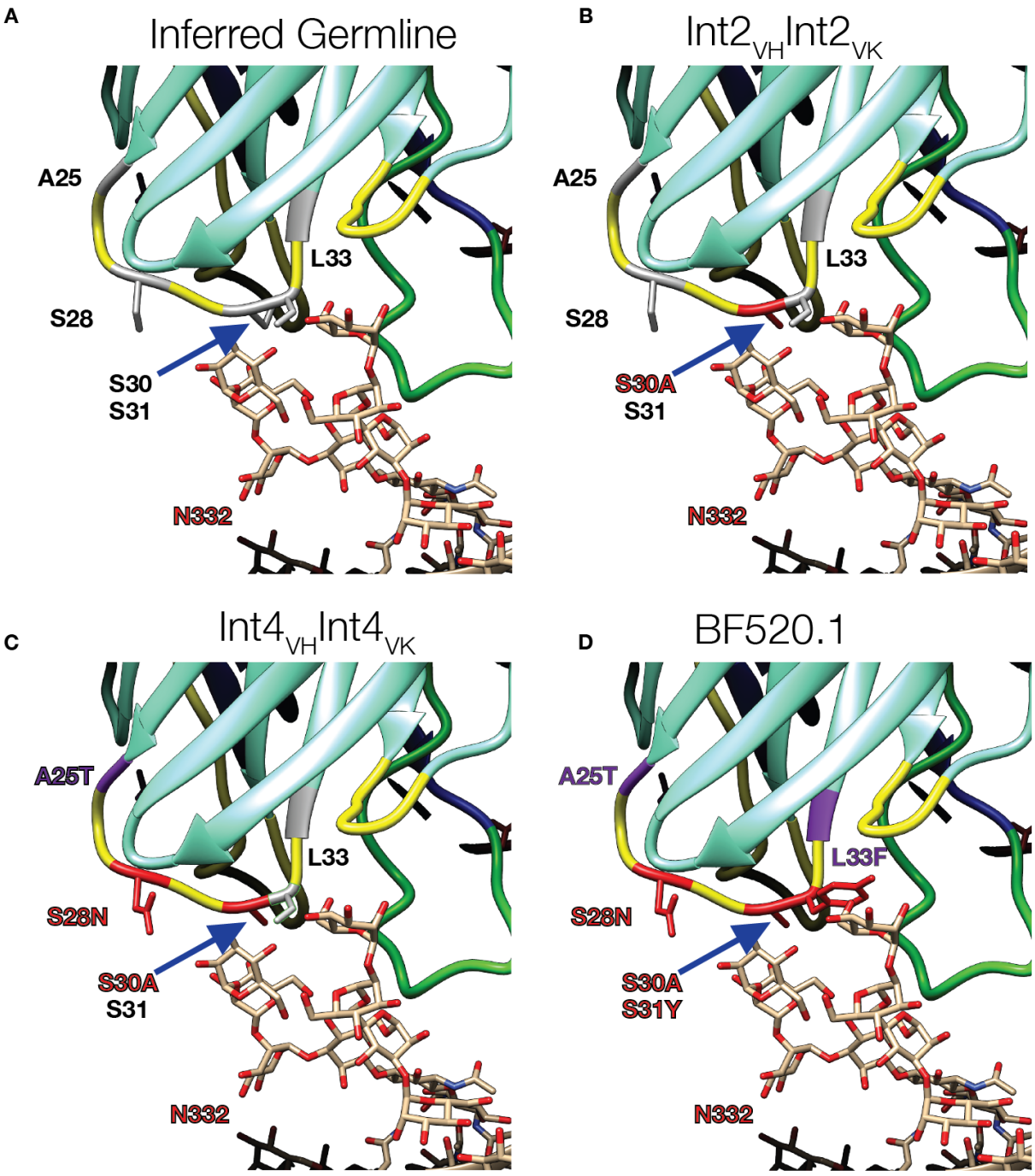

Figure 4.6: Early CDRL1 mutations are critical for neutralization by BF520.1. **(A)** The modeled structure of the inferred germline Ab. Amino acids shown in gray are residues that are mutated during lineage development. Amino acid substitutions occurring in CDRL1 (red) and the flanking framework regions (purple) are shown for **(B)** $Int2_{VH}Int2_{VK}$, **(C)** $Int4_{VH}Int4_{VK}$, and **(D)** mature BF520.1 sequences. The structure of the Fab domain is based on the BF520.1 Fab model shown in figure 3.5.

References

1. Lane HC. 2010. Pathogenesis of HIV infection: total CD4+ T-cell pool, immune activation, and inflammation. Top HIV Med 18:2-6.

2. Sattentau QJ, Weiss RA. 1988. The CD4 antigen: physiological ligand and HIV receptor. Cell 52:631-3.

3. Lyumkis D, Julien JP, de Val N, Cupo A, Potter CS, Klasse PJ, Burton DR, Sanders RW, Moore JP, Carragher B, Wilson IA, Ward AB. 2013. Cryo-EM structure of a fully glycosylated soluble cleaved HIV-1 envelope trimer. Science 342:1484-90.

4. Merk A, Subramaniam S. 2013. HIV-1 envelope glycoprotein structure. Curr Opin Struct Biol 23:268-76.

5. Richman DD, Wrin T, Little SJ, Petropoulos CJ. 2003. Rapid evolution of the neutralizing antibody response to HIV type 1 infection. Proc Natl Acad Sci U S A 100:4144-9.

6. Li B, Decker JM, Johnson RW, Bibollet-Ruche F, Wei X, Mulenga J, Allen S, Hunter E, Hahn BH, Shaw GM, Blackwell JL, Derdeyn CA. 2006. Evidence for potent autologous neutralizing antibody titers and compact envelopes in early infection with subtype C human immunodeficiency virus type 1. J Virol 80:5211-8.

7. Gray ES, Moore PL, Choge IA, Decker JM, Bibollet-Ruche F, Li H, Leseka N, Treurnicht F, Mlisana K, Shaw GM, Karim SS, Williamson C, Morris L, Team CS. 2007. Neutralizing antibody responses in acute human immunodeficiency virus type 1 subtype C infection. J Virol 81:6187-96.

8. Bar KJ, Tsao CY, Iyer SS, Decker JM, Yang Y, Bonsignori M, Chen X, Hwang KK, Montefiori DC, Liao HX, Hraber P, Fischer W, Li H, Wang S, Sterrett S, Keele BF, Ganusov VV, Perelson AS, Korber BT, Georgiev I, McLellan JS, Pavlicek JW, Gao F, Haynes BF, Hahn BH, Kwong PD, Shaw GM. 2012. Early low-titer neutralizing antibodies impede HIV-1 replication and select for virus escape. PLoS Pathog 8:e1002721.

9. Wei X, Decker JM, Wang S, Hui H, Kappes JC, Wu X, Salazar-Gonzalez JF, Salazar MG, Kilby JM, Saag MS, Komarova NL, Nowak MA, Hahn BH, Kwong PD, Shaw GM. 2003. Antibody neutralization and escape by HIV-1. Nature 422:307-12.

10. Moore PL, Ranchobe N, Lambson BE, Gray ES, Cave E, Abrahams MR, Bandawe G, Mlisana K, Abdool Karim SS, Williamson C, Morris L, Study C, Immunology NCfHAV. 2009. Limited neutralizing antibody specificities drive neutralization escape in early HIV-1 subtype C infection. PLoS Pathog 5:e1000598.

11. Hraber P, Seaman MS, Bailer RT, Mascola JR, Montefiori DC, Korber BT. 2014. Prevalence of broadly neutralizing antibody responses during chronic HIV-1 infection. AIDS 28:163-9.

12. Gray ES, Madiga MC, Hermanus T, Moore PL, Wibmer CK, Tumba NL, Werner L, Mlisana K, Sibeko S, Williamson C, Abdool Karim SS, Morris L, Team CS. 2011. The neutralization breadth of HIV-1 develops incrementally over four years and is associated with CD4+ T cell decline and high viral load during acute infection. J Virol 85:4828-40.

13. Landais E, Huang X, Havenar-Daughton C, Murrell B, Price MA, Wickramasinghe L, Ramos A, Bian CB, Simek M, Allen S, Karita E, Kilembe W, Lakhi S, Inambao M, Kamali A, Sanders EJ, Anzala O, Edward V, Bekker LG, Tang J, Gilmour J, Kosakovsky-Pond SL, Phung P, Wrin T, Crotty S, Godzik A, Poignard P. 2016. Broadly Neutralizing Antibody Responses in a Large Longitudinal Sub-Saharan HIV Primary Infection Cohort. PLoS Pathog 12:e1005369.

14. Lee JH, de Val N, Lyumkis D, Ward AB. 2015. Model Building and Refinement of a Natively Glycosylated HIV-1 Env Protein by High-Resolution Cryoelectron Microscopy. Structure 23:1943-1951.

15. Barnes CO, Gristick HB, Freund NT, Escolano A, Lyubimov AY, Hartweger H, West AP, Jr., Cohen AE, Nussenzweig MC, Bjorkman PJ. 2018. Structural characterization of a highly-potent V3-glycan broadly neutralizing antibody bound to natively-glycosylated HIV-1 envelope. Nat Commun 9:1251.

16. Lee JH, Andrabi R, Su CY, Yasmeen A, Julien JP, Kong L, Wu NC, McBride R, Sok D, Pauthner M, Cottrell CA, Nieusma T, Blattner C, Paulson JC, Klasse PJ, Wilson IA, Burton DR, Ward AB. 2017. A Broadly Neutralizing Antibody Targets the Dynamic HIV Envelope Trimer Apex via a Long, Rigidified, and Anionic beta-Hairpin Structure. Immunity 46:690-702.

17. Scharf L, Wang H, Gao H, Chen S, McDowall AW, Bjorkman PJ. 2015. Broadly Neutralizing Antibody 8ANC195 Recognizes Closed and Open States of HIV-1 Env. Cell 162:1379-90.

18. Blattner C, Lee JH, Sliepen K, Derking R, Falkowska E, de la Pena AT, Cupo A, Julien JP, van Gils M, Lee PS, Peng W, Paulson JC, Poignard P, Burton DR, Moore JP, Sanders RW, Wilson IA, Ward AB. 2014. Structural delineation of a quaternary, cleavage-dependent epitope at the gp41-gp120 interface on intact HIV-1 Env trimers. Immunity 40:669-80.

19. Wibmer CK, Moore PL, Morris L. 2015. HIV broadly neutralizing antibody targets. Curr Opin HIV AIDS 10:135-43.

20. Garces F, Lee JH, de Val N, de la Pena AT, Kong L, Puchades C, Hua Y, Stanfield RL, Burton DR, Moore JP, Sanders RW, Ward AB, Wilson IA. 2015. Affinity Maturation of a Potent Family of HIV Antibodies Is Primarily Focused on Accommodating or Avoiding Glycans. Immunity 43:1053-63.

21. MacLeod DT, Choi NM, Briney B, Garces F, Ver LS, Landais E, Murrell B, Wrin T, Kilembe W, Liang CH, Ramos A, Bian CB, Wickramasinghe L, Kong L, Eren K, Wu CY, Wong CH, Investigators IPC, The IAHIVRN, Kosakovsky Pond SL, Wilson IA, Burton DR, Poignard P. 2016. Early Antibody Lineage Diversification and Independent Limb Maturation Lead to Broad HIV-1 Neutralization Targeting the Env High-Mannose Patch. Immunity 44:1215-26.

22. Sok D, Laserson U, Laserson J, Liu Y, Vigneault F, Julien JP, Briney B, Ramos A, Saye KF, Le K, Mahan A, Wang S, Kardar M, Yaari G, Walker LM, Simen BB, St John EP, Chan-Hui PY, Swiderek K, Kleinstein SH, Alter G, Seaman MS, Chakraborty AK, Koller D, Wilson IA, Church GM, Burton DR, Poignard P. 2013. The effects of somatic hypermutation on neutralization and binding in the PGT121 family of broadly neutralizing HIV antibodies. PLoS Pathog 9:e1003754.

23. Bonsignori M, Kreider EF, Fera D, Meyerhoff RR, Bradley T, Wiehe K, Alam SM, Aussedat B, Walkowicz WE, Hwang KK, Saunders KO, Zhang R, Gladden MA, Monroe A, Kumar A, Xia SM, Cooper M, Louder MK, McKee K, Bailer RT, Pier BW, Jette CA, Kelsoe G, Williams WB, Morris L, Kappes J, Wagh K, Kamanga G, Cohen MS, Hraber PT, Montefiori DC, Trama A, Liao HX, Kepler TB, Moody MA, Gao F, Danishefsky SJ, Mascola JR, Shaw GM, Hahn BH, Harrison SC, Korber BT, Haynes BF. 2017. Staged induction of HIV-1 glycan-dependent broadly neutralizing antibodies. Sci Transl Med 9.

24. Alam SM, Aussedat B, Vohra Y, Meyerhoff RR, Cale EM, Walkowicz WE, Radakovich NA, Anasti K, Armand L, Parks R, Sutherland L, Scearce R, Joyce MG, Pancera M, Druz A, Georgiev IS, Von Holle T, Eaton A, Fox C, Reed SG, Louder M, Bailer RT, Morris L, Abdool-Karim SS, Cohen M, Liao HX, Montefiori DC, Park PK, Fernandez-Tejada A, Wiehe K, Santra S, Kepler TB, Saunders KO, Sodroski J, Kwong PD, Mascola JR, Bonsignori M, Moody MA, Danishefsky S, Haynes BF. 2017. Mimicry of an HIV broadly neutralizing antibody epitope with a synthetic glycopeptide. Sci Transl Med 9.

25. Buchacher A, Predl R, Strutzenberger K, Steinfellner W, Trkola A, Purtscher M, Gruber G, Tauer C, Steindl F, Jungbauer A, et al. 1994. Generation of human monoclonal antibodies against HIV-1 proteins; electrofusion and Epstein-Barr virus transformation for peripheral blood lymphocyte immortalization. AIDS Res Hum Retroviruses 10:359-69.

26. Freund NT, Wang H, Scharf L, Nogueira L, Horwitz JA, Bar-On Y, Golijanin J, Sievers SA, Sok D, Cai H, Cesar Lorenzi JC, Halper-Stromberg A, Toth I, Piechocka-Trocha A, Gristick HB, van Gils MJ, Sanders RW, Wang LX, Seaman MS, Burton DR, Gazumyan A, Walker BD, West AP, Jr., Bjorkman PJ, Nussenzweig MC. 2017. Coexistence of potent HIV-1 broadly neutralizing antibodies and antibody-sensitive viruses in a viremic controller. Sci Transl Med 9.

27. Mouquet H, Scharf L, Euler Z, Liu Y, Eden C, Scheid JF, Halper-Stromberg A, Gnanapragasam PN, Spencer DI, Seaman MS, Schuitemaker H, Feizi T, Nussenzweig MC, Bjorkman PJ. 2012.

Complex-type N-glycan recognition by potent broadly neutralizing HIV antibodies. Proc Natl Acad Sci U S A 109:E3268-77.

28. Walker LM, Huber M, Doores KJ, Falkowska E, Pejchal R, Julien JP, Wang SK, Ramos A, Chan-Hui PY, Moyle M, Mitcham JL, Hammond PW, Olsen OA, Phung P, Fling S, Wong CH, Phogat S, Wrin T, Simek MD, Principal Investigators PG, Koff WC, Wilson IA, Burton DR, Poignard P. 2011. Broad neutralization coverage of HIV by multiple highly potent antibodies. Nature 477:466-70.

29. Sok D, Pauthner M, Briney B, Lee JH, Saye-Francisco KL, Hsueh J, Ramos A, Le KM, Jones M, Jardine JG, Bastidas R, Sarkar A, Liang CH, Shivatare SS, Wu CY, Schief WR, Wong CH, Wilson IA, Ward AB, Zhu J, Poignard P, Burton DR. 2016. A Prominent Site of Antibody Vulnerability on HIV Envelope Incorporates a Motif Associated with CCR5 Binding and Its Camouflaging Glycans. Immunity 45:31-45.

30. Bonsignori M, Liao HX, Gao F, Williams WB, Alam SM, Montefiori DC, Haynes BF. 2017. Antibody-virus co-evolution in HIV infection: paths for HIV vaccine development. Immunol Rev 275:145-160.

31. Hoot S, McGuire AT, Cohen KW, Strong RK, Hangartner L, Klein F, Diskin R, Scheid JF, Sather DN, Burton DR, Stamatatos L. 2013. Recombinant HIV envelope proteins fail to engage germline versions of anti-CD4bs bNAbs. PLoS Pathog 9:e1003106.

32. Stamatatos L, Pancera M, McGuire AT. 2017. Germline-targeting immunogens. Immunol Rev 275:203-216.

33. Goo L, Chohan V, Nduati R, Overbaugh J. 2014. Early development of broadly neutralizing antibodies in HIV-1-infected infants. Nat Med 20:655-8.

34. Muenchhoff M, Adland E, Karimanzira O, Crowther C, Pace M, Csala A, Leitman E, Moonsamy A, McGregor C, Hurst J, Groll A, Mori M, Sinmyee S, Thobakgale C, Tudor-Williams G, Prendergast AJ, Kloverpris H, Roider J, Leslie A, Shingadia D, Brits T, Daniels S, Frater J, Willberg CB, Walker BD, Ndung'u T, Jooste P, Moore PL, Morris L, Goulder P. 2016. Nonprogressing HIV-infected children share fundamental immunological features of nonpathogenic SIV infection. Sci Transl Med 8:358ra125.

35. Ditse Z, Muenchhoff M, Adland E, Jooste P, Goulder P, Moore PL, Morris L. 2018. HIV-1 Subtype C-Infected Children with Exceptional Neutralization Breadth Exhibit Polyclonal Responses Targeting Known Epitopes. J Virol 92.

36. Simonich CA, Williams KL, Verkerke HP, Williams JA, Nduati R, Lee KK, Overbaugh J. 2016. HIV-1 Neutralizing Antibodies with Limited Hypermutation from an Infant. Cell 166:77-87.

37. Sanders RW, Derking R, Cupo A, Julien JP, Yasmeen A, de Val N, Kim HJ, Blattner C, de la Pena AT, Korzun J, Golabek M, de Los Reyes K, Ketas TJ, van Gils MJ, King CR, Wilson IA, Ward AB, Klasse PJ, Moore JP. 2013. A next-generation cleaved, soluble HIV-1 Env trimer, BG505 SOSIP.664 gp140, expresses multiple epitopes for broadly neutralizing but not non-neutralizing antibodies. PLoS Pathog 9:e1003618.

38. Verkerke HP, Williams JA, Guttman M, Simonich CA, Liang Y, Filipavicius M, Hu SL, Overbaugh J, Lee KK. 2016. Epitope-Independent Purification of Native-Like Envelope Trimers from Diverse HIV-1 Isolates. J Virol 90:9471-82.

39. Tang G, Peng L, Baldwin PR, Mann DS, Jiang W, Rees I, Ludtke SJ. 2007. EMAN2: an extensible image processing suite for electron microscopy. J Struct Biol 157:38-46.

40. Suloway C, Shi J, Cheng A, Pulokas J, Carragher B, Potter CS, Zheng SQ, Agard DA, Jensen GJ. 2009. Fully automated, sequential tilt-series acquisition with Leginon. J Struct Biol 167:11-8.

41. Rantalainen K, Berndsen ZT, Murrell S, Cao L, Omorodion O, Torres JL, Wu M, Umotoy J, Copps J, Poignard P, Landais E, Paulson JC, Wilson IA, Ward AB. 2018. Co-evolution of HIV Envelope and Apex-Targeting Neutralizing Antibody Lineage Provides Benchmarks for Vaccine Design. Cell Rep 23:3249-3261.

42. Stark H. 2010. GraFix: stabilization of fragile macromolecular complexes for single particle cryo-EM. Methods Enzymol 481:109-26.

43. Wong SS, Wong LJ. 1992. Chemical crosslinking and the stabilization of proteins and enzymes. Enzyme Microb Technol 14:866-74.

44. Taylor BS, Hammer SM. 2008. The challenge of HIV-1 subtype diversity. N Engl J Med 359:1965-6.

45. Dampier W, Nonnemacher MR, Mell J, Earl J, Ehrlich GD, Pirrone V, Aiamkitsumrit B, Zhong W, Kercher K, Passic S, Williams JW, Jacobson JM, Wigdahl B. 2016. HIV-1 Genetic Variation Resulting in the Development of New Quasispecies Continues to Be Encountered in the Peripheral Blood of Well-Suppressed Patients. PLoS One 11:e0155382.

46. Gautam R, Nishimura Y, Pegu A, Nason MC, Klein F, Gazumyan A, Golijanin J, Buckler-White A, Sadjadpour R, Wang K, Mankoff Z, Schmidt SD, Lifson JD, Mascola JR, Nussenzweig MC, Martin MA. 2016. A single injection of anti-HIV-1 antibodies protects against repeated SHIV challenges. Nature 533:105-109.

47. Klein F, Halper-Stromberg A, Horwitz JA, Gruell H, Scheid JF, Bournazos S, Mouquet H, Spatz LA, Diskin R, Abadir A, Zang T, Dorner M, Billerbeck E, Labitt RN, Gaebler C, Marcovecchio P, Incesu RB, Eisenreich TR, Bieniasz PD, Seaman MS, Bjorkman PJ, Ravetch JV, Ploss A, Nussenzweig MC. 2012. HIV therapy by a combination of broadly neutralizing antibodies in humanized mice. Nature 492:118-22.

48. Mascola JR, Stiegler G, VanCott TC, Katinger H, Carpenter CB, Hanson CE, Beary H, Hayes D, Frankel SS, Birx DL, Lewis MG. 2000. Protection of macaques against vaginal transmission of a pathogenic HIV-1/SIV chimeric virus by passive infusion of neutralizing antibodies. Nat Med 6:207-10.

49. Shingai M, Nishimura Y, Klein F, Mouquet H, Donau OK, Plishka R, Buckler-White A, Seaman M, Piatak M, Jr., Lifson JD, Dimitrov DS, Nussenzweig MC, Martin MA. 2013. Antibody-mediated immunotherapy of macaques chronically infected with SHIV suppresses viraemia. Nature 503:277-80.

50. Caskey M, Klein F, Lorenzi JC, Seaman MS, West AP, Jr., Buckley N, Kremer G, Nogueira L, Braunschweig M, Scheid JF, Horwitz JA, Shimeliovich I, Ben-Avraham S, Witmer-Pack M, Platten M, Lehmann C, Burke LA, Hawthorne T, Gorelick RJ, Walker BD, Keler T, Gulick RM, Fatkenheuer G, Schlesinger SJ, Nussenzweig MC. 2015. Viraemia suppressed in HIV-1-infected humans by broadly neutralizing antibody 3BNC117. Nature 522:487-91.

51. Caskey M, Schoofs T, Gruell H, Settler A, Karagounis T, Kreider EF, Murrell B, Pfeifer N, Nogueira L, Oliveira TY, Learn GH, Cohen YZ, Lehmann C, Gillor D, Shimeliovich I, Unson-O'Brien C, Weiland D, Robles A, Kummerle T, Wyen C, Levin R, Witmer-Pack M, Eren K, Ignacio C, Kiss S, West AP, Jr., Mouquet H, Zingman BS, Gulick RM, Keler T, Bjorkman PJ, Seaman MS, Hahn BH, Fatkenheuer G, Schlesinger SJ, Nussenzweig MC, Klein F. 2017. Antibody 10-1074 suppresses viremia in HIV-1-infected individuals. Nat Med 23:185-191.

52. Burton DR, Hangartner L. 2016. Broadly Neutralizing Antibodies to HIV and Their Role in Vaccine Design. Annu Rev Immunol 34:635-59.

53. Haynes BF, Montefiori DC. 2006. Aiming to induce broadly reactive neutralizing antibody responses with HIV-1 vaccine candidates. Expert Rev Vaccines 5:579-95.

54. Klein F, Mouquet H, Dosenovic P, Scheid JF, Scharf L, Nussenzweig MC. 2013. Antibodies in HIV-1 vaccine development and therapy. Science 341:1199-204.

55. Kong L, Lee JH, Doores KJ, Murin CD, Julien JP, McBride R, Liu Y, Marozsan A, Cupo A, Klasse PJ, Hoffenberg S, Caulfield M, King CR, Hua Y, Le KM, Khayat R, Deller MC, Clayton T, Tien H, Feizi T, Sanders RW, Paulson JC, Moore JP, Stanfield RL, Burton DR, Ward AB, Wilson IA. 2013. Supersite of immune vulnerability on the glycosylated face of HIV-1 envelope glycoprotein gp120. Nat Struct Mol Biol 20:796-803.

56. Pancera M, Zhou T, Druz A, Georgiev IS, Soto C, Gorman J, Huang J, Acharya P, Chuang GY, Ofek G, Stewart-Jones GB, Stuckey J, Bailer RT, Joyce MG, Louder MK, Tumba N, Yang Y, Zhang B, Cohen MS, Haynes BF, Mascola JR, Morris L, Munro JB, Blanchard SC, Mothes W, Connors M, Kwong PD. 2014. Structure and immune recognition of trimeric pre-fusion HIV-1 Env. Nature 514:455-61.

57. Schmidt AG, Xu H, Khan AR, O'Donnell T, Khurana S, King LR, Manischewitz J, Golding H, Suphaphiphat P, Carfi A, Settembre EC, Dormitzer PR, Kepler TB, Zhang R, Moody MA, Haynes BF, Liao HX, Shaw DE, Harrison SC. 2013. Preconfiguration of the antigen-binding site during affinity maturation of a broadly neutralizing influenza virus antibody. Proc Natl Acad Sci U S A 110:264-9.

58. Eisen HN, Chakraborty AK. 2010. Evolving concepts of specificity in immune reactions. Proc Natl Acad Sci U S A 107:22373-80.

59. Thorpe IF, Brooks CL, 3rd. 2007. Molecular evolution of affinity and flexibility in the immune system. Proc Natl Acad Sci U S A 104:8821-6.

60. Finton KA, Friend D, Jaffe J, Gewe M, Holmes MA, Larman HB, Stuart A, Larimore K, Greenberg PD, Elledge SJ, Stamatatos L, Strong RK. 2014. Ontogeny of recognition specificity and functionality for the broadly neutralizing anti-HIV antibody 4E10. PLoS Pathog 10:e1004403.

61. Klein F, Diskin R, Scheid JF, Gaebler C, Mouquet H, Georgiev IS, Pancera M, Zhou T, Incesu RB, Fu BZ, Gnanapragasam PN, Oliveira TY, Seaman MS, Kwong PD, Bjorkman PJ, Nussenzweig MC. 2013. Somatic mutations of the immunoglobulin framework are generally required for broad and potent HIV-1 neutralization. Cell 153:126-38.

62. Davenport TM, Gorman J, Joyce MG, Zhou T, Soto C, Guttman M, Moquin S, Yang Y, Zhang B, Doria-Rose NA, Hu SL, Mascola JR, Kwong PD, Lee KK. 2016. Somatic Hypermutation-Induced Changes in the Structure and Dynamics of HIV-1 Broadly Neutralizing Antibodies. Structure 24:1346-1357.

Chapter 5. Summary and Future Directions

The entry of enveloped viruses occurs through the attachment of viral glycoproteins to host-cell receptors followed by fusion of viral and host-cell membranes. These glycoproteins not only serve a critical role in infection but also represent a major target of neutralizing antibodies (nAbs). During natural infection, nAbs play a key role in the immune response against enveloped viruses by binding to viral glycoproteins, yet a major gap has existed in our understanding of the mechanisms by which nAbs act. The objective of this dissertation was to shed light on antibody-mediated mechanisms of neutralization of enveloped viruses and the ability of nAbs to inhibit viral glycoprotein function by examining two significant human pathogens, influenza and HIV-1.

In Chapter 2, I described the impact of bivalency on the ability of IgG to arrest viral infectivity by comparing the neutralization of virus by intact IgG and monovalent Fab domains. I observed that the Ab-mediated inhibition of HA function occurs by multiple complementary mechanisms and is largely dependent on the specific epitope that is targeted and on the bivalent nature of IgG molecules. Using cryo-electron tomography (cryo-ET) in combination with biophysical assays, I revealed that the ability of nAbs to aggregate influenza virus particles enhances the inhibition of HA at an early stage of fusion peptide-induced membrane disruption through the occlusion of infectious virions, even at concentrations well below antigen saturation. Unexpectedly, HC19, a nAb that targets the receptor binding site towards the distal end of HA (1), also inhibited the ability of HA to undergo low pH-induced conformational changes that are necessary for fusion to occur. Epitopes further down the HA stem do not exhibit cross-linking across separate particles; however, bivalent interspike cross-linking by FI6v3 IgG within a given virus particle appeared to be critical for its neutralizing activity. This chapter is one of few studies to date (2, 3) that structurally characterizes the interactions between full-length IgG and whole virus, but this work is unique in that it provides functional consequences for the complex interactions observed by cryo-ET. Furthermore, this study underscores the necessity to consider bivalent interactions when developing a general model of antibody-mediated neutralization.

In Chapter 3, I provide structural characterization of the first, and currently, the best described broadly neutralizing antibody (bnAb) isolated from an HIV-1 infected infant (4). Until recently, the ability of

infants to mount a neutralizing antibody response against HIV-1 was largely unknown (5). Therefore, earlier research relied on characterization of bnAbs from chronically infected adults. Infant-derived bnAb, BF520.1, is exceptional in that it developed within one year post-infection and did so with few mutations. This contrasts with observations of adult-derived bnAbs, which generate after several years of extensive somatic hypermutation (6-10). Prior to this study, it was unclear if infant-derived bnAbs target novel epitopes or those similar to bnAbs isolated in adults. My work indicated that BF520.1 binds a familiar epitope that is commonly targeted by adult bnAbs, namely, the V3-glycan region (11-13). Although the majority of bnAbs characterized to date have focused on the contacts mediated by the antibody variable heavy chain, we identified that maturation in the BF520.1 variable light chain was particularly important for HIV Env binding and neutralization by making extensive contacts with the N332 glycan.

Chapter 4 expands on BF520.1 development by beginning to characterize early antibody lineage intermediates. $Int2_{VH}Int2_{VK}$ and $Int4_{VH}Int4_{VK}$ are both early antibody lineage intermediates that bridge the development from a weakly neutralizing Ab ($Int2_{VH}Int2_{VK}$), to an intermediate exhibiting heterologous breadth ($Int4_{VH}Int4_{VK}$). Processing of cryo-EM data collected for $Int4_{VH}Int4_{VK}$ is currently on-going with a goal of achieving high resolution structural information for comparison with the mature BF520.1 structure.

Overall, the results obtained during my studies suggest novel directions for future research, which will ideally provide new insights into mechanisms of antibody mediated neutralization, and illuminate the developmental pathway of BF520.1 which may be an attractive template for vaccine design against HIV-1.

5.1 High resolution characterization of the HA trimer stabilized by HC19 at neutral and low pH

Results in Chapter 2 suggest that neutralization by HC19 acts through multiple complementary mechanisms by arresting HA function at two distinct stages of the fusion pathway. Although high resolution structures of HC19 in complex with HA1 suggest that neutralization is achieved by blocking receptor engagement (1), HC19 and likely similar antibodies that bind to HA1, appear to be able to inhibit later stages of HA's conformational changes that are required for lipid mixing. HC19 binds to the HA trimer in such a fashion that the fusion peptides can still be released, and then bind to and perturb the target membrane. This data is consistent with an HA fusion activation pathway where the fusion peptide can be released prior to HA1 dissociation without requiring full HA spike reorganization (14-16). Another HA1-targeted nAb, HC63,

was previously shown to inhibit HA activation; however, in that case, the antibody itself bridges two HA1 subunits of the same trimer, preventing their dissociation (17, 18). For HC19, Fab interacts with a single protomer (1), and hence, I infer that it acts by stabilizing the subunit's conformation and indirectly, the HA1-HA1 “cage” that prevents the full refolding of the HA2 subunit. Alternatively, it is conceivable that with Fab bound to the HC19 epitope at the apex of the spike, the fusion machinery may be sterically blocked from drawing the two membranes into close enough proximity to fuse, despite allowing fusion peptide insertion into the target membrane.

Negative-stain EM analysis of the soluble bromelain-released HA trimer bound by HC19 Fab and exposed to acidic pH indicated that the trimeric spike overall remained intact. A key piece of information that remains unresolved are the interactions between HC19 and HA that mediates stabilization under acidic conditions. A step to illuminate these interactions would be to solve the high resolution structure of HC19 bound to HA at low pH using cryo-EM single-particle techniques. While the HA1 trimeric interface should remain largely intact, I anticipate a thinning of the HA stalk, which would indicate fusion peptide release or relaxation within the HA2 subunit. A recent study used cryo-electron tomography and subtomogram averaging techniques to observe the structure of HA under acidic conditions. Although they noted a thinning of the HA stalk, the data lacked the resolution necessary to observe detailed structural information (19). It is also possible that the structure of HA2 upon fusion-peptide release may be highly dynamic and thus limit the achievable resolution within the HA2 domain by cryo-EM.

In combination with cryo-EM, it would be advantageous to use Hydrogen-Deuterium exchange Mass Spectrometry (HDX-MS). HDX-MS probes the local structure of native proteins, providing a fingerprint of structural dynamics with the resolution desired to provide a detailed fingerprint of ligand-induced structural changes and isolate-specific differences in protein structure (14, 20-24). HDX-MS alone does not provide three-dimensional structural information, but measures structural dynamics or flexibility of protein segments as they exist under experimental conditions. In combination with structural information provided by cryo-EM, HDX-MS would be a powerful method for characterizing structural alterations in HA2 that may be too dynamic and flexible to characterize cryo-EM alone.

A research study from our lab probed the conformational dynamics of BHA at pH conditions approaching fusion activation (14). Garcia and colleagues observed that regions in HA2 showed dynamic

differences, with the N-terminal fusion peptide showing the greatest amount of solvent exposure in response to pH. Additionally, HA1-HA2 interfacial peptides, specifically peptides spanning the HA1 hinge domain, also exhibited more dynamic behavior at low pH. In contrast, the HA1 trimeric interface at pH 5.6 appeared to become more protected from solvent exposure compared to neutral pH. I hypothesize that HC19 bound to BHA under fusion activating conditions will allow significant dynamic behavior of regions of HA2, specifically the N-terminal fusion peptide. Furthermore, I predict that the HA1 hinge region resting above HA2 would become stabilized by HC19, possibly restricting exposure of HA2's B-loop. This would further support a fusion activation pathway suggested by others, where fusion peptide release precedes HA1 dissociation (14, 15, 19). Furthermore, in additional to blocking receptor binding, the restriction of HA2 rearrangement through stabilization of the HA1 trimeric interface, may be important considerations when developing vaccination strategies or therapeutic intervention.

5.2 Cryo-EM reconstruction of BF520.1 lineage intermediates with BG505.SOSIP trimers

The focus of Chapter 2 was to render a structural model of BF520.1 in complex with heterologous BG505.SOSIP trimer. In combination with the antibody's developmental pathway, defined by collaborators, we revealed that development of the variable light chain and specifically mutations in the CDRL1 loop were important for the broad and potent neutralization observed by BF520.1. We also noted that the presence of the N332 glycan is critical for BF520.1 binding and neutralization, and is the major feature of the targeted epitope (4). One caveat in the proposed model is our assumption that the structure of BF520.1 Fab generated by predictive software accurately reflects the native structure of BF520.1. Although overall fold architecture of Fab is relatively invariant between antibodies, loop positioning between the generated structures in our study, specifically for CDRH3, was highly variable. To address this concern, I will be crystallizing BF520.1, as well as two lineage intermediates that were selected in Chapter 4 to obtain a more accurate description of loop positioning. This will allow us to accurately assign loop positioning and better attribute the interactions of CDRH3 with BG505.SOSIP trimer.

In our proposed model, the mutations observed in CDRL1 that occur early in development are thought to make extensive contact with the N332 glycan, which may account for the measured binding of early lineage intermediates to BG505.SOSIP trimers (see Chapter 4). However, high resolution structures

of the BF520.1 lineage intermediates in complex with SOSIP trimer, and a thorough analysis of interactions between the Ab lineage and SOSIPs lacking N332 will be required to either support or refute these claims. To this end, a dataset of $Int4_{VH}Int4_{VK}$ in complex with BG505.SOSIP trimer is currently being processed. For $Int2_{VH}Int2_{VK}$, the lower binding affinity results in a large population of unbound trimers on electron microscopy grids. To overcome heterogeneity in proteins and protein complexes, studies have often relied on glutaraldehyde fixation to form more stable samples (25-28). I propose to chemically crosslink $Int2_{VH}Int2_{VK}$ to BG505.SOSIP to saturate binding sites, providing an appropriate sample condition for structural determination by cryo-EM. On-going single-particle cryo-EM analysis will provide higher resolution detail to illustrate how antibody-Env contacts evolved over the course of affinity maturation.

Additionally, our current data does not describe the effect of framework mutations on paratope stability and must be further explored using additional methodologies such as HDX-MS (29). We have speculated that contacts between the CDRL1 loop and N332 glycan are established at an early stage of maturation, and may become stabilized by framework mutations around CDRL1, providing an anchor for the developmental pathway of BF520.1. Alternatively, framework mutations may increase the Fab's overall flexibility to promote binding to a broad range of diverse HIV-1 isolates. Once x-ray crystal structures are determined for BF520.1, $Int4_{VH}Int4_{VK}$ and $Int2_{VH}Int2_{VK}$, HDX-MS should be performed to monitor the dynamic behavior of the Fab along the BF520.1 maturation pathway.

5.3 Co-evolution of BF520.1 development with autologous founder virus

Our current work has largely focused on characterizing the interactions between the BF520.1 antibody lineage and the heterologous HIV-1 isolate, BG505. Although BF520.1 has potent and broad heterologous neutralization, it is not able to neutralize the autologous BF520 founder virus that initiated the BF520.1 response, despite binding to BF520 trimer (4). Although BF520.1 does not neutralize the transmitted autologous virus, recent data by collaborators show that BF520 variants isolated from 6 months of age (M6) become sensitive to neutralization, which is ~2.2 months after infection was detected (4). Similar to the mature mAb BF520.1, the early lineage intermediates were not able to neutralize the transmitted autologous envelope. It remains unclear what differences exist between the BF520 founder virus and the M6 variant. Therefore, it would also be of interest to use HDX-MS to parse out differences in

the dynamic behavior of both the transmitted founder virus and M6 variant. Perhaps the BF520 founder virus exhibits more dynamic behavior around the BF520.1 epitope and alters the presentation of glycan or key residues that are contacted by CDR-loops. As BF520 evolves, the M6 variant may differ in the accessibility of the epitope or changes in glycan positioning compared to the earlier variant.

In a recent study of the co-evolution of V1/V2 apex-targeting antibody and HIV-1, comparison of complexes at early and late time points revealed that, within the antibody lineage, the CDRH3 loop rigidified, and the bnAb angle of approach steepened as maturation progressed (30). The BF520.1 bnAb is well-suited for a similar study. We have expressed and purified both the BF520 founder virus and BF520 M6 variant, providing early and late Env trimer constructs. Binding affinity of the BF520.1 lineage to both BF520 and the BF5201 M6 variant will be performed by BLI to monitor changes in binding affinity during development. This data will help direct sample optimization for cryo-EM analysis, which may or may not require glutaraldehyde fixation. Cryo-EM structures should be solved for the early and late intermediate, as well as mature BF520.1 bound to the BF520 founder and M6 isolate. I aim to learn how BF520 Env structure, which initiated BF520.1 development, remains resistant to neutralization despite binding to the mature BF520.1. Furthermore, I hope to illuminate how evolution of BF520, often a method of viral escape, imparts sensitivity to neutralization. We suggested in Chapter 3 that early mutations in CDRL1 made extensive contacts with the N332 glycan. I hypothesize that early intermediates containing these mutations also bind the N332 glycan of the BF520 founder virus. However, other features of the epitope are not optimally presented, perhaps due to highly dynamic behavior, which prevents neutralization. Still, the weak binding may help drive viral diversification. I predict that the M6 variant presents a more stable epitope to later antibody intermediates that improves variable heavy chain contacts in addition to maintaining CDRL1–N332 glycan contacts, therefore, becoming sensitive to neutralization. High resolution structural information of the co-evolutionary pathway between BF520.1 and virus will shed light on the complex interplay between the antibody response and HIV-1, and may provide an exemplary model for the design of germline targeted immunogens to direct a similar developmental pathway by vaccination strategies.

5.4 Concluding remarks

Taken together, the results obtained during my studies have shown that using a combination of biophysical and structural approaches can provide new insights into the mechanisms of antibody mediated neutralization against viral glycoproteins. The importance of bivalent Fab presentation by full-length antibodies likely applies to other viral pathogens where a high copy number of antigens exist on the viral surface and allows for complex binding to occur. Furthermore, our work with BF520.1 characterizes the unique ability of infants to respond against infection with HIV-1 without extensive affinity maturation commonly observed in adults; characteristics that are highly desirable for vaccine development. Ultimately, my work has unveiled complex ways that antibodies can neutralize virus and underscores the need for continued exploration of the mechanisms by which they act.

References

1. Bizebard T, Daniels R, Kahn R, Golinelli-Pimpaneau B, Skehel JJ, Knossow M. 1994. Refined three-dimensional structure of the Fab fragment of a murine IgG1, lambda antibody. Acta Crystallographica Section D, Biological Crystallography 50:768-777.
2. Hai R, Krammer F, Tan GS, Pica N, Eggink D, Maamary J, Margine I, Albrecht RA, Palese P. 2012. Influenza viruses expressing chimeric hemagglutinins: globular head and stalk domains derived from different subtypes. J Virol 86:5774-81.
3. Harris AK, Meyerson JR, Matsuoka Y, Kuybeda O, Moran A, Bliss D, Das SR, Yewdell JW, Sapiro G, Subbarao K, Subramaniam S. 2013. Structure and accessibility of HA trimers on intact 2009 H1N1 pandemic influenza virus to stem region-specific neutralizing antibodies. Proc Natl Acad Sci U S A 110:4592-7.
4. Simonich CA, Williams KL, Verkerke HP, Williams JA, Nduati R, Lee KK, Overbaugh J. 2016. HIV-1 Neutralizing Antibodies with Limited Hypermutation from an Infant. Cell 166:77-87.
5. Goo L, Chohan V, Nduati R, Overbaugh J. 2014. Early development of broadly neutralizing antibodies in HIV-1-infected infants. Nat Med 20:655-8.
6. Klein F, Mouquet H, Dosenovic P, Scheid JF, Scharf L, Nussenzweig MC. 2013. Antibodies in HIV-1 vaccine development and therapy. Science 341:1199-204.
7. West AP, Jr., Scharf L, Scheid JF, Klein F, Bjorkman PJ, Nussenzweig MC. 2014. Structural insights on the role of antibodies in HIV-1 vaccine and therapy. Cell 156:633-48.
8. Doria-Rose NA, Schramm CA, Gorman J, Moore PL, Bhiman JN, DeKosky BJ, Ernandes MJ, Georgiev IS, Kim HJ, Pancera M, Staupe RP, Altae-Tran HR, Bailer RT, Crooks ET, Cupo A, Druz A, Garrett NJ, Hoi KH, Kong R, Louder MK, Longo NS, McKee K, Nonyane M, O'Dell S, Roark RS, Rudicell RS, Schmidt SD, Sheward DJ, Soto C, Wibmer CK, Yang Y, Zhang Z, Program NCS, Mullikin JC, Binley JM, Sanders RW, Wilson IA, Moore JP, Ward AB, Georgiou G, Williamson C, Abdool Karim SS, Morris L, Kwong PD, Shapiro L, Mascola JR. 2014. Developmental pathway for potent V1V2-directed HIV-neutralizing antibodies. Nature 509:55-62.
9. Sok D, Laserson U, Laserson J, Liu Y, Vigneault F, Julien JP, Briney B, Ramos A, Saye KF, Le K, Mahan A, Wang S, Kardar M, Yaari G, Walker LM, Simen BB, St John EP, Chan-Hui PY, Swiderek K, Kleinstein SH, Alter G, Seaman MS, Chakraborty AK, Koller D, Wilson IA, Church GM, Burton DR, Poignard P. 2013. The effects of somatic hypermutation on neutralization and binding in the PGT121 family of broadly neutralizing HIV antibodies. PLoS Pathog 9:e1003754.
10. Landais E, Moore PL. 2018. Development of broadly neutralizing antibodies in HIV-1 infected elite neutralizers. Retrovirology 15:61.
11. Wibmer CK, Moore PL, Morris L. 2015. HIV broadly neutralizing antibody targets. Curr Opin HIV AIDS 10:135-43.
12. Carrow EW, Vujcic LK, Glass WL, Seamon KB, Rastogi SC, Hendry RM, Boulos R, Nzila N, Quinnan GV, Jr. 1991. High prevalence of antibodies to the gp120 V3 region principal neutralizing determinant of HIV-1MN in sera from Africa and the Americas. AIDS Res Hum Retroviruses 7:831-8.
13. Sok D, Pauthner M, Briney B, Lee JH, Saye-Francisco KL, Hsueh J, Ramos A, Le KM, Jones M, Jardine JG, Bastidas R, Sarkar A, Liang CH, Shivatare SS, Wu CY, Schief WR, Wong CH, Wilson IA, Ward AB, Zhu J, Poignard P, Burton DR. 2016. A Prominent Site of Antibody Vulnerability on HIV Envelope Incorporates a Motif Associated with CCR5 Binding and Its Camouflaging Glycans. Immunity 45:31-45.
14. Garcia NK, Guttman M, Ebner JL, Lee KK. 2015. Dynamic changes during acid-induced activation of influenza hemagglutinin. Structure 23:665-76.
15. White JM, Wilson IA. 1987. Anti-peptide antibodies detect steps in a protein conformational change: low-pH activation of the influenza virus hemagglutinin. J Cell Biol 105:2887-96.

16. White JM, Delos SE, Brecher M, Schornberg K. 2008. Structures and mechanisms of viral membrane fusion proteins: multiple variations on a common theme. Crit Rev Biochem Mol Biol 43:189-219.

17. Barbey-Martin C, Gigant B, Bizebard T, Calder LJ, Wharton SA, Skehel JJ, Knossow M. 2002. An antibody that prevents the hemagglutinin low pH fusogenic transition. Virology 294:70-4.

18. Knossow M, Gaudier M, Douglas A, Barrere B, Bizebard T, Barbey C, Gigant B, Skehel JJ. 2002. Mechanism of neutralization of influenza virus infectivity by antibodies. Virology 302:294-8.

19. Fontana J, Cardone G, Heymann JB, Winkler DC, Steven AC. 2012. Structural changes in Influenza virus at low pH characterized by cryo-electron tomography. J Virol 86:2919-29.

20. Davenport TM, Guttman M, Guo W, Cleveland B, Kahn M, Hu SL, Lee KK. 2013. Isolate-specific differences in the conformational dynamics and antigenicity of HIV-1 gp120. J Virol 87:10855-73.

21. Konermann L, Pan J, Liu YH. 2011. Hydrogen exchange mass spectrometry for studying protein structure and dynamics. Chem Soc Rev 40:1224-34.

22. Marcsisin SR, Engen JR. 2010. Hydrogen exchange mass spectrometry: what is it and what can it tell us? Anal Bioanal Chem 397:967-72.

23. Guttman M, Cupo A, Julien JP, Sanders RW, Wilson IA, Moore JP, Lee KK. 2015. Antibody potency relates to the ability to recognize the closed, pre-fusion form of HIV Env. Nat Commun 6:6144.

24. Lewis HA, Wang C, Zhao X, Hamuro Y, Conners K, Kearins MC, Lu F, Sauder JM, Molnar KS, Coales SJ, Maloney PC, Guggino WB, Wetmore DR, Weber PC, Hunt JF. 2010. Structure and dynamics of NBD1 from CFTR characterized using crystallography and hydrogen/deuterium exchange mass spectrometry. J Mol Biol 396:406-30.

25. Wong SS, Wong LJ. 1992. Chemical crosslinking and the stabilization of proteins and enzymes. Enzyme Microb Technol 14:866-74.

26. Shukla AK, Westfield GH, Xiao K, Reis RI, Huang LY, Tripathi-Shukla P, Qian J, Li S, Blanc A, Oleskie AN, Dosey AM, Su M, Liang CR, Gu LL, Shan JM, Chen X, Hanna R, Choi M, Yao XJ, Klink BU, Kahsai AW, Sidhu SS, Koide S, Penczek PA, Kossiakoff AA, Woods VL, Jr., Kobilka BK, Skiniotis G, Lefkowitz RJ. 2014. Visualization of arrestin recruitment by a G-protein-coupled receptor. Nature 512:218-222.

27. Stark H. 2010. GraFix: stabilization of fragile macromolecular complexes for single particle cryo-EM. Methods Enzymol 481:109-26.

28. Southworth DR, Agard DA. 2011. Client-loading conformation of the Hsp90 molecular chaperone revealed in the cryo-EM structure of the human Hsp90:Hop complex. Mol Cell 42:771-81.

29. Davenport TM, Gorman J, Joyce MG, Zhou T, Soto C, Guttman M, Moquin S, Yang Y, Zhang B, Doria-Rose NA, Hu SL, Mascola JR, Kwong PD, Lee KK. 2016. Somatic Hypermutation-Induced Changes in the Structure and Dynamics of HIV-1 Broadly Neutralizing Antibodies. Structure 24:1346-1357.

30. Liao HX, Lynch R, Zhou T, Gao F, Alam SM, Boyd SD, Fire AZ, Roskin KM, Schramm CA, Zhang Z, Zhu J, Shapiro L, Program NCS, Mullikin JC, Gnanakaran S, Hraber P, Wiehe K, Kelsoe G, Yang G, Xia SM, Montefiori DC, Parks R, Lloyd KE, Scearce RM, Soderberg KA, Cohen M, Kamanga G, Louder MK, Tran LM, Chen Y, Cai F, Chen S, Moquin S, Du X, Joyce MG, Srivatsan S, Zhang B, Zheng A, Shaw GM, Hahn BH, Kepler TB, Korber BT, Kwong PD, Mascola JR, Haynes BF. 2013. Co-evolution of a broadly neutralizing HIV-1 antibody and founder virus. Nature 496:469-76.